PROFILING OF LOW-OCCUPANCY, KINETICALLY PRIVILEGED ELECTROPHILE SENSORS IN THE C. ELEGANS CYSTEINOME: A WINDOW INTO ENDOGENOUS REDOX SIGNALING

A Dissertation

Presented to the Faculty of the Graduate School

of Cornell University

In Partial Fulfillment of the Requirements for the Degree of

Doctor of Philosophy

By

Daniel Ahmet Urul

December 2020

PROFILING OF LOW-OCCUPANCY, KINETICALLY PRIVILEGED ELECTROPHILE SENSORS IN THE *C. ELEGANS* CYSTEINOME: A WINDOW INTO ENDOGENOUS REDOX SIGNALING

Daniel Ahmet Urul, PhD

Cornell University 2020

Recent advances in the pharmacokinetic understanding of irreversible inhibitors have led to renewed interest in covalent drug development. A major driving force behind this therapeutics renaissance is the emergence of a "redox-sensing proteome" that facilitates key intracellular signaling pathways and acute stress responses by utilizing reactive electrophilic species (RES) in lieu of canonical signaling biomolecules. The ability to detect RES at endogenous concentrations and convert RES flux into a downstream output is engendered by "kinetically privileged" cysteine residues able to facilitate rapid covalent modification. Thus, mining the cysteinome for such uniquely reactive targets can guide future pharmaceutical strategies. Indeed, several contemporary profiling techniques have been developed to capture these cysteines and their associated RES-sensor proteins. However, despite their continued usefulness, many of these systems require heavy exogenous dosing of the RES of interest. In treating the system with minimal temporal or spatial control, many RES-sensing proteins that undergo low endogenous modification of an otherwise "kinetically privileged" cysteine sensor may be missed, and the pathways facilitated by the ones that

are captured may be obfuscated by the breadth of accompanying off-target effects. Furthermore, many of these methods are incompatible with live-animal models, further reducing the biological context within which these "low-occupancy" sensors operate.

To better elucidate these RES sensors and their impact as signaling mediators, a novel profiling method must be able to facilitate controlled RES deployment within a whole-organism context. This work describes the development of one such method, adapting a comprehensive screening platform for the direct identification of novel, low-occupancy RES sensors for use in *C. elegans,* a renowned model organism. Following proof-of-concept targeted labeling of a known RES sensor *in vivo,* we uncovered novel redox-sensing functionality in S-adenosylhomocysteine hydrolase (SAHH) through pilot cysteinomic profiling efforts in *C. elegans*. This highly conserved SAHH also allowed us to investigate the nature of RES-sensing conservation across species, forming a basis through which sensing capability in seemingly disparate species can inform functionality in a human context. With the potential to further fine-tune future profiling efforts with tissue- and organelle-specificity, *C. elegans* offers a significant avenue for deepening our comprehension of RES-mediated signaling pathways with relevance to human biology.

BIOGRAPHICAL SKETCH

Daniel Urul was born in Woonsocket, Rhode Island on July 30th, 1992, to Nulufer and Ercan Urul, a pair of successful restaurant owners who had independently immigrated from Turkey years prior. Around early 2007, he moved with his family to Jacksonville, Florida, where he completed his high school studies. It was during this time that his affinity for chemistry began to surface, fostered by several excellent high school science teachers. This interest continued to grow as he began his undergraduate studies at the University of Florida in 2010 as an Honors Program member. With the aid of an undergraduate research scholarship from the Howard Hughes Medical Institute, he began work under Professor Steven Bruner, culminating in a thesis project characterizing putative siderophore-specific iron-sulfur reductases. After graduating with a B.S. in chemistry *summa cum laude* and a minor in mathematics, he remained at UF for another year, working in the computational biochemistry lab of Professor Kenneth Merz as a technical reader and assistant to then-Ph.D. candidate Mona Minkara, now a Northeastern University professor and advocate for the blind scientist community. Now committed to pursuing graduate studies, he went on to join the lab of Professor Yimon Aye at Cornell University, receiving support from the NSF Graduate Research Fellowship Program. Here, he worked towards expanding the group's emergent T-REX redox signaling elucidation platform, utilizing *C. elegans* as a focal organism for uncovering low-occupancy redox sensors in endogenous, biologically relevant conditions. With the Aye lab's transition to EPFL (Swiss Federal Institute of Technology) over the summer of 2018, Daniel spent over a year abroad in Lausanne, Switzerland, gaining valuable collaborative experience as his studies came to a close. Having now returned to the US, Daniel is looking to either take on postdoctoral training or gain experience in the industrial side of biochemistry research upon graduating, with a desire to return to the Northeast once more.

Dedicated to the memory of Hasan Okumuş, the first scientist I ever knew.

Her zaman bir kitap yazabileceğime inandın. Zamanında bitiremediğim için her zaman pişman olacağım.

ACKNOWLEDGEMENTS

First and foremost, I wish to express sincere gratitude to my advisor, Professor Yimon Aye, for her guidance and tutelage throughout an unforgettable graduate career. From the very beginning, she has afforded me countless opportunities to learn and improve as an aspiring scientist. She challenged me to exit my academic comfort zone, and kept faith in me during times of personal struggle. I carry with me the tools to succeed going forward thanks to her tireless support and mentorship, and for that, I am incredibly grateful.

I would also like to express thanks to both of my committee members: Professor Kelly Liu for sharing her *C. elegans* expertise with our lab over the years, and Professor Rick Cerione for offering valuable support and insight throughout my candidacy. In addition, I would like to thank the labs of Professor Pierre Gönczy and Professor Beat Fierz of EPFL, both of whom have aided our lab in numerous incalculable ways as we found our footing in Switzerland.

Furthermore, I would like to thank the National Science Foundation for supporting my pursuits in the Aye Lab through the GRFP (No. DGE-1650441).

I am also immeasurably grateful to every member of the Aye Lab who I have had the privilege to work with. Between the insightful lessons of senior postdoctoral members, the intellectual and personal support of my graduate peers, and the boundless enthusiasm of our undergraduate mentees and Masters students, I come away from the Aye Lab with so many treasured memories and experiences. I could not have asked for better teammates to travel with on my graduate school journey.

Of course, I would not have been on this journey in the first place were it not for those who inspired me to pursue science as a career and passion. I owe much to Professor Steven Bruner for introducing me to the wider world of biochemical research

as an undergraduate mentor, and to Professor Mona Minkara for encouraging me to explore different approaches both to the study of chemistry and to my own development, both as a researcher and as a person. I am also incredibly thankful to Professor Mark Orazem for offering me an invaluable perspective at a difficult crossroad in my academic life; his advice helped me to truly grasp what I wanted out of my career, something that I will never forget.

I would be remiss if I did not acknowledge the incredible outpouring of emotional support that my friends outside of academia have selflessly given me for the past five years. I especially want to thank Oliver Nelson and their cats for what must now be thousands of Skype hours accompanying me on busy late nights, and I want to thank Dr. Athéna Patterson-Orazem for her many reassurances, plant nursery pictures, and freely dispensed pearls of wisdom as I navigated my own path through graduate education.

Finally, I cannot stress enough that none of this would have been possible without the love and support of my family. My sister, Selina, has always been my most enthusiastically vocal advocate, and my parents have worked tirelessly every day of their lives to ensure that I could fully commit to my studies and achieve the potential they always believed I had. I cannot quite express in words just how lucky I am to have them in my life.

TABLE OF CONTENTS

LIST OF FIGURES

LIST OF TABLES

LIST OF ABBREVIATIONS

ACTG-1	Actin Gamma 1
AdoD	Ademosine Deaminase
AHCY	S-Adenosylhomocysteine Hydrolase (alternate acronym)
Akt3	RAC-gamma serine/threonine-protein kinase isoform 3
ARE	Antioxidant Response Element
βME/BME	β-mercapthoethanol
BSA	Bovine Serum Albumin
C. elegans	*Caenorhabditis elegans*
CKMT	Creatine Kinase, Mitochondrial
CMV	Cytomegalovirus promoter
CNDP2	Carnosine Dipeptidase 2
C-REX	*C. elegans*-compatible G-REX
Cy5	Cyanine-5
Cys / C	Cysteine
D. rerio	*Danio rerio*
ddH_2O	Double-Distilled Water
dHNE	2-Nonenal
DNA	Deoxyribonucleic Acid
DNase	Deoxyribonuclease
DTNB	5,5'-Dithiobis-(2-Nitrobenzoic Acid)
3-DZA	3-Deazaadenosine
EDTA	Ethylenediaminetetraacetic Acid
FBS	Fetal Bovine Serum
FUDR	Floxuridine/5-Fluorodeoxyuridine

Fwd	Forward primer
GAPDH	Glyceraldehyde-3-Phosphate Dehydrogenase
GFP	Green Fluorescent Protein
G-REX	Global/Genome-wide Reactive Electrophiles and Oxidants
GSR	Glutathione-Disulfide Reductase
Halo/HaloTag	HaloTag® (Haloalkane dehalogenase Tag)
HDE	4-Hydroxydodecenal
HEK293T	Human Embryonic Kidney 293 (mutant SV40 large T antigen)
HeLa	Henrietta Lacks (cell line)
HEPES	4-(2-Hydroxyethyl)-1-Piperazineethanesulfonic Acid
HNE	4-Hydroxynonenal
HRP	Horseradish Peroxidase
(s)HSP	(Small) Heat Shock Protein
hHSPB7	Small Heat Shock Protein B7 (human)
zHspb7	Small Heat Shock Protein B7 (zebrafish)
Ht-	HaloTag-targeting
Ht-PreHNE	HaloTag-targeting Precursor HNE
IPTG	Isopropyl β-D-1-Thiogalactopyranoside
Keap1	Kelch-like ECH-associated Protein 1
L1/L2/L3/L4	Larval Stage 1/2/3/4
LB	Luria Broth
LC/MS-MS	Liquid Chromatography with Tandem Mass Spectrometry
LDE	Lipid-derived Electrophile
MBP	Maltose Binding Protein
MEM (media)	Minimal Essential Media
Met / M	Methionine

mRFP	Momomeric Red Fluorescent Protein
N2	Bristol N2 (*C. elegans* background)
NEAA	Non-Essential Amino Acids
NGM	Nematode Growth Media
Ni-NTA	Nickel - Nitrilotriacetic Acid
NP-40	Nonidet P-40
Nrf2	Nuclear Factor Erythroid 2–Related Factor 2
ORF	Open Reading Frame
PBS	Phosphate-Buffered Saline
PDB	Protein Data Bank
PEI	Polyethylenimine
PMSF	Phenylmethylsulfonyl Fluoride
PVDF	Polyvinylidene Fluoride
RES	Reactive Electrophilic Species
Rev	Reverse primer
RNase	Ribonuclease
ROS	Reactive Oxidative Species
SAH	S-Adenosylhomocysteine
hSAHH	S-Adenosylhomocysteine Hydrolase (human)
CeSahh	S-Adenosylhomocysteine Hydrolase (*C. elegans*)
SAM	S-Adenosylmethionine
SDS	Sodium Dodecyl Sulfate
SILAC	Stable Isotope Labeling with Amino Acids in Cell Culture
SP6	SP6 promoter system
SUMO	Small Ubiquitin-like Modifier
Sypro	Sypro ™ Ruby Stain

T7	T7 promoter system
TBS	Tris-Buffered Saline
TBST	Tris-Buffered Saline + Tween20
TBTA	Tris(benzyltriazolylmethyl)amine
TCEP	Tris(2-carboxyethyl)phosphine
TEV	Tobacco Etch Virus (protease or cleavage site)
TMR	Tetramethylrhodamine
TOM70	Translocase of the Mitochondrial Outer Membrane 70
(m)TOR	(Mammalian) Target of Rapamycin
T-REX	T-REX™ (Targetable Reactive Electrophiles and Oxidants)
Tris	Tris(hydroxymethyl)aminomethane
Ube2N	Ubiquitin-Conjugating Enzyme E2 N
Ube2V1/2V2	Ubiquitin-Conjugating Enzyme E2 Variant 1/E2 Variant 2
UTR	Untranslated Region
UV	Ultraviolet Light (365 nm unless stated otherwise)
WT	Wild-Type

LIST OF SYMBOLS

α-	Anti- (with reference to antibodies)
°C	(Degrees) Celsius
Da	Dalton
g	gram
L	Liter
m	Meter
M	Molar
mol	Moles
pK_a	Acid Dissociation Constant (log scale)
r	"Labeling Rate" (See Figure 1-7)
R	Intrinsic Kinetic "Rate" (see Figure 1-2)
$k_{on/off}$	On/Off Rate Constant (see Figure 1-7)
K_m	Michaelis Constant
v	Volume
V	Voltage
v_{max}	Maximum Catalytic Rate

k	kilo-
c	centi-
m	milli-
μ	micro-

CHAPTER 1

INTRODUCTION

PREFACE

Figures from the following chapter have appeared in a previously published work. They have been adapted for presentation in this work with permissions from Methods in Enzymology (Copyright 2020 Elsevier Books)

Long, M. J. C.; Urul, D. A.; Aye, Y. REX technologies for profiling and decoding the electrophile signaling axes mediated by Rosetta Stone proteins. Methods in Enzymology vol. 633 (2020). (doi: 10.1016/bs.mie.2019.02.039)

1.1 Role of reactive electrophilic species as facilitators of endogenous signaling pathways and acute stress response

An increasingly significant proportion of modern drug discovery efforts are fueled by ongoing investigations into the mechanisms and targets of covalent inhibitors.[1,2] Initial forays into covalent drug design, though lucrative, fostered justifiable concerns regarding toxicity induced by off-target effects, which were amplified by the relative irreversibility of covalent binders onto off-targets with low turnover.[3] However, recent advances in the knowledge of factors that engender covalent warhead specificity, [4] as well as our ability to exactly determine and characterize on-target sites, have allowed for the renewed development of selective covalent drug candidates with high efficacy, low dosage requirements, and reduced incidence of drug resistance (**Figure 1-1**).[2,5] Modern drug development roadmaps, then, require investigation into the identification of novel targets with discernable specificity of covalent binding partners *in vivo,* whose modification can be linked to known disease states with as-yet insufficient therapeutic options.

Concurrent with this resurgence in the collective interest in covalent inhibitors is our broadening knowledge of endogenous intracellular signaling mechanisms that govern and fine-tune nearly all aspects of biology. Much of our understanding of signaling mechanisms has been informed by decades of fruitful research into uncovering canonical signaling pathways propagated by small, non-reactive

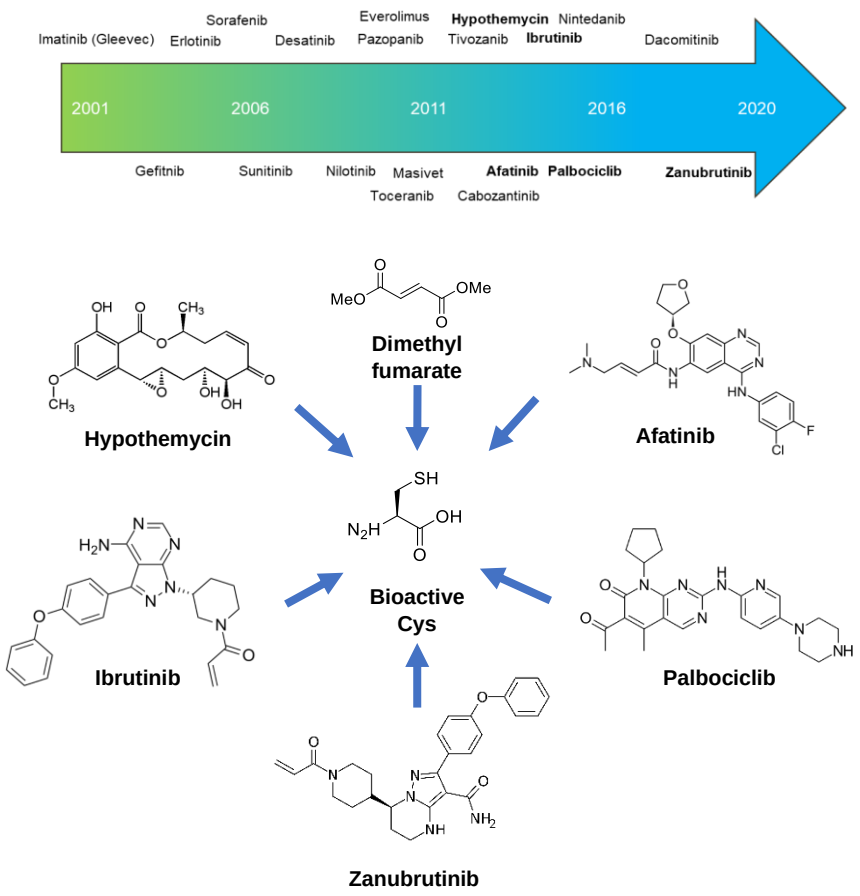

Figure 1-1. A snapshot of the history of modern cysteine-targetable covalent drug development. Recent developments in the understanding of off-target effect and warhead specificity have led to a resurgence in residue-specific covalent therapeutics, including anti-cancer therapeutics (such as the kinase inhibitors shown above) and drugs for multiple sclerosis treatment (dimethyl fumarate; brand name Tecfidera).

biomolecules. These stable signaling mediators are numerous in type and kind, functioning as variable "currencies" that are exchanged along a pathway until a downstream response is ultimately elicited.[6] Some constitute a form of small-molecule covalent modification, such as methylation,[7] acetylation,[8] or phosphorylation;[9] others are comprised of low-molecular weight proteins including ubiquitin,[10] SUMO,[11] and products of interferon-stimulated gene expression.[12] Regardless of kind, many of these

"currencies" ultimately incur one of three outcomes: a gain-of-function response, which can be achieved via low levels of upstream modification;[13–15] controlled shut-down of a target;[16,17] or a dominant loss-of-function where a small increase in labelled protein elicits an amplified down-regulated response.[18] Regardless of function, however, nearly all of the aforementioned signaling currencies commonly require an enzyme to facilitate transfer of signal.[6] The end result is a complex web of interchanging pathways whereby said enzymes function as controllable nodes for fine-tuning signaling and response to exogenous prompts.

Separate from these enzymatically-controlled mediators, however, is an emergent category of highly reactive small-molecule signaling currencies, which can be broadly categorized as reactive oxidative species (ROS)[19] or reactive electrophilic species (RES).[20–23] ROS and RES can occur and accumulate intracellularly from a number of sources,[23] such as through oxidative damage[24] or leakage from electron transfer pathways.[25] Prior to our current understanding of these molecules in endogenous conditions, ROS and RES were largely studied in the context of toxic accumulation, which can lead to cancer occurrence and multiple disease states.[6] However, the zeitgeist surrounding ROS and RES has shifted considerably towards their roles in facilitating key health-promoting signaling pathways or health-preserving stress responses at far lower concentrations than observed in deleterious situations.[19,20,22] As just one example, ROS has been implicated in a significant role in cell growth when deployed in a tightly

controlled manner.[26] Meanwhile, RES, while shown to be equally crucial in maintaining physiological health through intracellular signaling, does not yet have a defined consensus in terms of affected cellular outcomes and phenotypes.[23] As such, preferential RES targets in an endogenous environment have become a potential mine for druggable targets in the event of disease-relevant signaling misregulation.

Prominent among these biologically relevant RES targets are reactive, solvent-exposed cysteine residues, which have long been associated with control and disease-relevant perturbation of redox biology.[27–29] These cysteines are what can enable RES signaling propagation in all manner of proteins, either as a primary function or a secondary "moonlighting" function of a previously-characterized enzyme.[6,30,31] Much attention has been brought to assessing the redox state of surface-accessible cysteine residues as a potential predictive factor of RES modification [32]. For example, induction of low pK_a by proximity to charged amino acids,[33] presence of hydrogen bonding,[34] or positioning at the N cap of an α-helix[35] have been individually investigated as predictive elements.[28] However, while pK_a can be a factor in determining general reactivity of a specific cysteine, there still exists intriguingly differential kinetic labeling behavior among solvent-exposed cysteines across different RES sensor proteins that cannot be explained by redox state alone.[36] As such, it is crucial to develop methods for directly interrogating the cysteineome of a known biological system to tease out targets that are most relevant in an endogenous state.

1.2 Contemporary methods for screening and identifying RES-sensor candidates

Early attempts to identify and understand these RES-sensing targets involved variants of "bolus-dosing" exposure experiments, whereby the target biological environment is exposed to an excess of exogenous RES, and RES-modified proteins are subsequently identified using any number of downstream readouts.[23] Paired with downstream enrichment and mass spectroscopy techniques, this strategy has helped to facilitate a jump-start in our understanding of enzyme-independent redox signaling.[37] However, there are issues that can hinder attempts at pinpointing precise elements of signal mediation (see Figure 1-6a). The excess of active RES introduced to the system can swamp both RES sensors and non-sensors alike, yielding many off-target results from downstream profiling. Furthermore, assessing the downstream output of any one RES-modified protein becomes difficult due to the myriad number of signaling pathways triggered by all swamped RES sensors, resulting in confounding biological outcomes.[31] Even if a RES sensor's downstream effects can be isolated from the resulting amalgamation, it can only be discussed in the context of RES overload; behavior in an endogenous setting, where RES presence is governed by cellular machinery, may not be reliably concluded from such results.

Subsequent efforts to modify or otherwise mitigate the disadvantages of bolus-dosing techniques have made this strategy more attractive for purposes of high-throughput proteomic profiling. One prolific example is the isoTOP-ABPP (Activity-

based Protein Profiling) platform, which extracts high-resolution indirect readouts of potential cysteine sensors from a bolus-dosing strategy (**Figure 1-2a**).[38,39] ABPP combines a reactive group of interest with a readout tag to produce a landscape of reactive targets within the proteome of a given system.[40,41] This system was further tuned to identify RES targets by chasing *in vivo* bulk RES exposure with a functionalized affinity probe, such as iodoacetamide (IA) in the case of investigating the reactive cysteinome. The accuracy of the ensuing readouts allow for the detection of highly reactive cysteine sites that may feature specificity to certain RES; for example, 4-hydroxynonenal (HNE), a lipid-derived electrophile (LDE) resulting from peroxidative activity,[42] has been linked to specific cysteine sensors in ZAK and RTN4, among other protein hits, using this method.[39]

However, despite the vast improvements and continued relevance of this and associated platforms, there is still a reliance on bolus dosing to produce RES-modified targets, which may fundamentally alter the behavior of a putative RES sensor in a way that does not accurately reflect its activity in a basal signaling context. Additionally, the indirect readout by affinity probe signal drop-out introduces an intrinsic limitation to the available cysteinome that can be interrogated, based on the probe selected. IA-based

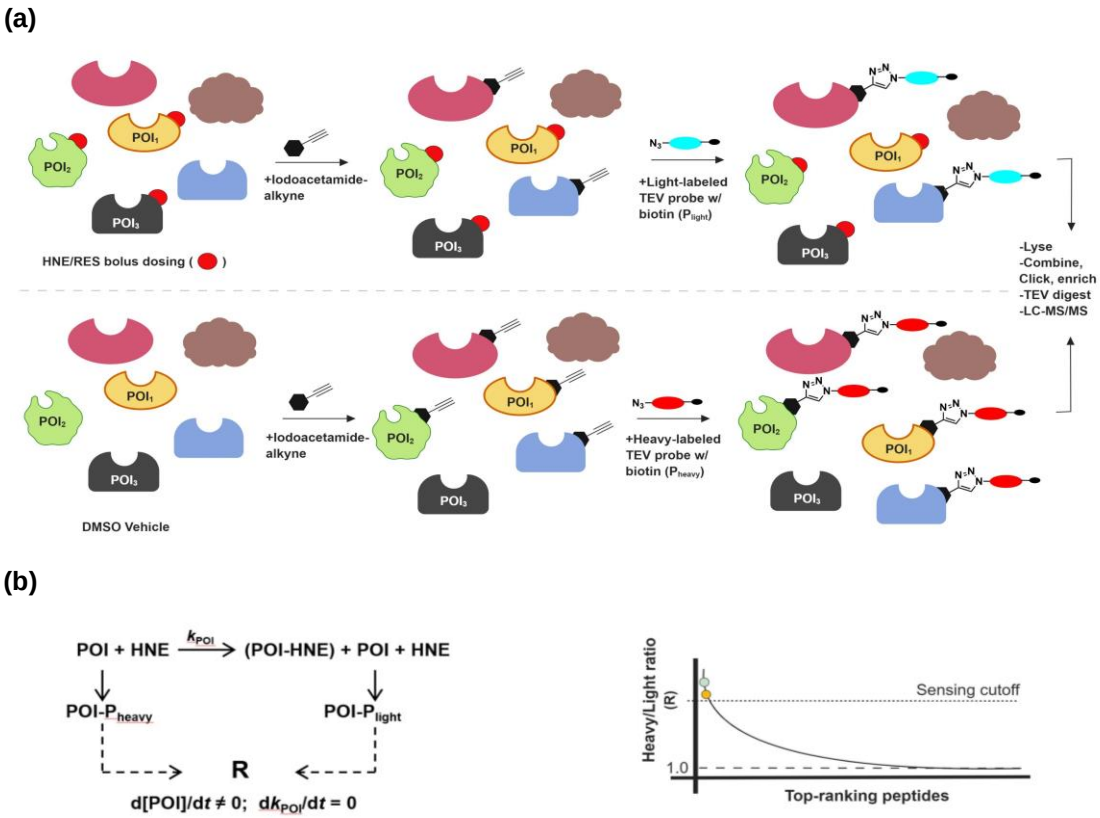

Figure 1-2. IsoTOP-ABPP, a robust contemporary method for RES sensor detection. **(a)** Lysates are treated either with a chosen RES (such as HNE or other LDE) or vehicle, then are treated with an alkynylated iodoacetamide affinity probe. Streptavadin-biotin enrichment and follow-up MS/MS enables the indirect identification of HNE-sensing proteins within the profiled system. **(b)** The ratio of heavy- to light-labeled proteins produces an "R" value that offers a relative comparison of intrinsic kinetics among RES-sensing hits. This can be used to establish a "cutoff" beyond which proteins are not considered RES-sensitive.

isoTOP-ABPP, for instance, can reliably profile up to 2,000 out of over 200,000 unique cysteines.[43] Additionally, IA signal drop-out may capture other phenomena beyond RES modification that can affect binding of said probe.

Techniques to turn away from active RES bolus-dosing and towards intracellular biosynthesis have been developed in recent years to try and address this gap. One such

case involves treatment of cells with an LDE precursor that can be metabolized *in vivo,* such as linoleic acid (LA).[44] In this instance, LA treatment followed with Kdo-lipid A-driven metabolism can mimic endogenous RES generation (**Figure 1-3**). This experiment can be run with functionalized LA to enable SILAC-derived proteomic readouts. Success has also been achieved with more direct readouts of modified proteins, such as through capture of proteins with active LDE-derived aldehyde tags after a RES biosynthesis event, such as ferroptosis.[45] However, central to this suite of tools remains the issue of precise control over RES generation and release, producing variable readouts that can be affected by cell type or organelle locale. Both of the above techniques, for example, produce a suite of mitochondria-localized targets, but this may be a result of localized LDE generation rather than a lack of RES-sensing targets elsewhere in the cell.

1.3 Development of a comprehensive discovery-to-characterization platform for low-occupancy RES sensors

Collectively, the aforementioned profiling strategies and their modern contemporaries highlight several key factors that must be addressed by any incoming high-throughput technique. Any new RES-sensor profiling tool must allow precise control over RES release in terms of both time and locale, while maintaining sub-stoichiometric concentrations within the cell to mimic a basal environment as closely

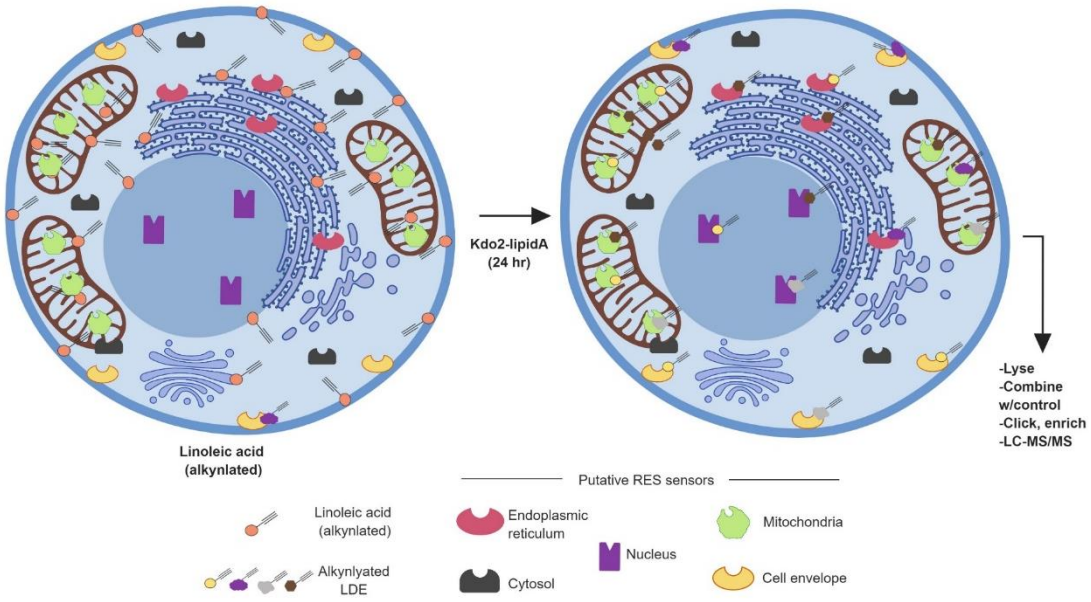

Figure 1-3. Internal LDE generation models endogenous RES conditions. Alkynylated linoleic acid is introduced into the cell, resulting in integration into cellular phospholipids. This is followed by Kdo-lipid A-driven metabolism to produce alkynated HNE, resulting in quasi-endogenous RES exposure.

as possible. To tackle these obstacles, our lab developed the REX (Reactive Electrophiles and oXidants) technology platform, a toolbox constructed around the central conceit of spatio-temporally controlled, intracellular release and delivery of a selected RES to putative redox-sensing proteins of interest (POI) in a manner resembling that of low-concentration, endogenous conditions.[46–50] At the core of this platform is the introduction of a bioinert, photocaged LDE precursor probe, which is both alkyne-appended and functionalized to bind to an artificial protein – HaloTag[51] – expressed in the target biological system (see Table 2-1). Unbound probe is then washed out of the system, allowing the expression of HaloTag to cap the concentration of LDE

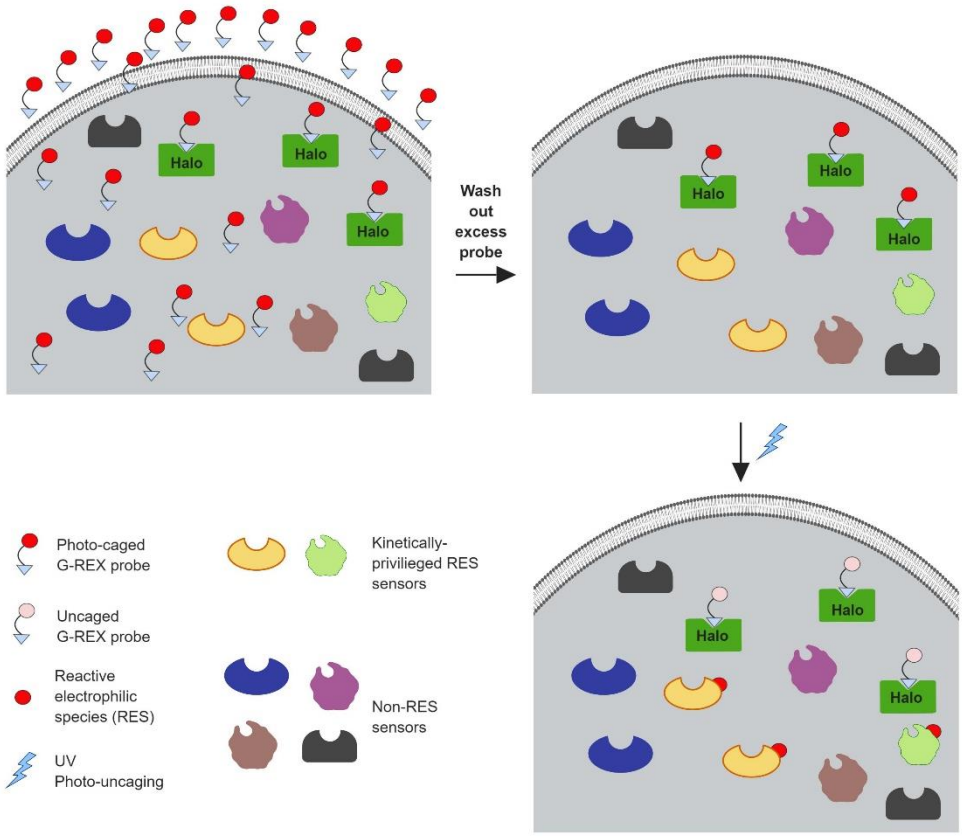

Figure 1-4. General schematic of G-REX, a platform for detection of low-occupancy RES sensors through controlled LDE release. The system is first fed an excess of photocaged LDE precursor, functionalized such that it selectively binds to and saturates HaloTag. Excess probe is then washed out, and a photouncaging step releases the LDE in a transient, low-concentration burst.

that is subsequently released into the system via a photouncaging step. From this core, several techniques can be derived under the REX umbrella that together can form a pipeline between the discovery of novel redox sensors and the specific characterization of their RES modification, producing a self-sufficient platform for interrogating basal redox signaling in compatible biological environments.

At the discovery end of this pipeline is Genome-wide REX (G-REX), a technique to probe the reactive cysteinome in a spatio-temporally controlled fashion (**Figure 1-4**)[36,49,50]. In a standard G-REX experiment, a biological system is engineered to express HaloTag in a specific locale of interest (such as cell type or organelle). This HaloTag is then saturated with the precursor probe, which is then released as bioactive LDE via photouncaging. The LDE then binds to available redox-sensing cysteines, effectively tagging proteins that are suited to detect small fluctuations in LDE that more closely resemble those of a signaling pathway modulated by cellular machinery. These sensors can then be identified through a range of downstream proteomics tools, including SILAC or TMT-based profiling.

This controlled release of a capped amount of LDE is what enables G-REX to identify a range of RES sensors that may otherwise be masked in a high-RES environment. In such excess, cysteine and protein abundance may weigh more prominently in determining detected hits, especially over an extended treatment period. By comparison, in pilot G-REX experiments, released HNE, which is produced in a relatively quick ($t_{1/2}$ < 1 min.) photouncaging step, could be limited to approximately 1 μM in HEK293T cells when factoring in HaloTag expression and HNE clearance kinetics.[36] This substoichiometric condition, which better approximates endogenous signaling, allows the intrinsic binding kinetics of individual cysteines to play a more prominent role (**Figure 1-5a**). The end result leads to the detection of "low-occupancy"

(a)

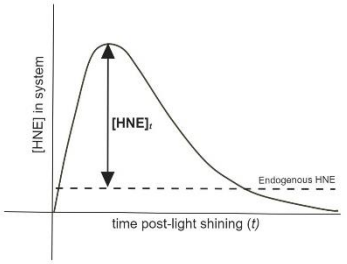

$$d[POI]/dt = 0;\ dk_{POI}/dt = 0$$

$$d[POI_1\text{-}HNE]/dt = k_1[POI]_1[HNE]_t$$
$$d[POI_2\text{-}HNE]/dt = k_2[POI]_2[HNE]_t$$
$$\ldots$$
$$d[POI_n\text{-}HNE]/dt = k_n[POI]_n[HNE]_t$$

(b)

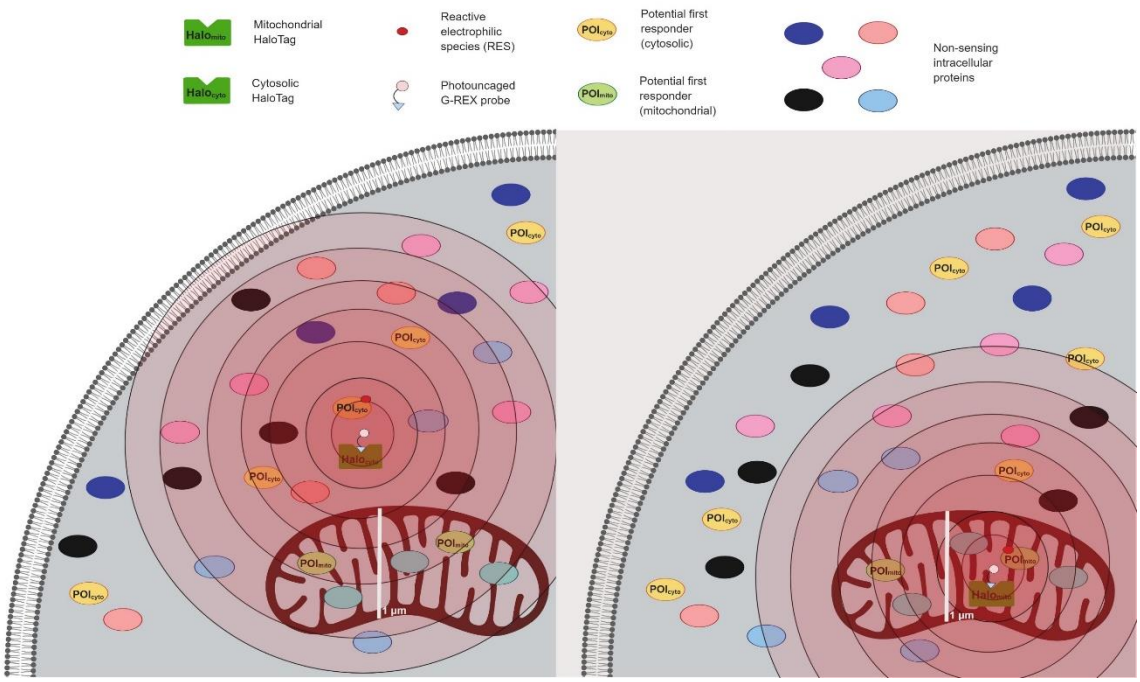

Figure 1-5. Advantages of G-REX enabled controlled LDE release. **(a)** Via a brief, transient pulse of HNE (left), G-REX can capture labeling of low-occupancy RES sensors possessing kinetically privileged cysteine residues bestowing a rate k_n (right). **(b)** Localization of HaloTag can control the spatial landscape of RES release, given that diffusion is limited by cystosolic off-targets; for instance, cystosolic HaloTag (left) may unreliably probe RES sensors within and adjacent to the mitochondria, which may be better captured by mitochondrial localization of Halotag (right).

sensors: proteins with transient, low-percentage total labeling facilitated by cysteines that rapidly react with available RES. Said cysteines are said to be "kinetically

privileged," allowing their associated proteins to respond first to a limited change in environmental RES before other proteins that may feature greater total RES modification. Early foundational work in developing the G-REX platform led to the elucidation of one such pair of low-occupancy targets: Ube2V1 and Ube2V2,[49] each of which facilitate independent signaling pathways that intersect at a common UbE2N node.[52,53]

This controlled release engendered by HaloTag localization also enables us to have a better understanding of the exact proteomic landscape being interrogated in a given experiment. RES diffusion within the cell – from any starting point – is limited by the sheer quantity of modifiable targets that can sequester it (**Figure 1-5b**). As such, localized RES sensors can be missed or artificially underrepresented based on the origin of RES within a system. Locale-specific context for the same protein can also be discerned from differential results depending on RES origin, in a manner analogous to localized ROS sensing.[54,55]

With targets identified, the other end of the pipeline requires a platform to precisely determine the consequence of RES modification of putative sensor proteins. For this, we employ Targetable REX (T-REX) to both validate the RES sensitivity of a given hit and investigate the downstream implications of its labeling (**Figure 1-6**).[36,46–50,56,57] T-REX utilizes proximity-driven directed labeling of a candidate RES sensor by way of fusion to a HaloTag via a TEV-cleavable linker, which is then saturated with an

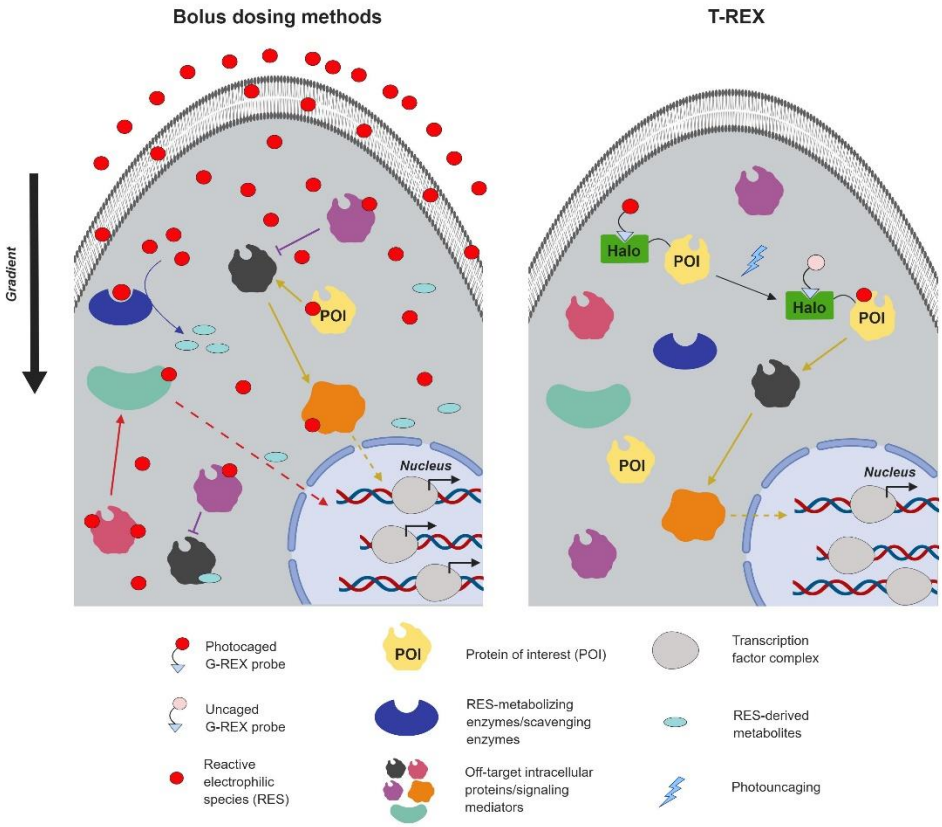

Figure 1-6. General schematic of T-REX-targeted labeling of a specific RES-sensing protein of interest (POI). In a bolus-dosing schematic, the sheer quantity of off-targets labeled will confound many downstream outputs (left). Instead, HaloTag-POI constructs are generated, and the choice of RES is delivered to the POI after loading its photocaged precursor onto the neighboring HaloTag, enabling activation of a specific pathway (right).

LDE precursor of choice. Upon photouncaging, the released LDE briefly remains in the solvent cage of the construct, whereby the kinetics of cysteine labeling compete with the diffusion kinetics of the probe (**Figure 1-7**) [47,48]. From this point, the RES-labeling efficiency of the protein in question can be evaluated downstream, typically by cleaving the HaloTag from the purported sensor and utilizing quantitative techniques (enrichment, fluorescent labeling, etc.) to assess RES modification. Following this, T-

REX can be used to controllably affect signaling pathways mediated by a known sensor protein, completing the pipeline (**Figure 1-6**).

The capability of T-REX to both validate and interrogate known and novel RES sensors was first demonstrated via seminal proof-of-concept work using Keap1 as the target.[46,47] Keap1 is a well-documented redox sensor that plays an integral role in controlling expression of the antioxidant response element (ARE).[58] Specifically, RES-mediated Keap1 modification stabilizes and prevents degradation of the transcription factor Nrf2, which itself governs ARE activation when accumulated.[59,60] Beyond being able to quantify the labeling efficiency of Keap1, T-REX was also successfully used to visualize Nrf2 upregulation upon controlled HNE delivery to Keap1 in HNE293T cells.[46–48] Next, extending beyond known sensors, T-REX was used to similarly characterize redox-sensing capability and behavior of novel targets identified through medium-throughput screens – such as the Akt3 kinase isozyme – quantifying labeling efficiency and extent of downstream response in the process.[61] Finally, T-REX-driven investigation into the outcomes of UbE2V1/2V2 labeling demonstrated a capability to tease out the signaling function of low-occupancy RES sensors discovered exclusively through G-REX, completing the self-contained end-to-end pipeline. In this case, modification of either protein both led to UbE2N stimulation, which in turn upregulated a different pathway based on the associated modified protein (NFKB[52] and DDR[53] pathways, respectively) without itself being RES-modified.[62]

This breadth of RES sensors with differential labeling behavior reveals another key asset that T-REX affords, and one that highlights the value G-REX-mediated discovery provides to our understanding of endogenous cell signaling. Comparison to a split-system control (**Figure 1-7a**) demonstrates that HNE delivery to the target RES sensor is akin to a pseudo-intramolecular reaction; transfer occurs within a solvent cage, and diffused HNE does not sufficiently interact with the HaloTagged construct to produce a measurable second-order reaction. As such, delivery efficiency emerges as a ratio of rates from a pseudo-first-order intramolecular RES transfer and a pseudo-first-order RES diffusion rate. This allows for T-REX evaluated proteins to be "ranked" in terms of relative labeling kinetics, assuming equal diffusion kinetics across the board (**Figure 1-7b**). While other profiling methods do have relative rate assessments baked into their outputs, including ABPP (**Figure 1-2b**), the combined G-REX/T-REX pipeline can extend this assessment to kinetically privileged sensors on low-occupancy proteins, allowing for direct comparison to more completely labeled proteins (**Figure 1-8**). Expanding the pool of redox sensors characterized this way may enable us to derive functional predictions from relative rate. For example, assessing the redox sensors discussed thus far seems to suggest that increased cysteine reactivity correlates with the "directness" of signal propagation, with higher-rate cysteines (Keap1, Akt3) directly effecting downstream responses,[47,48,61,63] and Ube2V1/Ube2V2 affecting Ube2N in an allosteric manner to affect a response.[49]

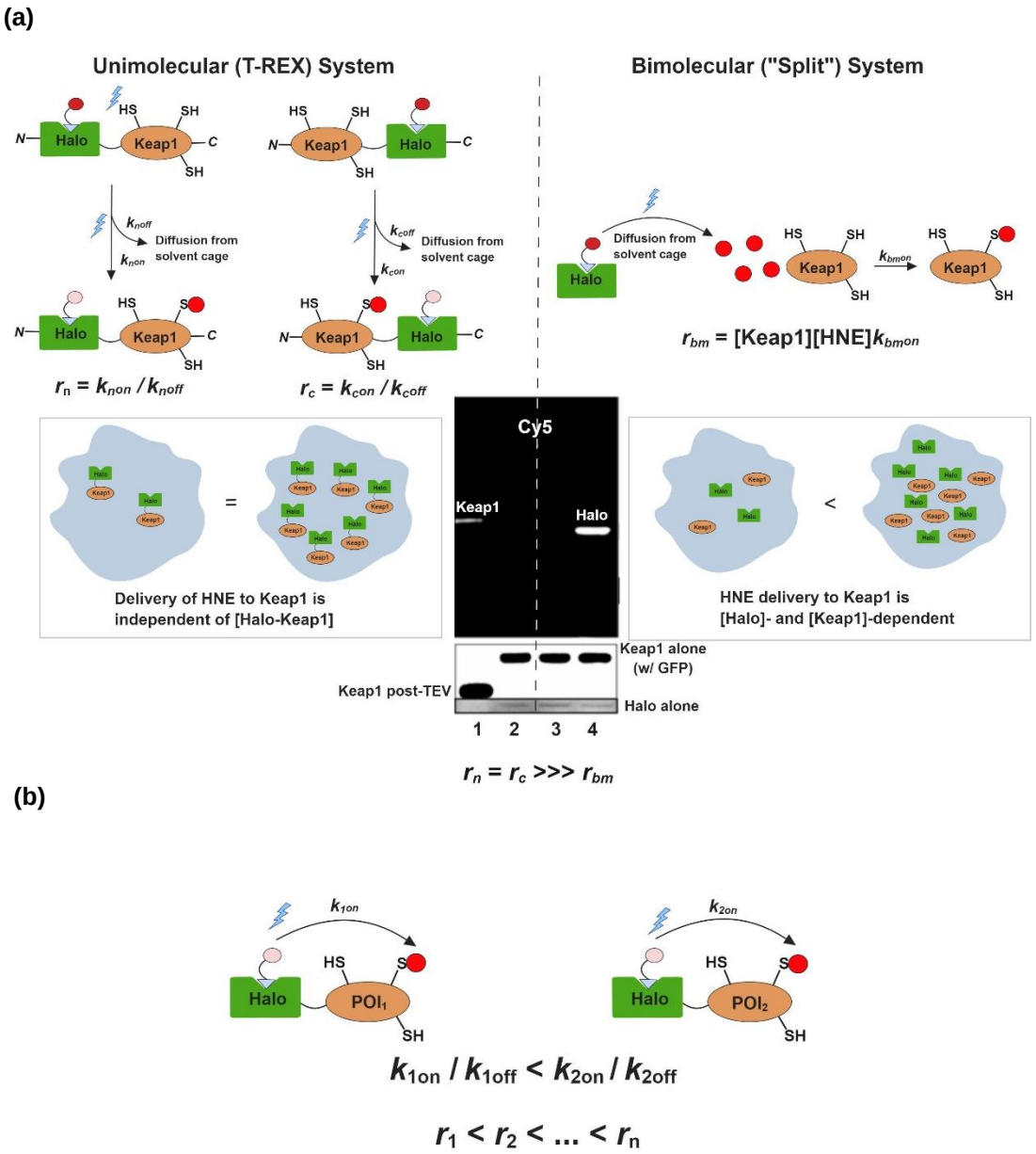

Figure 1-7. T-REX as a means of evaluating relative rates of cysteine modification. **(a)** T-REX-mediated delivery to a putative RES sensor behaves in a pseudo-intramolecular fashion; the released RES either remains within the complex via modifying the RES sensor (k_{on}) or diffuses out of the solvent cage (k_{off}) (left). This behavior is not concentration dependent, in contrast with a bimolecular "split" system (right), and is not dependent on the positioning of the HaloTag and RES sensor (N- or C- terminus). **(b)** A ratio of k_{on} to k_{off} can produce a "labeling rate" r, which can be used to rank cysteine sensors relative to each other.

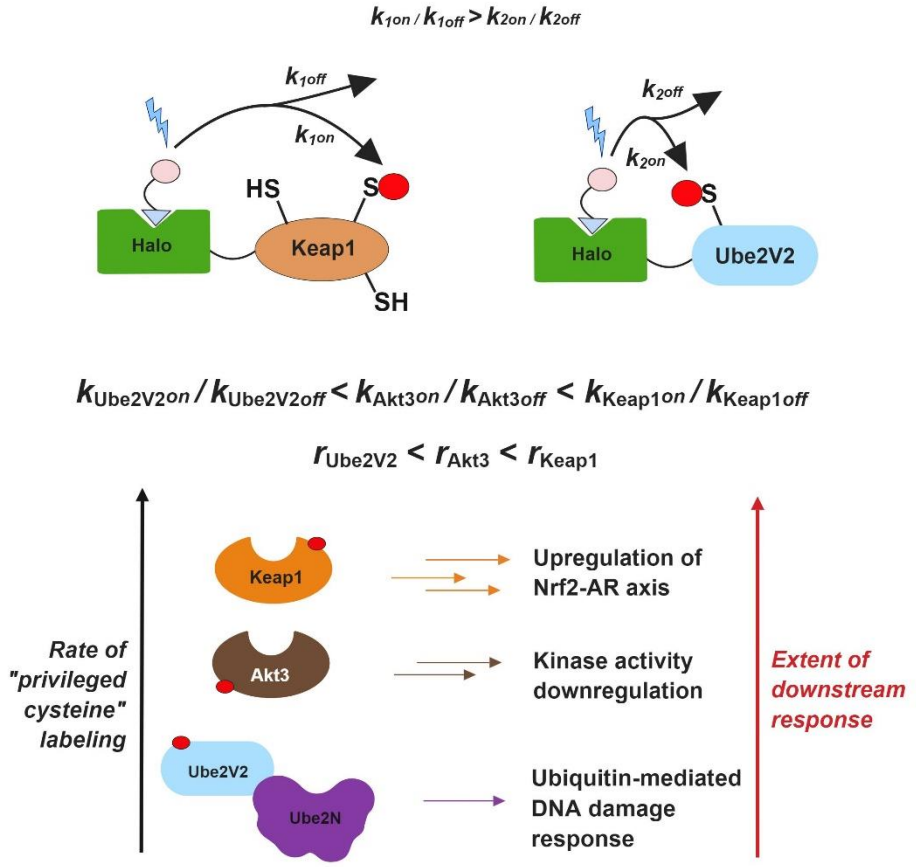

Figure 1-8. T-REX-derived relative kinetic rankings may offer insight into RES-sensing function. Higher-ranked RES sensors, like Keap1 and Akt3, may be more involved in direct translation of RES presence to downstream signal flux. Lower-ranked sensors, like UbE2V2 (and UbE2V1), may mediate a more indirect path via allosteric interaction with an intermediate (such as UbE2N).

It should be noted that the REX technology umbrella does share a few shortcomings that can be accommodated for. Genetic modification is required to produce HaloTag constructs, and as such a model system must be amenable to transgene expression at minimum; further, there is the risk of perturbance of the innate cell environment with the HaloTag transgene. This construct is also saturated with a

xenobiotic probe that must be exogenously delivered, as opposed to internally generated; however, this probe is inert and non-toxic, a marked improvement compared to bolus-dosing with RES. Additionally, G-REX in isolation does not provide a cleanly comparative ranking of labeling kinetics between hits. T-REX can account for this as discussed prior, but how the pseudo-first order rates measured through T-REX compare to the second-order labeling rates that would govern endogenous RES signaling are not fully known (though T-REX evaluation of additional G-REX hits may provide clarity to this relationship). Despite these concerns, however, the controllable specificity and ability to detect low-occupancy sensors in a basal RES signaling pathway significantly outweigh these disadvantages.

1.4 *C. elegans* as a model system for discovery of low-occupancy RES sensors

The next step for expanding this all-in-one REX platform is to progress to proteomic profiling in live animal models, to be able to capture full biological context when profiling RES sensors responsible for mediating cell signaling in basal environments. REX technologies have already proven to be transposable to whole-animal models in the form of zebrafish embryos (*D. rerio*).[61] Zebrafish have been well-established as a powerful model for assessing redox biology and stress response in cardiovascular health[64] and early-stage vertebrate development,[65,66] and their transparency at the embryonic stage enables compatibility with light-based techniques.[67]

However, our interest in native redox signaling extends beyond embryonic development; we next sought to incorporate a model that can enable the study of redox signaling through a whole organism with measurable phenotypes across a complete lifespan.

To that end, we turned to *C. elegans*, a central, irreplaceable model organism within developmental biology. *C. elegans* is a nematode with a relatively small, fully sequenced genome, transparent body, a rapid and well-characterized life cycle, and an invariable cell count from animal to animal, making it uniquely suited to studies of metabolic disease states and lifespan regulation.[68–70] It is also genetically tractable – with well-established protocols for manipulation[71] – and easy to maintain transgenic populations; *C. elegans* feature male/hermaphroditic sexual dimorphism, and as such, populations of hermaphroditic worms can self-propagate. Taken together, *C. elegans* provides an opportunity for whole-organism profiling through G-REX, as it can be reasonable adapted to fit the generic REX protocol (**Figure 1-9**; see Chapter 3).[72]

Incorporating *C. elegans* also affords an opportunity to investigate the relative transposability of signaling pathways and mediators found in disparate organisms to those analogous in humans. Cysteine residues are generally highly conserved across species due to their critical roles in mediating structural and functional support, though that alone does not guarantee that any one reactive cysteine will serve the same purpose as a privileged sensor across species. Given that substrate binding sites of many known

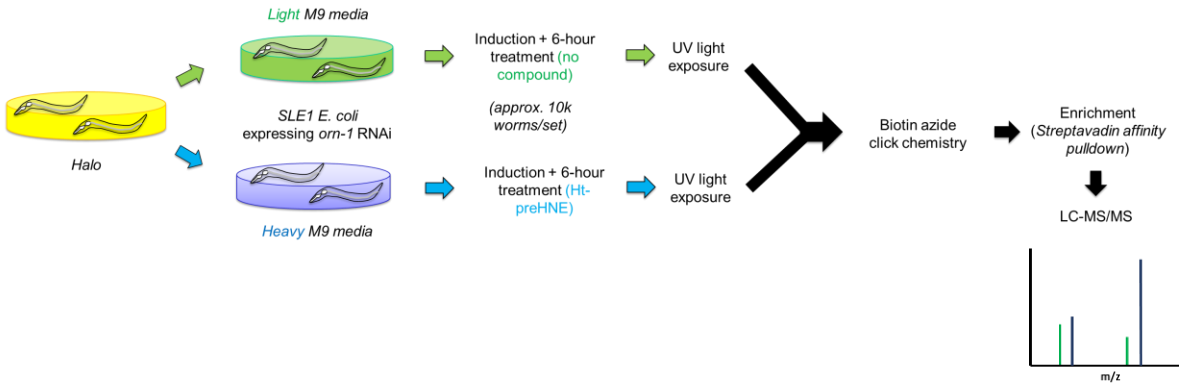

Figure 1-9. Example schematic of a hypothetical G-REX experiment in *C. elegans*, dubbed C-REX. Localized release of RES *in vivo* within adult worm populations can potentially yield unique results at a tissue- or organelle-specific level (See Chapter 3).

enzymes have demonstrated trackable plasticity through evolution,[73–75] it is possible that, by applying phylogenetic analyses to RES-sensor cysteines discovered through G-REX of a well-understood model organism, we can better predict the occurrence of RES-sensing cysteines in the human homologs. Evolution and tuning of an allosteric RES-sensing site is not without precedent,[76] and *C. elegans* signaling pathways have already been widely deployed to analyze many key lifespan-related pathways analogous to mammalian systems, including insulin/IGF-1 and TOR/mTOR signaling mechanisms .[77] Connecting these studies through phylogenetic analysis may unlock low-occupancy RES-sensing nodes hidden in mammalian systems that can in turn yield therapeutic targets in diseased states. There is also the opportunity to fine-tune how we predict RES sensing in candidate cysteines in the first place, as aforementioned investigations into, as an example, redox-state modulation, may not create a complete picture.

Ultimately, through this pairing of such a unique and well-characterized model organism with a compatible, high-throughput platform for redox discovery, we aim to provide a system that can accelerate our understanding of the endogenous small-molecule signaling paradigm. By first demonstrating compatibility of the REX platform in *C. elegans,* then utilizing G-REX to uncover a candidate redox sensor, we aim to glean knowledge of the sensing capacity of an analogous human sensor through phylogenetic analysis and subsequent biochemical validation. The following chapters demonstrate work towards this goal in three steps: (1) establishing compatibility of the REX platform, (2) assessing the conservation of sensing between a *C. elegans* G-REX hit and its human ortholog, and (3) discerning the transposability of phylogenetic analysis via analysis of a zebrafish-derived redox-sensor.

1.5 References

1. Singh, J., Petter, R. C., Baillie, T. A. & Whitty, A. The resurgence of covalent drugs. *Nat. Rev. Drug Discov.* **10**, 307–317 (2011).
2. Sutanto, F., Konstantinidou, M. & Dömling, A. Covalent inhibitors: A rational approach to drug discovery. *RSC Med. Chem.* **11**, 876–884 (2020).
3. Kola, I. & Landis, J. Can the pharmaceutical industry reduce attrition rates? *Nat. Rev. Drug Discov.* **3**, 711–715 (2004).
4. Gehringer, M. & Laufer, S. A. Emerging and Re-Emerging Warheads for Targeted Covalent Inhibitors: Applications in Medicinal Chemistry and Chemical Biology. *J. Med. Chem.* **62**, 5673–5724 (2019).
5. Pammolli, F., Magazzini, L. & Riccaboni, M. The productivity crisis in pharmaceutical R&D. *Nat. Rev. Drug Discov.* **10**, 428–438 (2011).
6. Long, M. J. C. & Aye, Y. The Die Is Cast: Precision Electrophilic Modifications Contribute to Cellular Decision Making. *Chem. Res. Toxicol.* **29**, 1575–1582 (2016).
7. Paik, W. K., Paik, D. C. & Kim, S. Historical review: the field of protein methylation. *Trends Biochem. Sci.* **32**, 146–152 (2007).
8. Verdin, E. & Ott, M. 50 years of protein acetylation: From gene regulation to epigenetics, metabolism and beyond. *Nat. Rev. Mol. Cell Biol.* **16**, 258–264 (2015).
9. Chen, Z. & Cole, P. A. Synthetic approaches to protein phosphorylation. *Curr. Opin. Chem. Biol.* **28**, 115–122 (2015).
10. Patterson, C. & Höhfeld, J. Molecular Chaperones and the Ubiquitin-Proteasome System. in *Protein Degradation* vol. 2 1–30 (Wiley-VCH Verlag GmbH & Co. KGaA, 2008).
11. Flotho, A. & Melchior, F. Sumoylation: A regulatory protein modification in health and disease. *Annu. Rev. Biochem.* **82**, 357–385 (2013).
12. Schneider, W. M., Chevillotte, M. D. & Rice, C. M. Interferon-stimulated genes: A complex web of host defenses. *Annu. Rev. Immunol.* **32**, 513–545 (2014).
13. Wu, R. *et al.* A large-scale method to measure absolute protein phosphorylation stoichiometries. *Nat. Methods* **8**, 677–683 (2011).
14. Dar, A. C. & Shokat, K. M. The evolution of protein kinase inhibitors from antagonists to agonists of cellular signaling. *Annu. Rev. Biochem.* **80**, 769–795 (2011).

15. Tsai, C. F. *et al.* Large-scale determination of absolute phosphorylation stoichiometries in human cells by motif-targeting quantitative proteomics. *Nat. Commun.* **6**, 2–9 (2015).

16. Martin, C. & Zhang, Y. The diverse functions of histone lysine methylation. *Nat. Rev. Mol. Cell Biol.* **6**, 838–849 (2005).

17. Holt, M. & Muir, T. Application of the protein semisynthesis strategy to the generation of modified chromatin. *Annu. Rev. Biochem.* **84**, 265–290 (2015).

18. Peisajovich, S. G., Garbarino, J. E., Wei, P. & Lim, W. A. Rapid Diversification of Cell Signaling Phenotypes by Modular Domain Recombination. *Science (80-.).* **328**, 368–372 (2010).

19. Pizzimenti, S., Toaldo, C., Pettazzoni, P., Dianzani, M. U. & Barrera, G. The 'Two-Faced' effects of reactive oxygen species and the lipid peroxidation product 4-Hydroxynonenal in the hallmarks of cancer. *Cancers (Basel).* **2**, 338–363 (2010).

20. Schopfer, F. J., Cipollina, C. & Freeman, B. A. Formation and signaling actions of electrophilic lipids. *Chem. Rev.* **111**, 5997–6021 (2011).

21. Shannon, D. A. & Weerapana, E. Covalent protein modification: The current landscape of residue-specific electrophiles. *Curr. Opin. Chem. Biol.* **24**, 18–26 (2015).

22. Poganik, J. R., Long, M. J. C. & Aye, Y. Getting the Message? Native Reactive Electrophiles Pass Two Out of Three Thresholds to be Bona Fide Signaling Mediators. *BioEssays* **40**, 1–12 (2018).

23. Parvez, S., Long, M. J. C., Poganik, J. R. & Aye, Y. Redox signaling by reactive electrophiles and oxidants. *Chem. Rev.* **118**, 8798–8888 (2018).

24. Marnett, L. J., Riggins, J. N. & West, J. D. Endogenous generation of reactive oxidants and electrophiles and their reactions with DNA and protein. *J. Clin. Invest.* **111**, 583–593 (2003).

25. Jastroch, M., Divakaruni, A. S., Mookerjee, S., Treberg, J. R. & Brand, M. D. Mitochondrial proton and electron leaks. *Essays Biochem.* **47**, 53–67 (2010).

26. Carol, R. J. & Dolan, L. The role of reactive oxygen species in cell growth: Lessons from root hairs. *J. Exp. Bot.* **57**, 1829–1834 (2006).

27. Liu, Q. *et al.* Developing irreversible inhibitors of the protein kinase cysteinome. *Chem. Biol.* **20**, 146–159 (2013).

28. Paulsen, C. E. & Carroll, K. S. Cysteine-mediated redox signaling: Chemistry, biology, and tools for discovery. *Chem. Rev.* **113**, 4633–4679 (2013).

29. Fra, A., Yoboue, E. D. & Sitia, R. Cysteines as redox molecular switches and targets of disease. *Front. Mol. Neurosci.* **10**, 1–9 (2017).

30. Copley, S. D. An evolutionary perspective on protein moonlighting. *Biochem. Soc. Trans.* **42**, 1684–1691 (2014).

31. Long, M. J. C. & Aye, Y. Privileged Electrophile Sensors: A Resource for Covalent Drug Development. *Cell Chem. Biol.* **24**, 787–800 (2017).

32. Marino, S. M. & Gladyshev, V. N. Analysis and functional prediction of reactive cysteine residues. *J. Biol. Chem.* **287**, 4419–4425 (2012).

33. Lutolf, M. P., Tirelli, N., Cerritelli, S., Cavalli, L. & Hubbell, J. A. Systematic modulation of Michael-type reactivity of thiols through the use of charged amino acids. *Bioconjug. Chem.* **12**, 1051–1056 (2001).

34. Roos, G., Foloppe, N. & Messens, J. Understanding the pKa of redox cysteines: The key role of hydrogen bonding. *Antioxidants Redox Signal.* **18**, 94–127 (2013).

35. Kortemme, T. & Creighton, T. E. Ionisation of cysteine residues at the termini of model α-helical peptides. Relevance to unusual thiol pKa values in proteins of the thioredoxin family. *J. Mol. Biol.* **253**, 799–812 (1995).

36. Liu, X., Long, M. J. C. & Aye, Y. Proteomics and Beyond: Cell Decision-Making Shaped by Reactive Electrophiles. *Trends Biochem. Sci.* **44**, 75–89 (2019).

37. Yang, J., Carroll, K. S. & Liebler, D. C. The expanding landscape of the thiol redox proteome. *Mol. Cell. Proteomics* **15**, 1–11 (2016).

38. Weerapana, E. *et al.* Quantitative reactivity profiling predicts functional cysteines in proteomes. *Nature* **468**, 790–797 (2010).

39. Wang, C., Weerapana, E., Blewett, M. M. & Cravatt, B. F. A chemoproteomic platform to quantitatively map targets of lipid-derived electrophiles. *Nat. Methods* **11**, 79–85 (2014).

40. Cravatt, B. F. & Sorensen, E. J. Chemical strategies for the global analysis of protein function. *Curr. Opin. Chem. Biol.* **4**, 663–668 (2000).

41. Speers, A. E. & Cravatt, B. F. Profiling Enzyme Activities In Vivo Using Click Chemistry Methods. *Chem. Biol.* **11**, 535–546 (2004).

42. Esterbauer, H., Schaur, R. J. & Zollner, H. Chemistry and biochemistry of 4-hydroxynonenal, malonaldehyde and related aldehydes. *Free Radic. Biol. Med.* **11**, 81–128 (1991).

43. Lawson, A. P. *et al.* Naturally occurring isothiocyanates exert anticancer effects by inhibiting deubiquitinating enzymes. *Cancer Res.* **75**, 5130–5142 (2015).

44. Beavers, W. N. *et al.* Protein Modification by Endogenously Generated Lipid Electrophiles: Mitochondria as the Source and Target. *ACS Chem. Biol.* **12**, 2062–2069 (2017).

45. Chen, Y. *et al.* Quantitative Profiling of Protein Carbonylations in Ferroptosis by an Aniline-Derived Probe. *J. Am. Chem. Soc.* **140**, 4712–4720 (2018).

46. Fang, X. *et al.* Temporally controlled targeting of 4-hydroxynonenal to specific proteins in living cells. *J. Am. Chem. Soc.* **135**, 14496–14499 (2013).

47. Lin, H. Y., Haegele, J. A., Disare, M. T., Lin, Q. & Aye, Y. A generalizable platform for interrogating target- and signal-specific consequences of electrophilic modifications in redox-dependent cell signaling. *J. Am. Chem. Soc.* **137**, 6232–6244 (2015).

48. Parvez, S. *et al.* T-REX on-demand redox targeting in live cells. *Nat. Protoc.* **11**, 2328–2356 (2016).

49. Zhao, Y., Long, M. J. C., Wang, Y., Zhang, S. & Aye, Y. Ube2V2 Is a Rosetta Stone Bridging Redox and Ubiquitin Codes, Coordinating DNA Damage Responses. *ACS Cent. Sci.* **4**, 246–259 (2018).

50. Van Hall-Beauvais, A., Zhao, Y., Urul, D. A., Long, M. J. C. & Aye, Y. Single-Protein-Specific Redox Targeting in Live Mammalian Cells and C. elegans. *Curr. Protoc. Chem. Biol.* **10**, e43 (2018).

51. Los, G. V. *et al.* HaloTag: A novel protein labeling technology for cell imaging and protein analysis. *ACS Chem. Biol.* **3**, 373–382 (2008).

52. Deng, L. *et al.* Activation of the Iκb kinase complex by TRAF6 requires a dimeric ubiquitin-conjugating enzyme complex and a unique polyubiquitin chain. *Cell* **103**, 351–361 (2000).

53. Hofmann, R. M. & Pickart, C. M. Noncanonical MMS2-Encoded Ubiquitin-Conjugating Enzyme Functions in Assembly of Novel Polyubiquitin Chains for DNA Repair. *Cell* **96**, 645–653 (1999).

54. Maron, B. A. & Michel, T. Subcellular localization of oxidants and redox modulation of endothelial nitric oxide synthase. *Circ. J.* **76**, 2497–2512 (2012).

55. Travasso, R. D. M., Sampaio dos Aidos, F., Bayani, A., Abranches, P. & Salvador, A. Localized redox relays as a privileged mode of cytoplasmic hydrogen peroxide signaling. *Redox Biol.* **12**, 233–245 (2017).

56. Long, M. J. C., Poganik, J. R. & Aye, Y. On-Demand Targeting: Investigating Biology with Proximity-Directed Chemistry. *J. Am. Chem. Soc.* **138**, 3610–3622 (2016).

57. Long, M. J. C., Poganik, J. R., Ghosh, S. & Aye, Y. Subcellular Redox Targeting: Bridging in Vitro and in Vivo Chemical Biology. *ACS Chem. Biol.* **12**, 586–600 (2017).

58. Dinkova-Kostova, A. T., Holtzclaw, W. D. & Kensler, T. W. The role of Keap1 in cellular protective responses. *Chem. Res. Toxicol.* **18**, 1779–1791 (2005).

59. Nguyen, T., Nioi, P. & Pickett, C. B. The Nrf2-antioxidant response element signaling pathway and its activation by oxidative stress. *J. Biol. Chem.* **284**, 13291–13295 (2009).

60. Hayes, J. D. & Dinkova-Kostova, A. T. The Nrf2 regulatory network provides an interface between redox and intermediary metabolism. *Trends Biochem. Sci.* **39**, 199–218 (2014).

61. Long, M. J. C. *et al.* Akt3 is a privileged first responder in isozyme-specific electrophile response. *Nat. Chem. Biol.* **13**, 333–338 (2017).

62. Cheng, J. *et al.* A small-molecule inhibitor of UBE2N induces neuroblastoma cell death via activation of p53 and JNK pathways. *Cell Death Dis.* **5**, (2014).

63. Parvez, S. *et al.* Substoichiometric Hydroxynonenylation of a Single Protein Recapitulates Whole-Cell-Stimulated Antioxidant Response. *J. Am. Chem. Soc.* **137**, 10–13 (2015).

64. Nguyen, C. T., Lu, Q., Wang, Y. & Chen, J. N. Zebrafish as a model for cardiovascular development and disease. *Drug Discov. Today Dis. Model.* **5**, 135–140 (2008).

65. Mugoni, V., Camporeale, A. & Santoro, M. M. Analysis of oxidative stress in Zebrafish embryos. *J. Vis. Exp.* 1–11 (2014) doi:10.3791/51328.

66. Timme-Laragy, A. R., Hahn, M. E., Hansen, J. M., Rastogi, A. & Roy, M. A. Redox stress and signaling during vertebrate embryonic development: Regulation and responses. *Semin. Cell Dev. Biol.* **80**, 17–28 (2018).

67. Kardash, E., Bandemer, J. & Raz, E. Imaging protein activity in live embryos using fluorescence resonance energy transfer biosensors. *Nat. Protoc.* **6**, 1835–1846 (2011).

68. Brenner, S. THE GENETICS OF CAENORHABDITIS ELEGANS. *Genetics* **77**, 71 LP – 94 (1974).

69. Antoshechkin, I. & Sternberg, P. W. The versatile worm: Genetic and genomic resources for Caenorhabditis elegans research. *Nat. Rev. Genet.* **8**, 518–532 (2007).

70. Volovik, Y., Marques, F. C. & Cohen, E. The nematode Caenorhabditis elegans:

A versatile model for the study of proteotoxicity and aging. *Methods* **68**, 458–464 (2014).

71. Fire, A. Integrative transformation of Caenorhabditis elegans . *EMBO J.* **5**, 2673–2680 (1986).

72. Larance, M. *et al.* Stable-isotope labeling with amino acids in nematodes. *Nat. Methods* **8**, 849–851 (2011).

73. Schrag, J. D., Winkler, F. K. & Cygler, M. Pancreatic lipases: Evolutionary intermediates in a positional change of catalytic carboxylates? *J. Biol. Chem.* **267**, 4300–4303 (1992).

74. Todd, A. E., Orengo, C. A. & Thornton, J. M. Plasticity of enzyme active sites. *Trends Biochem. Sci.* **27**, 419–426 (2002).

75. Devine, E. L., Oprian, D. D. & Theobald, D. L. Relocating the active-site lysine in rhodopsin and implications for evolution of retinylidene proteins. *Proc. Natl. Acad. Sci. U. S. A.* **110**, 13351–13355 (2013).

76. McMahon, M., Lamont, D. J., Beattie, K. A. & Hayes, J. D. Keap1 perceives stress via three sensors for the endogenous signaling molecules nitric oxide, zinc, and alkenals. *Proc. Natl. Acad. Sci. U. S. A.* **107**, 18838–18843 (2010).

77. Lapierre, L. R. & Hansen, M. Lessons from C. elegans: Signaling pathways for longevity. *Trends Endocrinol. Metab.* **23**, 637–644 (2012).

CHAPTER 2

PRECISION ELECTROPHILE TAGGING OF REDOX-SENSING PROTEINS IN LIVE C. ELEGANS

PREFACE

Figures and data from the following chapter have appeared in a previously published work. They have been adapted for presentation in this work with permissions from Biochemistry (Copyright 2018 American Chemical Society):

Long, M. J. C.; Urul, D. A.; Chawla, S.; Lin, H.; Zhao, Y.; Haegele, J. A.; Wang, Y; Aye, Y. Precision Electrophile Tagging in Caenorhabditis elegans. Biochemistry 57, 216–220 (2018). (doi: 10.1021/acs.biochem.7b00642)

2.1 Introduction

2.1.1 Adapting T-REX to the C. elegans model system

As outlined in the previous chapter, the genetic tractability, transparent body, and short, well-characterized development and lifespan of *C. elegans* makes it uniquely suited to incorporate into a system designed to interrogate electrophile signaling systems.[1] However, to do so, we must first establish that the fundamental T-REX platform is compatible with this model organism, which requires meeting three central criteria. First, we must be able to generate transgenic *C. elegans* lines expressing a target redox-sensing protein of interest (POI) fused to HaloTag. Following that, we must demonstrate that this HaloTag is active and can be accessed by otherwise-bioorthogonal photocaged RES precursors *in vivo*. Finally, light-activated release of the RES and subsequent labelling of the POI must be achievable in the live worms.

These steps can be reliably validated at several points along the general T-REX workflow (**Figure 2-1**). Transgene expression can be validated using fluorescent markers, either directly fused to the HaloTag or co-expressed in the final transgenic worm through dual-plasmid microinjection (see 2.4.3.1). Degree of saturation of HaloTag *in vivo* by our desired precursor probes can be evaluated through labelling of remaining unoccupied HaloTag with Halotag-functionalized TMR (Ht-TMR) (**Figure 2-1**; gray arrows). Finally, the fate of the RES after light-driven release from the precursor molecule can be determined by appending a terminal alkyne onto the desired

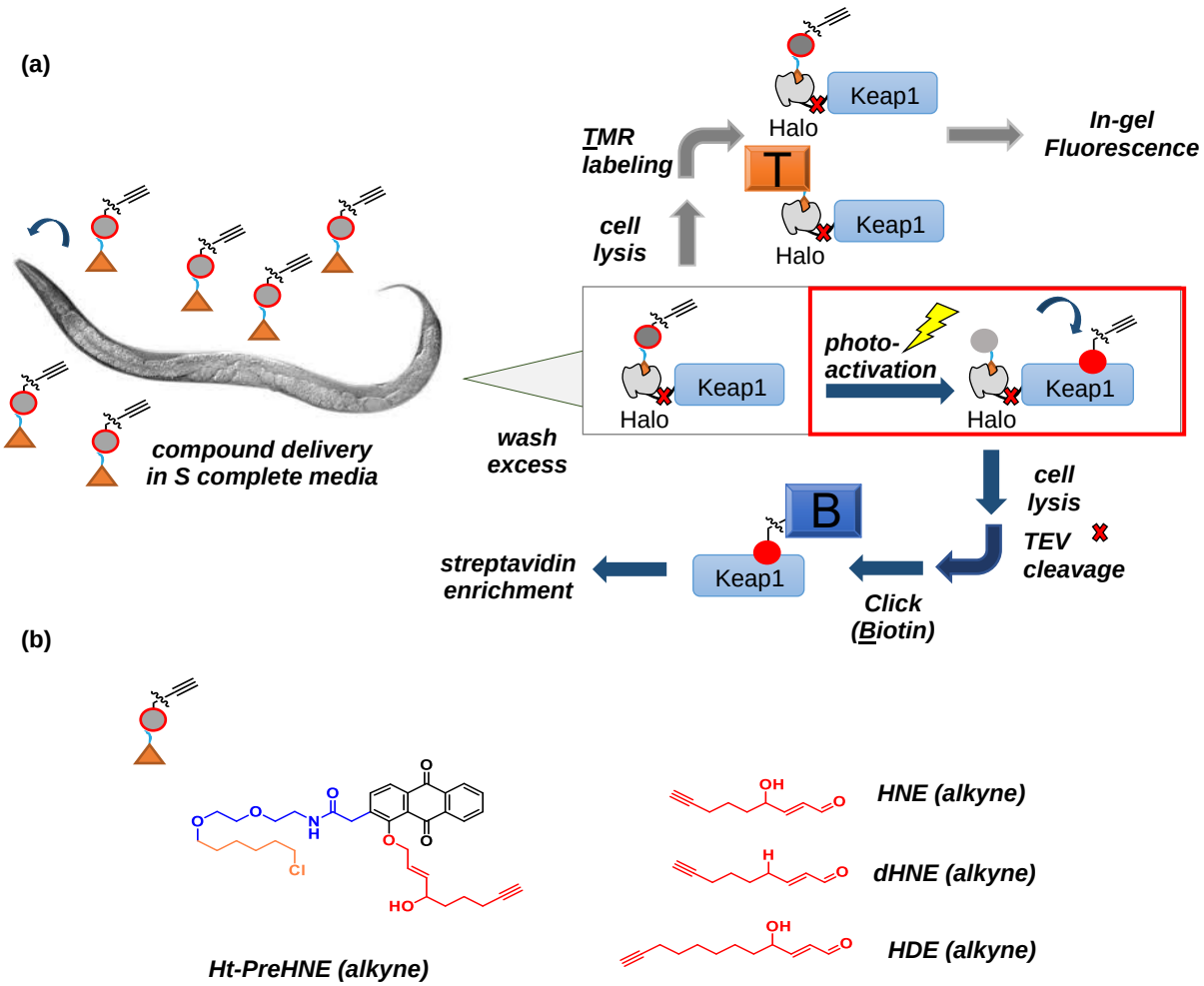

Figure 2-1. Overview of the T-REX protocol in *C. elegans*. **(a)** Basic schematic for T-REX compound delivery and downstream analysis. Full T-REX protocol is depicted with blue arrows (See 2.4.5, 2.4.6, 2.4.8), though evaluations of intermediate steps, such as HaloTag labeling and saturation (shown here in gray arrows; see 2.4.7), can be performed. T indicates TMR; B indicates biotin. **(b)** Summary of a photocaged, Halotag-functionalized, alkynylated LDE precursor (left) and examples from an expanding alkynylated LDE library (right). Components of the precursor include the LDE (red), the anthraquinone photocage (black), a linker region (blue), and the HaloTag-specific hexyl chloride terminus (orange).

RES, which enables the use of downstream azide-driven click chemistry. Thus, RES-labelled targets – such as the POI, or HaloTag in the case of unreleased probe – can be enriched through streptavidin pulldown following biotin azide click chemistry (**Figure**

2-1; blue arrows). A direct in-gel readout from fluorescent azide dyes to determine probe specificity can also be used as a readout. For this project, several candidate lipid-derived electrophiles (LDEs) from our existing REX toolbox – including HNE – will be featured.[2,3]

2.1.2 Utilization of Keap1 as an established RES sensor for C. elegans T-REX validation

In designing a proof-of-concept T-REX protocol to demonstrate in *C. elegans* – or any new model organism – we needed to select an existing known RES-sensor POI such that an inability to produce POI-targeted labelling *in vivo* could be attributed to failure adapting to the model system, and not to the POI itself. Few known RES sensors native to *C. elegans* were known to fit this criterion; for our purposes, then, we selected the human Keap1 (Kelch-like ECH-associating protein 1) as our sensor POI. In the broader context of redox and electrophile signaling, Keap1 has garnered significant interest for its function as a RES-sensing regulator of the antioxidant response element (ARE). Specifically, the steady-state binding of Keap1 to Nrf2 promotes proteasomal degradation of the latter, preventing Nrf2 from upregulating the ARE; this is interrupted upon RES binding to Keap1, allowing ARE activation and associated response to acute electrophile stress.[4–7] Previous work establishing T-REX methodology was successfully able to demonstrate RES labeling of Keap1 in a whole-cell context, with discernable consequences on Nrf2 upregulation.[3] While there is no

Keap1 ortholog in *C. elegans,*[8] its well-established state as a robust RES sensor is sufficient for use at this proof-of-concept stage.

2.2 Results and Discussion

2.2.1 Validation of transgene expression in C. elegans

To integrate *C. elegans* into our REX technology platform, we required a set of transgenic lines to both demonstrate proof-of-concept RES delivery to known sensor proteins (T-REX) and establish a starting point for future proteomic profiling (C-REX). To that end, several lines were created using an established transformation protocol, in which plasmids containing the target HaloTag construct were inserted via microinjection into the distal gonad cytoplasm core. In this manner, injected plasmids – typically the expression plasmid co-injected with a dominant marker for phenotypic screening – concatenate into extrachromosomal arrays, which are taken into the germ cell line and are subsequently propagated to progeny.[9–11] As a starting point, two transgenic lines each expressing a GFP-fused HaloTag construct were created, each expressed via a different promoter: Hlh8[12] or Hsp16[13,14] (See Appendix B). Expression in both lines was validated by fluorescent microscopy, as was *in vivo* HaloTag activity via Ht-TMR feeding (**Figure 2-2**). Transgene expression and labeling was further confirmed via Western blot and Cy5 labeling, respectively (**Figure 2-3**).

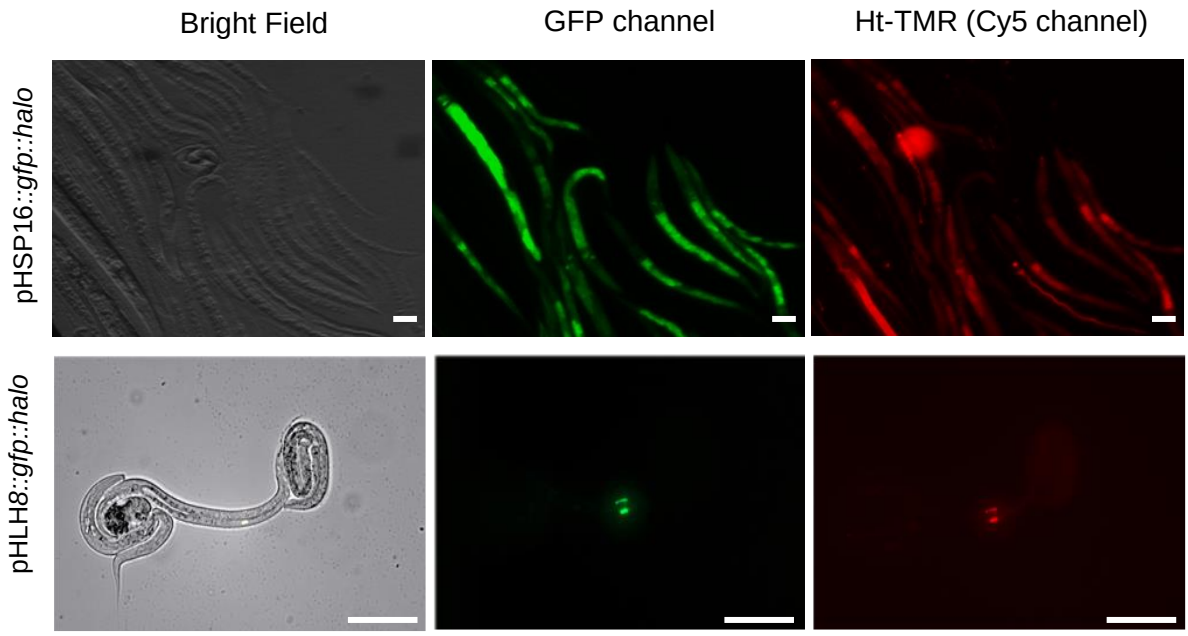

Figure 2-2. Demonstration of *in vivo* HaloTag activity in transgenic *C. elegans* lines. Two separate transgenic lines expressing *gfp::halo* fusion constructs under different promoters are shown after treatment with Ht-TMR in M9 media (See 2.4.7); the line featuring the *hsp16* promoter was exposed to heat-shock conditions (37°C) for 30 min, then imaged after 3 hours at 20°C. Scale bars represent 50 μm. *Performed with Dr. Joseph Haegele, Dr. Marcus Long, and Shivansh Chawla.*

These aforementioned lines were maintained via selection of worms expressing the co-transformed *rol6* phenotypic marker during routine passage. However, while we maintained these and additional such lines (see 2.2.6), we sought to create transgenic worms with genome-integrated HaloTag constructs as well. An additional two lines of this type were created, using gamma irradiation to induce DNA damage and facilitate integration of the co-injected transgenes and the selected *pmec7::mrfp* marker (**Figure 2-4**). Integration was confirmed via localized fluorescence of the touch-receptor neurons;[15] further, expression of the mitochondria-localized *tom70::mcherry::halo* construct was visible upon heat shock. The other transgenic line containing

Table 2-1. Photocaged precursor probes and HaloTag-functionalized TMR structure

Probe	Structure
Ht-preHNE (alkyne) **(1)**	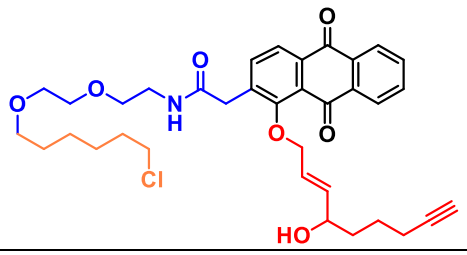
Ht-preHNE **(1-na)**	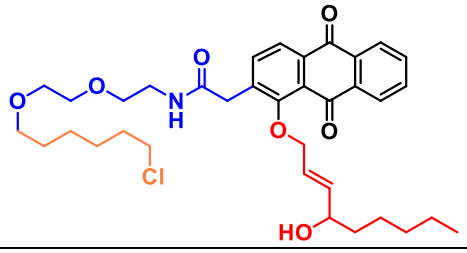
Ht-PredHNE (alkyne) **(2)**	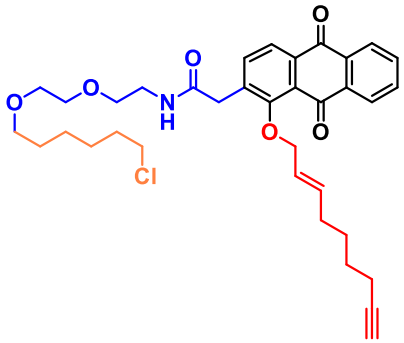
Ht-PreHDE (alkyne) **(3)**	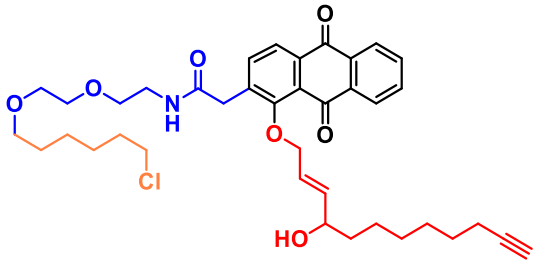
HNE (alkyne) **(4)**	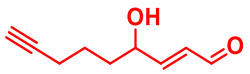
Ht-TMR	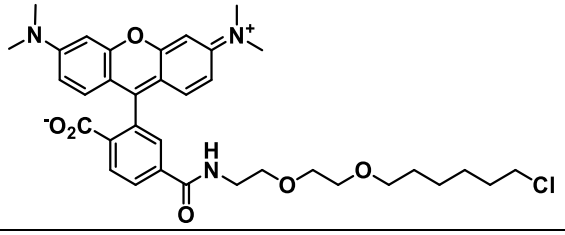

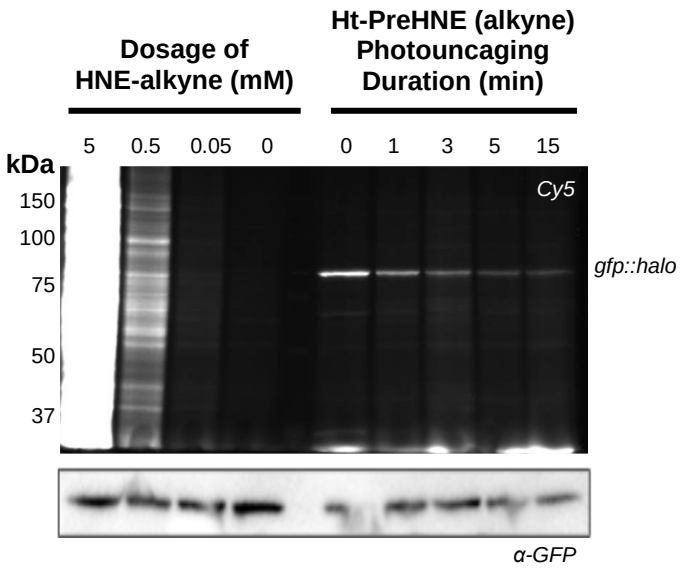

Figure 2-3. Qualitative evaluation of LDE uptake, HaloTag activity, and LDE photouncaging kinetics in *C. elegans* via in-gel Cy5 fluorescence. pHSP16.*::gfp::halo* worm lysates were evaluated after bolus dosing with HNE alkyne (left) and after treatment with excess Ht-preHNE (alkyne) followed by variable photouncaging durations (right). *Performed by Dr. Joseph Haegele*

halo::tev::keap1 – to be used for T-REX validation – was further confirmed via Western blot (**Figures 2-5** and **2-6**).

2.2.2 Validation of compound uptake and HaloTag activity in C. elegans

To be able to utilize these transgenic lines, we must demonstrate that they are able to uptake desired compounds by feeding such that active HaloTag constructs can be saturated *in vivo*. Previous treatment of the pHSP16.*::gfp::halo* worm line with Ht-TMR demonstrated that the expressed HaloTag constructs were functional and could be successfully labelled *in vivo* (**Figure 2-2**). By treating the lysate of *halo::tev::keap1* worms previously incubated with each of our photocaged LDE precursors (**Table 2-1**) with

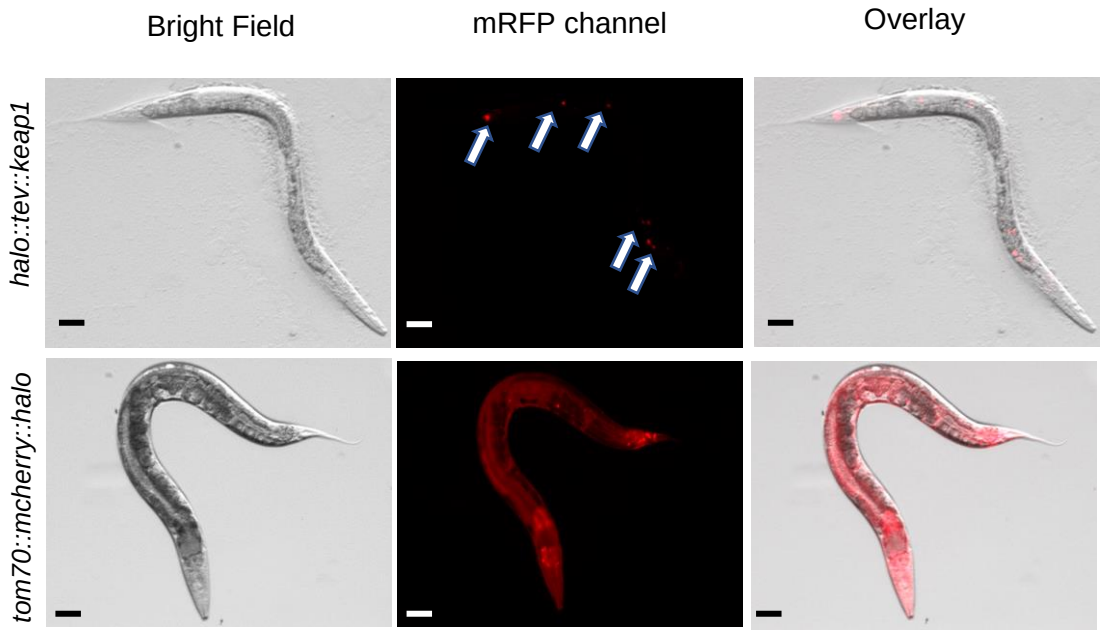

Figure 2-4. Transgenic *C. elegans* lines generated for T-REX validation (top) and later application towards combined G-REX/SILAC proteomics profiling (bottom). Both constructs are expressed under an *hsp16* heat-shock promoter. Both lines were co-injected with *pmec7::mrfp* transgene marker. Both lines were exposed to heat-shock conditions (37°C) for 30 min., then imaged after 3 hr. at 20°C. Scale bars represent 50 μm. *Performed with Dr. Marcus Long and Shivansh Chawla*

Ht-TMR, we could quantitate the extent of HaloTag saturation achieved by said precursors (**Figure 2-1,** top). In doing so, we achieved over 50% HaloTag saturation globally (**Figure 2-5**). Though there was some variability across our precursor molecules – with pre(HNE) alkyne yielding the best results – it did not seem to be affected by the presence or absence of the alkyne arm. Additionally, bolus treatment with an equivalent concentration of HNE-alkyne yielded minimal HaloTag labelling, further validating the specific binding of the Ht-functionalized precursors.

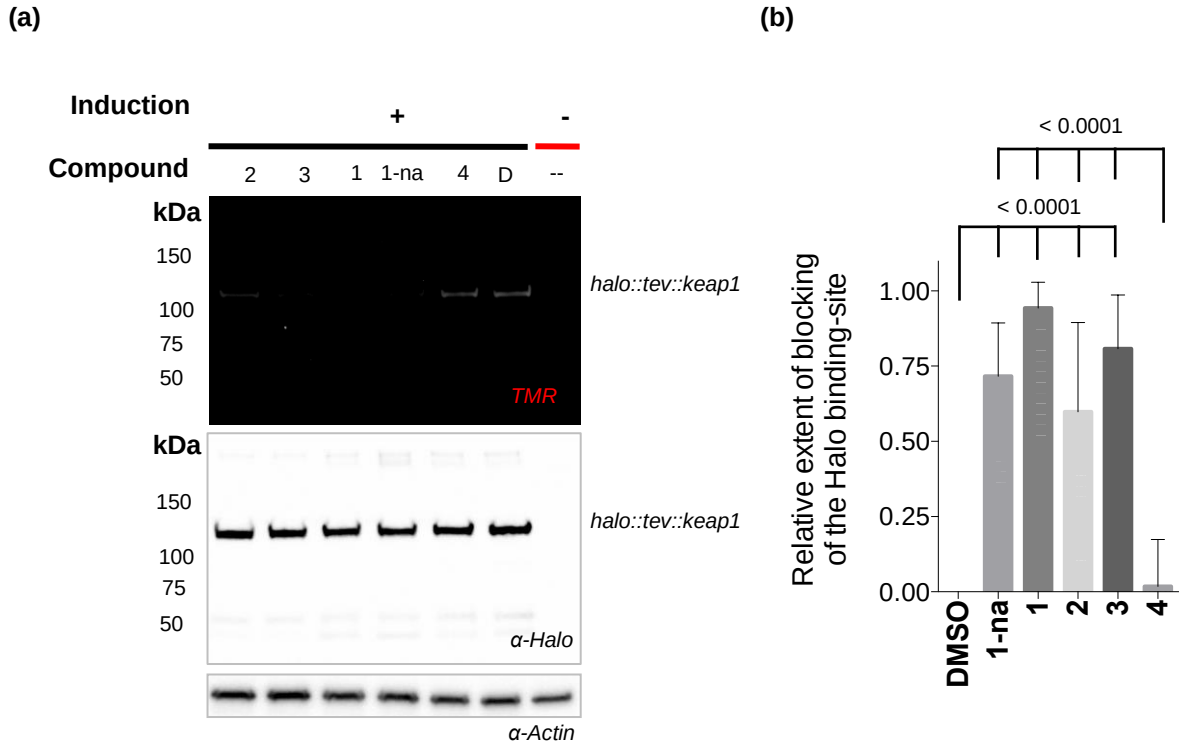

Figure 2-5. Evaluation of compound saturation of a HaloTag construct *in vivo* via Ht-TMR blocking assays. **(a)** In-gel fluorescent evaluation of unlabeled HaloTag construct after TMR treatment of worm lysates (See Table 2-1 for compounds). Validation of *halo::tev::keap1* expression, as well as normalization, was conducted by follow-up Western blot analysis. **(b)** Quantitation of Ht-TMR blocking due to occupation of the HaloTag binding site. Error bars show SEM (n = 8). *Performed with Dr. Marcus Long and Shivansh Chawla*

2.2.3 Validation of light-driven HNE release in C. elegans

Controllable protouncaging of the RES molecule is a critical component of T-REX, one that the transparent composition of *C. elegans* was well-suited for. To demonstrate this, we treated pHSP16*::gfp::halo* worms with Ht-PreHNE (alkyne) and exposed sub-populations of these worms to variable durations of UV light (**Figure 2-**

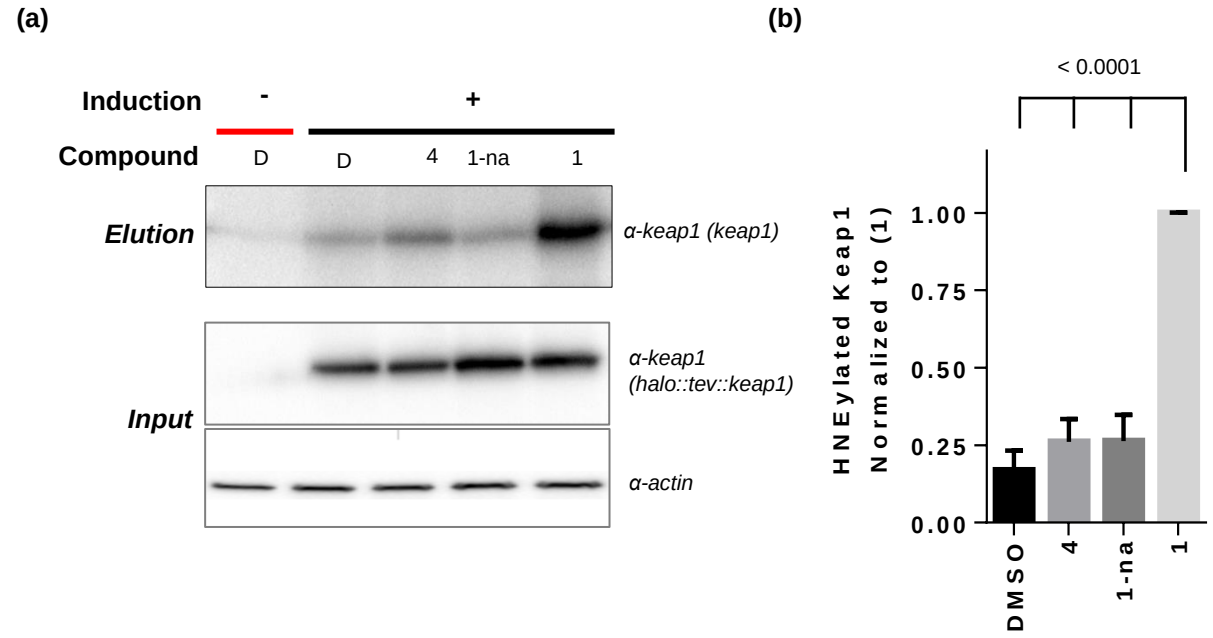

Figure 2-6. T-REX mediated selective delivery of HNE to Keap1 in *C. elegans*. **(a)** Quantitative analysis of HNE delivery to Keap1 via downstream Western blot analysis of worm lysates (See Table 2-1 for compounds). Elution signals were internally normalized to inputs withdrawn before pulldown. **(b)** Quantitation of T-REX-driven enrichment of labelled Keap1. Error bars show SEM (n ≥ 5). *Performed with Dr. Marcus Long and Shivansh Chawla*

3, right). On a 15-minute time scale, the loss of HNE (alkyne) from GFP::Halo, measured by the decreasing Cy5 signal, was readily apparent.

2.2.4 Controlled labeling of redox-sensing Keap1 in live C. elegans

Having demonstrated both the expression of active HaloTag constructs in *C. elegans* – including that of *halo::tev::keap1* – and the saturation of HaloTag by our photocaged LDEs, we proceeded to demonstrate T-REX-targeted delivery to Keap1 itself *in vivo*. Post-heat shock, we incubated *halo::tev::keap1* worms with Ht-preHNE (alkyne), alongside the non-alkynylated and non-photocaged variants. Following, we

enriched HNE (alkyne)-labelled proteins via biotin-streptavadin pulldown (**Figure 2-1**; blue arrows). By Western blot quantitation, we saw an approximate 70-80% increased enrichment of Keap1 compared to both non-alkynylated and non-photocaged (bolus) controls (**Figure 2-5**). The latter was particularly interesting in that bolus dosing did not yield any significant increase in Keap1 labelling compared to negative controls. Beyond being subject to a proteome's worth of off-target sequestration, it is also likely that reactive LDEs like HNE are subject to potential metabolic effects upon ingestion by *C. elegans,* which the photocaged variant is able to bypass.

2.2.5 Expansion of T-REX in C. elegans to other LDEs of interest

Thus far we have shown controllable labeling of an established RES sensor via T-REX using HNE as the RES of choice. However, our current library of photocaged LDEs extends beyond HNE,[3] several of which are shown here (**Figure 2-1; Table 2-1**). The alkenal-based LDEs featured here (HNE, dHNE, HDE) can each be efficiently used to saturate HaloTag constructs *in vivo* as photocaged precursor probes, similarly to their behavior in previous works (**Figure 2-5**). However, T-REX-targeted labeling of Keap1 *in vivo* upon LDE release proved to be inconsistent and, in general, subdued compared to HNE (data not shown). It is possible that the biological system in use and the target POI may be factors that effect delivery efficiency of different RES, even if said RES are functionally similar (such as the alkenal LDEs featured here). However,

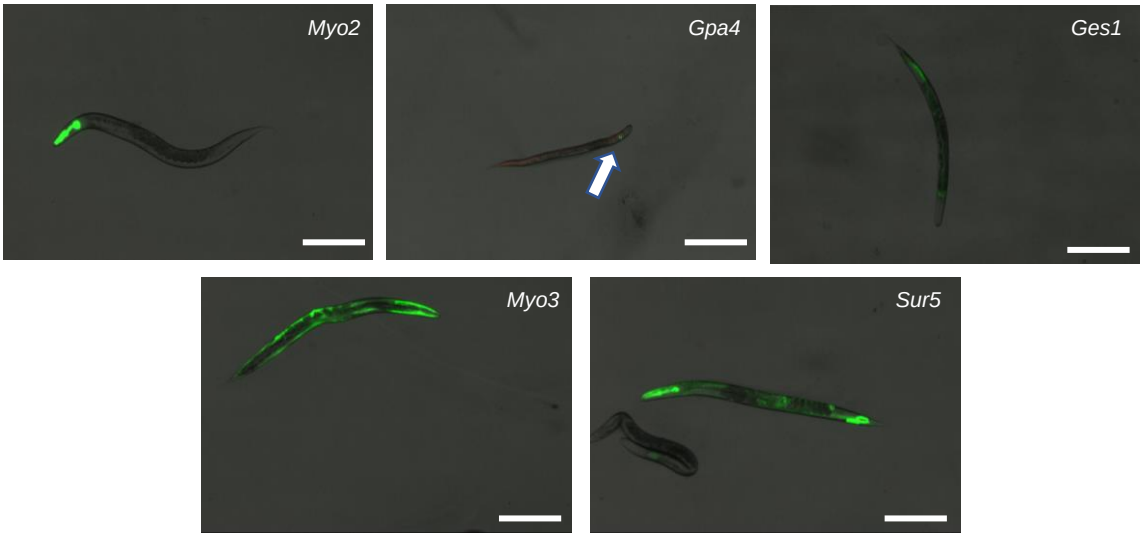

Figure 2-7. Expansion of the *C. elegans* transgenic library to include promoter-driven tissue-localized *gfp::halo* expression. Localization is extended to pharyngeal muscles (*myo-2*), intestines (*ges-1*), ASIR/ASIL sensory neurons (*gpa-4*), body-wall muscle (*myo-3*), or nuclei (*sur-5*). Scale bars represent 250 μm. *Lines generated by SunyBiotech*

such issues only further highlight the importance of expanding the available RES toolbox of any investigative platform such as T-REX.

2.2.6 Establishing tissue-specific expression of HaloTag constructs as a prelude to proteomic profiling in C. elegans

Having successfully conducted T-REX-directed labelling of a known RES sensor in *C. elegans,* we began to turn towards our future developments to fully integrate *C. elegans* into the REX technology pipeline. By this point we had already developed several HaloTag transgenic lines primed for usage in proteomic profiling. We were able to utilize pHSP16::*tom70::mcherry::halo* and pHSP16::*gfp::halo* lines, for example, to identify the RES-sensing function of the otherwise well-characterized s-adenosyl homocysteine

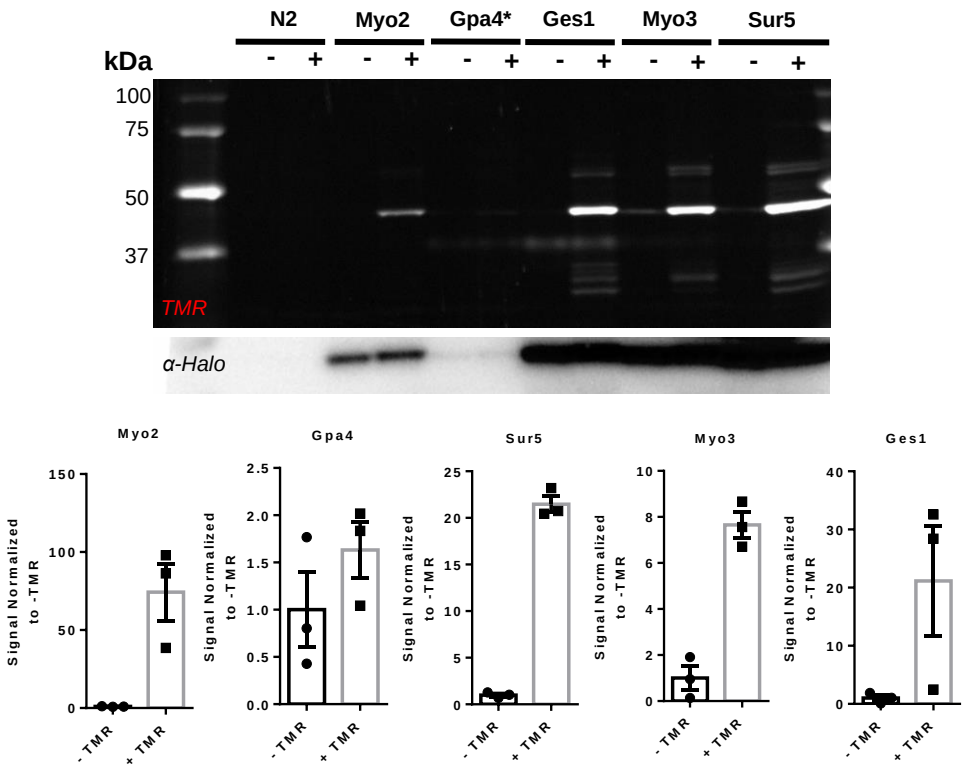

Figure 2-8. Assessment of *in vivo* Ht-TMR labelling of active HaloTag constructs of the extended *gfp::halo C. elegans* library. **(a)** In-gel fluorescent evaluation of TMR signal of labelled *gfp::halo* after worm treatment. Signal was internally normalized to follow-up Western blots. **(b)** Quantitation of TMR signal normalized to negative control. Error bars are SEM (n = 3). *Performed with Shivansh Chawla*

hydrolase (SAHH), and were able to further investigate this moonlighting function using our T-REX investigative toolset (see Chapter 3).

Our next query at this stage involved creating lines with tissue-specific HaloTag expression to facilitate discovery of RES sensor proteins that may only function or exist in specific cell types, and as such may be missed in a whole-organism profiling experiment. Mindfulness of localization was already a factor in early transgenic line generation; pHSP16::*tom70::mcherry::halo* was designed for RES release near

mitochondria,[16] and pHLH8::*gfp::halo* facilitated specific expression in mesodermal lineage cells.[17] To proceed with this inquiry in future studies, we obtained 5 unique transgenic lines, each featuring promoter-localized expression of *gfp::halo* (**Figure 2-7**). All lines obtained this way could be labelled with Ht-TMR, though TMR fluorescent signal varied accordingly with abundance of the cell type in the worm (**Figure 2-8**).

2.3 Conclusions

The successful targeted delivery of an LDE to a known RES sensor protein *in vivo* via T-REX represented a significant step forward in the integration of whole-organism models into the REX technology platform. By demonstrating spatiotemporally controlled labeling of Keap1 in *C. elegans,* we were able to clear the hurdles of precursor probe intake, saturation of active HaloTag, and light-driven LDE release. Future RES sensor candidates that emerge from proteomic profiling efforts within the REX platform can now be further interrogated through generation of transgenic lines designed for targeted labeling, with the added benefits of a whole-organism context. This includes gaining more valuable insight into downstream biochemical consequences or phenotypic outcomes of controlled RES sensor labeling.

However, such investigations require identifying novel sensors within these new whole-organismal contexts to begin with. Identification of low-occupancy RES sensors that facilitate endogenous signaling pathways requires the adaptation of G-REX[18] to

these whole-organism models. Transgenic lines expressing *gfp::halo* and *tom70::mcherry::halo* were created with this in mind. Future work will entail proteomic profiling across these transgenic lines, using low RES concentrations capped by HaloTag expression to identify kinetically privileged sensor candidates, which can then be isolated and further examined within the same model organism. Chapter 3 provides a sample of how such a pipeline can be envisioned, from discovery of a novel sensor candidate to characterization of its role in converting endogenous electrophile flux to a discernable biological outcome.

2.4 Experimental Details

2.4.1 Generation of Plasmids for HaloTag Fusion Construct Expression in C. elegans

(Performed by Dr. Marcus Long and Dr. Joseph Haegele)

Transgene inserts were designed with the intent of developing multiple *C. elegans* lines expressing HaloTag constructs to facilitate one of two goals: a proof-of-concept application of T-REX-mediated RES delivery to a known sensor protein *in vivo,* and development of a library of transgenic worm lines expressing HaloTag constructs for the purposes of RES sensor profiling via controlled release of transient, low-concentration RES. All plasmids constructed for this project were done so via ligase-

free cloning. For transgenic lines requiring *hlh-8* promoter, pJKL502 plasmids were utilized; for those requiring *hsp-16* instead, Lig778 destination plasmid was used instead. (See Appendix B)

2.4.2 C. elegans General Culture Methods

All *C. elegans* lines being maintained for active use were grown in 17°C or 20°C incubators depending on experimental factors and timelines. All lines were maintained using 100 mm NGM agarose plates (**Table 2-2**) seeded with OP50 *E. coli* lawns as a food source. Individual plates are maintained until the population of worms in a plate reaches near-confluence. Before food is depleted, worms are passaged to a new plate via heat-sterilized platinum wire pick. For integrated transgenic lines, 20 healthy worms are selected for passaging. For transgenic lines containing non-integrated extrachromosomal arrays, worms are screened for the dominant phenotypic marker, such as fluorescence, and are passaged accordingly. Unless otherwise indicated, all populations being grown for immediate experimental use were harvest prior to starvation conditions.

2.4.3 C. elegans Microinjection and Transgenic Line Generation

(Performed by Dr. Marcus Long)

2.4.3.1 Microinjection Protocol

Approximately a week before injection, 3-4 L4 worms were selected and seeded onto OP50 plates, then grown for at least 2 generations until a high number of young adult worms were available. 1-3 days before injection, agarose pads were prepared and set to dry out at room temperature. On the day of injection, healthy young adult worms were first picked and transferred to a clean, unseeded NGM plate until they sufficiently shed excess OP50. 2 drops of mineral oil were added to the now-desiccated agarose pads, and the pick, after being coated in the oil, was used to transfer 3-4 worms at a time onto the pad such that the gonads were visible. Upon loading 20-60 worms onto the agarose, a single gonad injection was performed with each worm using 150 ng/μL of DNA mix (1:1 mixture of expression plasmid and dominant marker plasmid, centrifuged 18000 g for 20 min prior to injection to clear precipitate). Worms were then transferred to Recovery Buffer (**Table 2-2**), and subsequently seeded onto OP50 plates (3-4 per plate). After 3 days of 16°C incubation, worms were screened for expression of the appropriate dominant phenotypic marker daily, for up to 5 days. During this time, transgenic worms were selected and moved to individual screening plates, and their progeny were scored in subsequent days for transmission. Typically, a transmission rate of 30-50% was expected of transgenic lines carrying extrachromosomal arrays.

2.4.3.2 Generation of Genome-integrated Transgenic Lines

Transgenic worms from the previous step were grown until an asynchronized population containing several hundred L4 transgenic worms could be achieved. The

Table 2-2. Buffers for *C. elegans* maintenance and T-REX protocols

Buffer/Media Name	**Composition**
NGM Agar/Agarose *Per 1mL of Agar/Agarose*	0.79 g Tris NaOH (pH 8.0) 2 g NaCl 3 g tryptone 17 g agar OR agarose 5 mg cholesterol
Recovery Buffer	5mM HEPES (pH 7.2) 3 mM $CaCl_2$ 3 mM $MgCl_2$ 66 mM NaCl 2.4 mM KCl, 4% glucose (w/v)
S-complete Media	S basal media (100 mM NaCl [EMD], 5.7 mM K2HPO4 [Fisher], 44.1 mM KH2PO4 [Fisher], 5 mg/L cholesterol) Trace metal solution (50 µM EDTA, 25 µM $FeSO_4$ •7 H_2O, 10 µM $MnCl_2$•4 H_2O, 10 µM $ZnSO_4$ •7 H_2O, 1 µM $CuSO_4$ •5 H_2O]) 3 mM $CaCl_2$ 3 mM $MgSO_4$ 10 mM sodium citrate 1x penicillin/streptomycin 1x nystatin
OP50 Stock Media *Per 1mL of OP50 Stock Media*	Spin down 2 mL of OP50 Resuspend in 1 mL S-complete media
Worm Lysis Buffer	1.5% NP-40 50 mM HEPES (pH 7.6) 2x Roche protease inhibitor cocktail 0.5 mM TCEP
10x Cy5 Click Mix *(*Add JUST before use)*	10% SDS 10 mM $CuSO_4$ 1 mM Cu-TBTA 20 mM TCEP* .1 mM Cy5-azide* *(Add t-BuOH separately)*
Resuspension Buffer	8% LDS 1 mM EDTA 50 mM HEPES (pH 7.6)

worm population was then subject to gamma irradiation (3600-4800 rads) and allowed to recover for several hours. Afterwards, transgenic young adult worms were picked and transferred to new OP50 plates in groups of 20 and allowed to grow until confluence. Then, transgenic young adults from these populations were similarly passaged. After at least one more round of passaging, young adult worms were picked and seeded individually on new plates, and their progeny were screened for Mendelian transgene inheritance.

After identifying such progeny populations, individual worms were picked from said groups and screened for homozygous transgenic progeny. Progeny identified this way were then back-crossed into the parent strain by plating 4-5 transgenic worms (all hermaphroditic) with 14-16 young adult male worms from the parent strain. Progeny from this back-cross was then screened for hermaphroditic worms that were heterozygous for the transgene. Worms from this progeny were picked, and their subsequent progeny was screened for homozygous transgenic worms. This back-cross was then repeated a minimum of 3 times.

2.4.4 Compound Dosing of C. elegans

(Performed with Dr. Marcus Long, Dr. Joseph Haegele, and Shivansh Chawla)

After determining the approximate number of confluent plates required for an experiment, each plate was seeded with a minimum of 20 transgenic worms (more if using a line with an extrachromosomal array with a low transmission rate) and allowed

to grow to confluence (but not starvation) at 17°C or 20°C. Typically, 1 x 100 mm confluent plate per condition was used for fluorescent-based click assays, and 5 x 100 mm plates per condition for biotin-streptavadin pulldown assays. If the transgenic line expressed the desired construct under a heat-shock promoter, a set number of plates were removed and transferred to a 37°C incubator and maintained there for 1 hr. During this time, if a "- induction" control was required (usually 2 x 100 mm plates per experiment), these worm plates were maintained in their original incubator conditions. All worm plates were then harvested using 2 mL of S complete media (**Table 2-2**) per plate. These were transferred to 2 mL tubes, which were then spun at 2000-6000 x g for 30 s. The resultant pellets were washed with fresh S complete media, and the process was repeated twice. Then, all "+ induction" and "- induction" worms were pooled and then split into 15 mL tubes depending on the number of conditions intended. To each 15 mL tube, 2 mL of S Complete media and 2.5 mL of OP50 Stock Media (**Table 2-2**) was added to the worm pellet.

To proceed with a bolus-dosing experiment, each condition was treated with variable concentrations of a pre-diluted, alkynylated LDE {such as HNE (alkyne)} stock for 1 hr, such that the final volume in each tube was 5 mL. "- compound" conditions were treated with an equivalent volume of equally diluted vehicle (DMSO). The tubes were then incubated via end-over-end rotation for 1 hr in the dark at room temperature. Afterwards, the worms were washed with S Complete media twice for 30

min, then once with 50 mM HEPES (pH 7.2) for 30 min. The worms were then transferred to 1.5 mL tubes and pelleted, with as much liquid supernatant removed as possible. These pellets were then flash frozen in liquid nitrogen and stored at -80°C until used (up to a week maximum, though typically used within 1-3 days).

2.4.5 T-REX Protocol in C. elegans

(Performed with Dr. Marcus Long, Dr. Joseph Haegele, and Shivansh Chawla)

C. elegans populations for T-REX experiments were prepared nearly identically to those for bolus dosing (See 2.4.4) up to the compound treatment step. At this stage, each tube was treated with .5 mL of a 10x (300 μM) stock of the appropriate photocaged precursor compound (**Table 2-1**) in S complete media. The tubes were then incubated via end-over-end rotation for 6 hr in the dark at room temperature. If a bolus-dosing condition was included as a control, this condition would be left untreated until the final hour of the incubation, at which point it would be treated with an equal concentration of LDE {HNE (alkyne)}and returned to end-over-end rotation. Afterwards, the worms were washed twice with S Complete media, then once with 50 mM HEPES media. Each worm pellet was then resuspended in 1.5-2 mL HEPES and transferred to a 6-well plate. These uncovered plates were then placed directly underneath a pre-warmed UV light source (365 nm, approx. 5 mW/cm^2) for 5 min. The worms were then transferred into 1.5 or 2 mL tubes and pelleted, then flash-frozen and stored in -80°C for up to a week maximum.

2.4.6 Preparation of C. elegans Lysate

Worm pellets were thawed on ice upon withdrawal from -80°C storage. Expected starting worm pellet volumes are ~10 μL for in-gel fluorescence assays, and ~60-100 μL for enrichment pulldowns. After thawing, 2-8 volumes of Worm Lysis Buffer (**Table 2-2**) were added, as well as ¼ volume of 0.7 mm zirconia beads. Samples were then vortexed for 30 s and freeze-thawed with liquid nitrogen. After thawing, this step was repeated twice more, with 15 s vortex steps instead. Afterward, all samples were centrifuged for 10 min at 20000 g at 4°C. Lysates were transferred to fresh tubes and quantitated via Bradford assay, then immediately used.

2.4.7 HaloTag Blocking Assays in C. elegans Lysate

(Performed with Dr. Marcus Long, Dr. Joseph Haegele, and Shivansh Chawla)

A portion of lysate from each condition is diluted to 1 mg/mL. Of this, 20 μL is withdrawn to be assessed. To each condition, 2 μL of stock Ht-TMR ligand was added such that the final concentration is 2 μM in 22 μL. These samples were then incubated at 37°C for 30 min. Following this, 6 μL of 4X Laemmli Buffer treated with 6% βME was added, and the samples were incubated for a further 5 min. Afterwards, samples were loaded onto an SDS-PAGE gel and analyzed for TMR fluorescent signal.

2.4.8 Click Chemistry in C. elegans Lysate

(Performed with Dr. Marcus Long, Dr. Joseph Haegele, and Shivansh Chawla)

2.4.8.1 In-gel (Cy5) Fluorescence Analysis

Following T-REX and/or bolus-dosing and worm lysate preparation, a volume of 21.3 μL per condition of 1 mg/mL diluted lysate was prepared. To each, 1.25 μL of t-BuOH and 2.5 μL of 10x Cy5 Click Mix (**Table 2-2**) were added. These samples were then incubated at 37°C for 30 min. Following this, 8 μL of 4X Laemmli Buffer treated with 6% βME was added, and the samples were incubated for a further 5 min.. Afterwards, samples were loaded onto an SDS-PAGE gel and analyzed for Cy5 fluorescent signal.

2.4.8.2 Biotin-Streptavidin Pulldown Analysis

Following T-REX and worm lysate preparation, a volume of 300-500 μL of each lysate was prepared to a final concentration of 1 mg/mL (or prepared to match the existing lowest-concentration lysate) using Worm Lysis Buffer (**Table 2-2**). Afterwards, TEV protease was added to each sample to a final concentration of 0.3 mg/mL, and each sample was incubated for 30 min at 37°C. Concurrently, streptavidin beads were being prepared for pre-clearance of endogenous biotinylated proteins from the lysates. These beads were washed twice in ddH_20 (30 min., room temperature) then once in 50 mM HEPES (30 min., room temperature). The lysates were then incubated with these beads (1:10 ratio of sample:beads by volume) for 2 hr at room temperature, using end-over-end rotation. Afterwards, lysates were spun down (2000 g, 1 min.) and removed.

After pre-clearance, lysates were prepared such that, in 350-600 mL final volume per sample, there contained 1% SDS, 5% t-BuOH, 1 mM $CuSO_4$, 0.1 mM CuTBTA, 2 mM TCEP, and 0.2 mM biotin azide. TCEP, followed immediately by biotin azide, were both added last to each sample prior to incubation. Once prepared, all samples were incubated at 37°C for 30 min.. Following this, pre-chilled (-20°C) pure EtOH was added to each lysate in a 1:4 lysate:EtOH ratio, to facilitate precipitation. Each sample was then moved to -80°C storage overnight.

The next day, lysates were centrifuged (20000 x g, 30 min., 4°C), and the resultant pellets were resuspended in 70% EtOH. They were then spun down again; this process was performed twice with 70% EtOH, then once with 100% acetone. After the final acetone resuspension and spin-down, samples were left exposed to air until the acetone had just evaporated (but before the pellets themselves dried out). At that point, each sample was resolubilized in 50 μL of pre-warmed Resuspension Buffer (**Table 2-2**) via sonication at 55°C for 15 minutes intervals until complete. To ensure complete resolubilization, samples were centrifuged (15000 x g, 5 min.) between each interval to check for remaining unsolubilized protein. Once complete, each sample was diluted to a final concentration of 0.5% LDS via 50 mM HEPES; samples were then centrifuged further (15000 x g, 5 min.) and transferred to clean tubes. A new set of streptavidin beads (prepared similarly to before) were added to each sample (at a 1:10 ratio of sample:beads by volume), and all samples were incubated for 2 hr. with end-over-end

rotation. The beads were then washed three times with 0.5% LDS in 50 mM HEPES for 30 min.; following this, the beads were boiled with 2x Lamelli Dye + 3% βME for 5 minutes to elute the enriched protein. Eluted samples were then assessed via Western blot.

2.5 References

1. Antoshechkin, I. & Sternberg, P. W. The versatile worm: Genetic and genomic resources for Caenorhabditis elegans research. *Nat. Rev. Genet.* **8**, 518–532 (2007).
2. Fang, X. *et al.* Temporally controlled targeting of 4-hydroxynonenal to specific proteins in living cells. *J. Am. Chem. Soc.* **135**, 14496–14499 (2013).
3. Lin, H. Y., Haegele, J. A., Disare, M. T., Lin, Q. & Aye, Y. A generalizable platform for interrogating target- and signal-specific consequences of electrophilic modifications in redox-dependent cell signaling. *J. Am. Chem. Soc.* **137**, 6232–6244 (2015).
4. Nguyen, T., Nioi, P. & Pickett, C. B. The Nrf2-antioxidant response element signaling pathway and its activation by oxidative stress. *J. Biol. Chem.* **284**, 13291–13295 (2009).
5. Hur, W. & Gray, N. S. Small molecule modulators of antioxidant response pathway. *Curr. Opin. Chem. Biol.* **15**, 162–173 (2011).
6. Bryan, H. K., Olayanju, A., Goldring, C. E. & Park, B. K. The Nrf2 cell defence pathway: Keap1-dependent and -independent mechanisms of regulation. *Biochem. Pharmacol.* **85**, 705–717 (2013).
7. Hayes, J. D. & Dinkova-Kostova, A. T. The Nrf2 regulatory network provides an interface between redox and intermediary metabolism. *Trends Biochem. Sci.* **39**, 199–218 (2014).
8. Choe, K. P., Przybysz, A. J. & Strange, K. The WD40 Repeat Protein WDR-23 Functions with the CUL4/DDB1 Ubiquitin Ligase To Regulate Nuclear Abundance and Activity of SKN-1 in Caenorhabditis elegans. *Mol. Cell. Biol.* **29**, 2704–2715 (2009).
9. Stinchcomb, D. T., Shaw, J. E., Carr, S. H. & Hirsh, D. Extrachromosomal DNA Transformation of Caenorhabditis elegans. *Mol. Cell. Biol.* **5**, 3484–3496 (1985).
10. Fire, A. Integrative transformation of Caenorhabditis elegans . *EMBO J.* **5**, 2673–2680 (1986).
11. Mello, C. & Fire, A. DNA Transformation. *Methods Cell Biol.* **48**, 451–482 (1995).
12. Meyers, S. G. & Corsi, A. K. C. elegans twist gene expression in differentiated cell types is controlled by autoregulation through intron elements. *Dev. Biol.* **346**, 224–236 (2010).
13. Stringham, E. G., Dixon, D. K., Jones, D. & Candido, E. P. M. Temporal and

spatial expression patterns of the small heat shock (hsp16) genes in transgenic Caenorhabditis elegans. *Mol. Biol. Cell* **3**, 221–233 (1992).

14. Shim, J., Im, S. H. & Lee, J. Tissue-specific expression, heat inducibility, and biological roles of two hsp16 genes in Caenorhabditis elegans. *FEBS Lett.* **537**, 139–145 (2003).

15. Hamelin, M., Scott, I. M., Way, J. C. & Culotti, J. G. The mec-7 β-tubulin gene of Caenorhabditis elegans is expressed primarily in the touch receptor neurons. *EMBO J.* **11**, 2885–2893 (1992).

16. Chacinska, A., Koehler, C. M., Milenkovic, D., Lithgow, T. & Pfanner, N. Importing Mitochondrial Proteins: Machineries and Mechanisms. *Cell* **138**, 628–644 (2009).

17. Harfe, B. D. *et al.* Analysis of a Caenorhabditis elegans twist homolog identifies conserved and divergent aspects of mesodermal patterning. *Genes Dev.* **12**, 2623–2635 (1998).

18. Zhao, Y., Long, M. J. C., Wang, Y., Zhang, S. & Aye, Y. Ube2V2 Is a Rosetta Stone Bridging Redox and Ubiquitin Codes, Coordinating DNA Damage Responses. *ACS Cent. Sci.* **4**, 246–259 (2018).

CHAPTER 3

EVALUATION OF HYDROXYNONENAL SENSING IN SAHH REVEALS A POTENTIAL STRESS-RESPONSE MEDIATED ROLE IN AGING

3.1 Introduction

3.1.1. Identification of S-adenosylhomocysteine hydrolase as a potential RES sensor in C. elegans

Thus far we have successfully integrated *C. elegans* as a critical whole-organism component of the REX technology platform, demonstrating a capability to interrogate the labeling behavior of a specific target protein via T-REX. However, to complete the pipeline from discovery to application within the platform, we must reliably demonstrate the biological relevance of uncovered redox-labeling behavior from first-responder proteins that have been identified via proteomic profiling in *C. elegans* ("C-REX"). Appreciable effects on well-characterized biological markers or phenotypic traits as a result of RES-driven modification would strongly implicate the presence of key secondary functions among these first-responder proteins.

Of the first-responder candidates to arise from our C-REX protocol (**Table 3-1**), we elected to focus our attention on S-adenosylhomocysteine hydrolase (SAHH; **Figure 3.1**). Previous quantitative profiling data obtained from pilot GREX work in HEK293T cells identified the human ortholog (hSAHH) among several native proteins responsive to HNE labeling under GREX-mediated conditions. Recurrence of this target in the form of its *C. elegans* ortholog (CeSahh) – coupled with a significant degree of sequence conservation between the two orthologs – highlighted a potential

Table 3-1. Enrichment ratios derived from *C. elegans* proteomics analysis. *Performed by Dr. Marcus Long, Dr. Souradyuti Ghosh, and Dr. Joseph Haegele.*

From Tg worms, *tom70::mcherry::halo* (proteins enriched with > 2 unique peptides)- Replicate 1	**Enrichment Ratio**
Probable arginine kinase F46H5.3	333
Alpha-3 tubulin	333
60S acidic ribosomal protein P0	38.4
Phosphate carrier protein, mitochondrial	10.3
Elongation factor 1-alpha	9.3
Malate dehydrogenase	6.4
Aldehyde dehydrogenase	5.6
40S ribosomal protein S3	4.3
Ribosomal Protein, Large subunit	4.1
ATP synthase subunit beta, mitochondrial	3.8
Elongation factor 2	3.7
S-adenosyl-L-homocysteine hydrolase (CeSahh) (6 unique peptides; 17% coverage)	3.5
Adenine Nucleotide Translocator	3.0
From Tg worms, *tom70::mcherry::halo* (proteins enriched with > 2 unique peptides)- Replicate 2	**Enrichment Ratio**
Uncharacterized protein CELE_C54C6.2	500
Tubulin alpha-2 chain	500
Elongation factor 2	500
Probable arginine kinase F46H5.3	333
Aconitate hydratase, mitochondrial	143
Elongation factor 1-alpha	5.9
S-adenosyl-L-homocysteine hydrolase (CeSahh) (12 unique peptides; 40% coverage)	7.9
Protein Up-regulated in Daf-2(gf)	1.4
From Tg worms, *gfp::halo* (proteins enriched with > 2 unique peptides)	**Enrichment Ratio**
Actin-4	17.6
Vitellogenin structural genes (yolk protein genes)	3.0
S-adenosyl-L-homocysteine hydrolase (CeSahh) (4 unique peptides; 11% coverage)	3.0

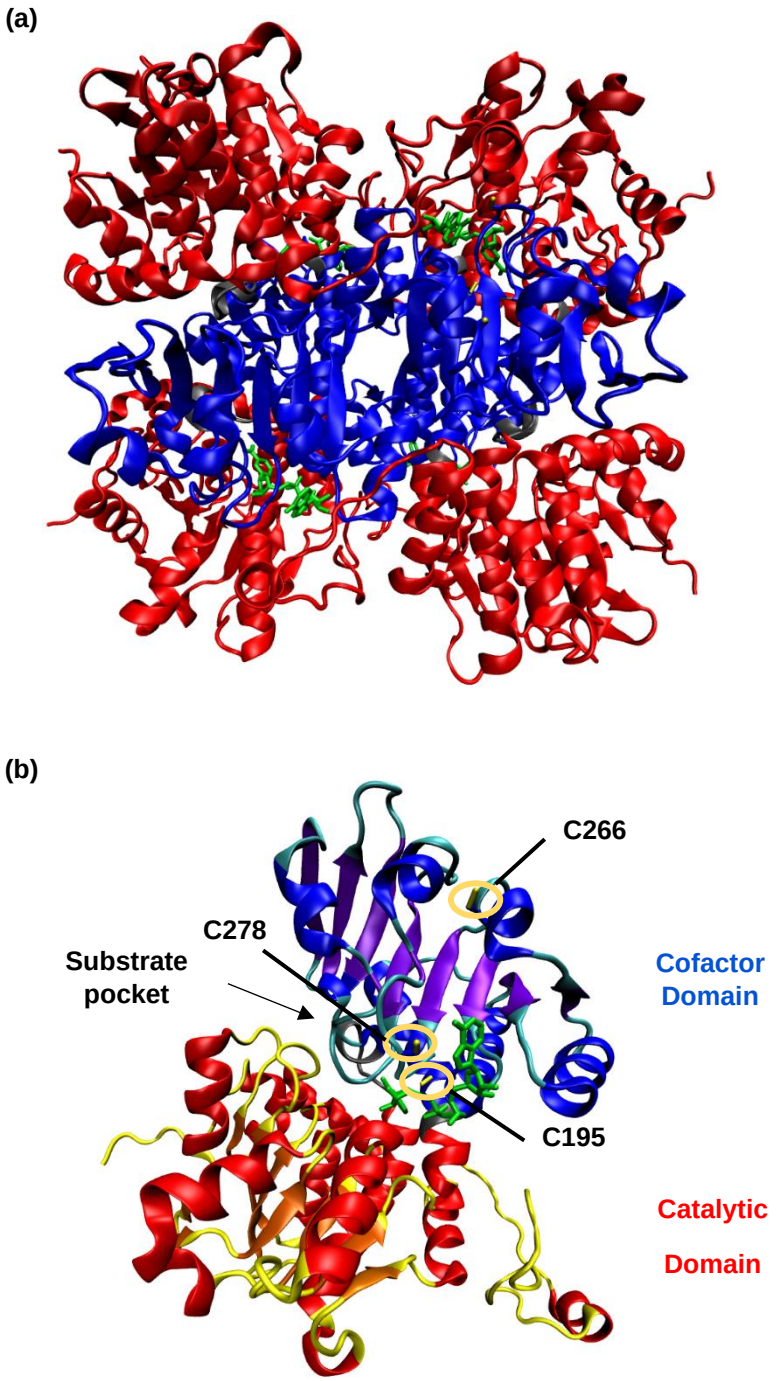

Figure 3-1. Structure of S-adenosylhomocysteine hydrolase human ortholog (hSAHH). **(a)** Full quaternary structure of hSAHH (PDB: 3NJ4). Catalytic domains are highlighted in red, cofactor domains in blue, NAD^+ cofactor in green, and linker regions in gray. **(b)** Structure of a single hSAHH chain. Catalytic and cofactor domains are shown with secondary structure features highlighted (alpha helices in blue/red, beta sheets in violet/orange, non-structured regions in cyan/yellow).

conserved "bridge" between the two species that carries significant implications for the relevance of results obtained from GREX profiling in *C. elegans* to human biology.

3.1.2 Putative importance of RES sensing in regulating the primary biological functions of SAHH

hSAHH is primarily characterized for its role as a metabolic enzyme critical to methionine cycle regulation (**Figure 3.2**) [1]. hSAHH functions in this capacity by directly controlling the concentration of S-adenosylhomocysteine (SAH), which itself negatively regulates a host of SAM-dependent methyltransferases.[2] SAHH has previously been studied in the greater context of methylation-based metabolic signaling,[3] and SAHH activity and associated regulation has itself been directly implicated in a range of disease-relevant biological outcomes, including cancer occurrence.[4,5] As a result, the presence of hSAHH among profiled RES-sensing candidates implies a potential translational link between RES flux and any key processes reliant on methyl transfer, such as epigenetic regulation in higher eukaryotes.[6]

The exact function and structure CeSahh, meanwhile, is less well understood. Though CeSahh has been established as an essential enzyme – as CeSahh-deficient gene knockouts are larval-lethal in *C. elegans* [7] – the implications of *C. elegans* methyltransferase activity potentially linked to SAH regulation have only recently become clearer.[8] However, at the same time, methionine metabolism has become more closely linked to certain shared phenotypes across multiple divergent species – particularly with regards

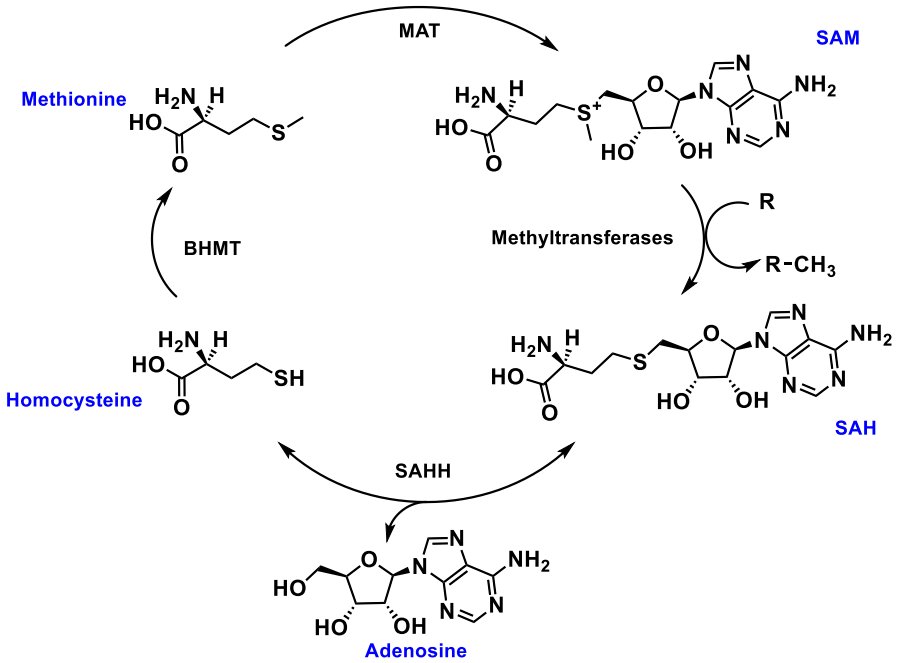

Figure 3-2. Role of hSAHH in methyltransferase regulation. SAHH facilitates the hydrolysis of SAH, itself a methyltransferase inhibitor. Homocysteine is then further metabolized by Betaine-homocysteine S-methyltransferase (BHMT) and S-adenosylmethionine synthetase (MAT) to regenerate SAM.

to lifespan and aging regulation – and associated orthologs of SAHH have been implicated in such common traits, at least in part.[9–11] Furthermore, while no published crystal structure exists for CeSahh, sequence conservation with hSAHH remains high.

As such, our objectives pertaining to the hSAHH/CeSahh orthologs are threefold. We must first identify the sensor residues of the two orthologs themselves, and determine the presence, if any, of a connective link between the two. Following, we look to determine a reproducible impact on the primary function of hSAHH/CeSahh – that of SAH metabolism – as a function of sensor labeling via TREX. Finally, we then demonstrate the downstream phenotypic impact of *in vivo* RES

labeling of SAHH, primarily through a return to the whole-organism *C. elegans* model. In doing so, through uncovering relevant biological consequences of RES-driven SAHH modification, we aim to establish a blueprint for a complete end-to-end path from sensor identification to characterization.

3.2 Results and Discussion

3.2.1 CeSahh emerges as a potential redox sensor in C. elegans

Our discovery of and interest in CeSahh for further study stemmed from results of quantitative profiling of HNE-labelled proteins in two separate strains of *C. elegans*. Each strain carried extrachromosomal arrays (*gfp::halo* or *tom70::mcherry:halo;* see Chapter 2) for the purposes of ubiquitous Halotag transgene expression, allowing for the combination of concepts from our REX technology platform and existing methods for *C. elegans* SILAC-based proteomics analysis (C-REX). Results from these analyses (**Table 3-1**) implicate CeSahh as a repeat HNE target upon selective, endogenous-like exposure to HNE alkyne. Furthering our interest was the discovery of hSAHH as an HNE-labelled hit in similar proteomic analyses conducted in HEK293T cells lines (conducted and analyzed by Dr. Yi Zhao; data not shown). Repeated occurrences of labelled CeSahh across two unique transgenic lines, coupled with an occurrence in a human cell line, prompted us to zero in on this enzyme as a candidate RES sensor.

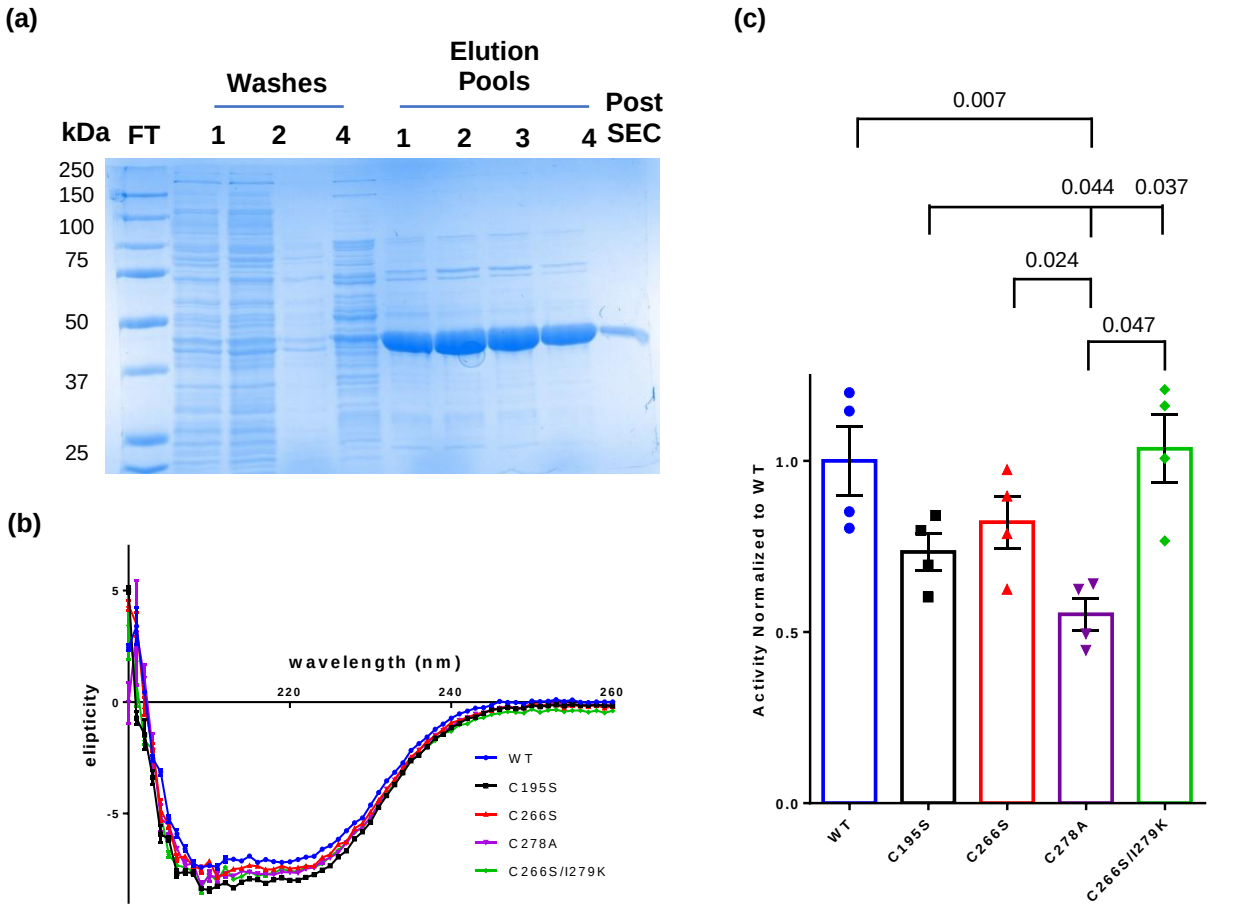

Figure 3-3. Protein-level validation of hSAHH and hSAHH candidate loss-of-sensing mutants. **(a)** Coomassie stain gel of representative Ni-NTA purification of WT hSAHH succeeding recombinant expression in BL21 DE3 *E. coli,* followed by SEC purification. Flowthrough (FT), washes, and elution pools were collected as per the general purification protocol (3.2.6.1). **(b)** Circular dichroism analysis of relevant hSAHH sensing-deficient and sensing-recovery mutants, as compared to WT hSAHH. A wavelength range of 200-280 nm was established, with an averaging time of 5 s, at 25°C. **(c)** Basal SAH hydrolysis activity of relevant hSAHH sensing-deficient and sensing-recovery mutants, normalized to WT hSAHH. Error bars show SEM (n = 4). *Performed with Sanjna Surya and Dr. Marcus Long*

3.2.2 Identification of first-responder cysteine redox sensors of human SAHH

Though our interest in SAHH was largely borne from quantitative profiling in *C. elegans,* we opted to begin our study of candidate cysteine sensor residues in the more

well-characterized human ortholog. Prior preliminary LC/MS-MS data analysis of HNEylated hSAHH post T-REX in HEK293T cells suggested several potential cysteine candidates, albeit at low-confidence due to unavoidable inherent limitations . Among these candidates, C195 and C266 were selected for further evaluation. Both belong to a group of 10 surface-accessible cysteine residues conserved among higher eukaryotes; further, C195 is one of 3 such cysteine residues to demonstrate a potential for RES modification.[12] As such, we generated putative RES-sensing deficient hSAHH mutants – C195S and C266S – to evaluate alongside the WT enzyme (see Appendix B for gene sequences). Said mutants were checked prior to use via circular dichroism analysis of the recombinantly expressed proteins, as well as a basal evaluation of their hydrolase activity (**Figure 3-3**). In doing so, we observed no significant changes to the secondary structure or folding behavior between WT hSAHH and the candidate loss-of-sensing mutants. In general, basal hydrolase activity (see **Figure 3-13**) was sufficiently comparable across all tested mutants, though some variation was present.

To determine a differential HNE sensing capability of each mutant, we performed T-REX using Halo-hSAHH and evaluated the resultant protein labeling by alkynylated HNE via streptavidin-biotin enrichment and pulldown. We first confirmed the sensing capability of the WT enzyme, demonstrating an approximate 2.5-fold increase in hSAHH enrichment post T-REX (**Figure 3-4**) when normalized to enrichment signal from untreated hSAHH. In doing so, we also determined an

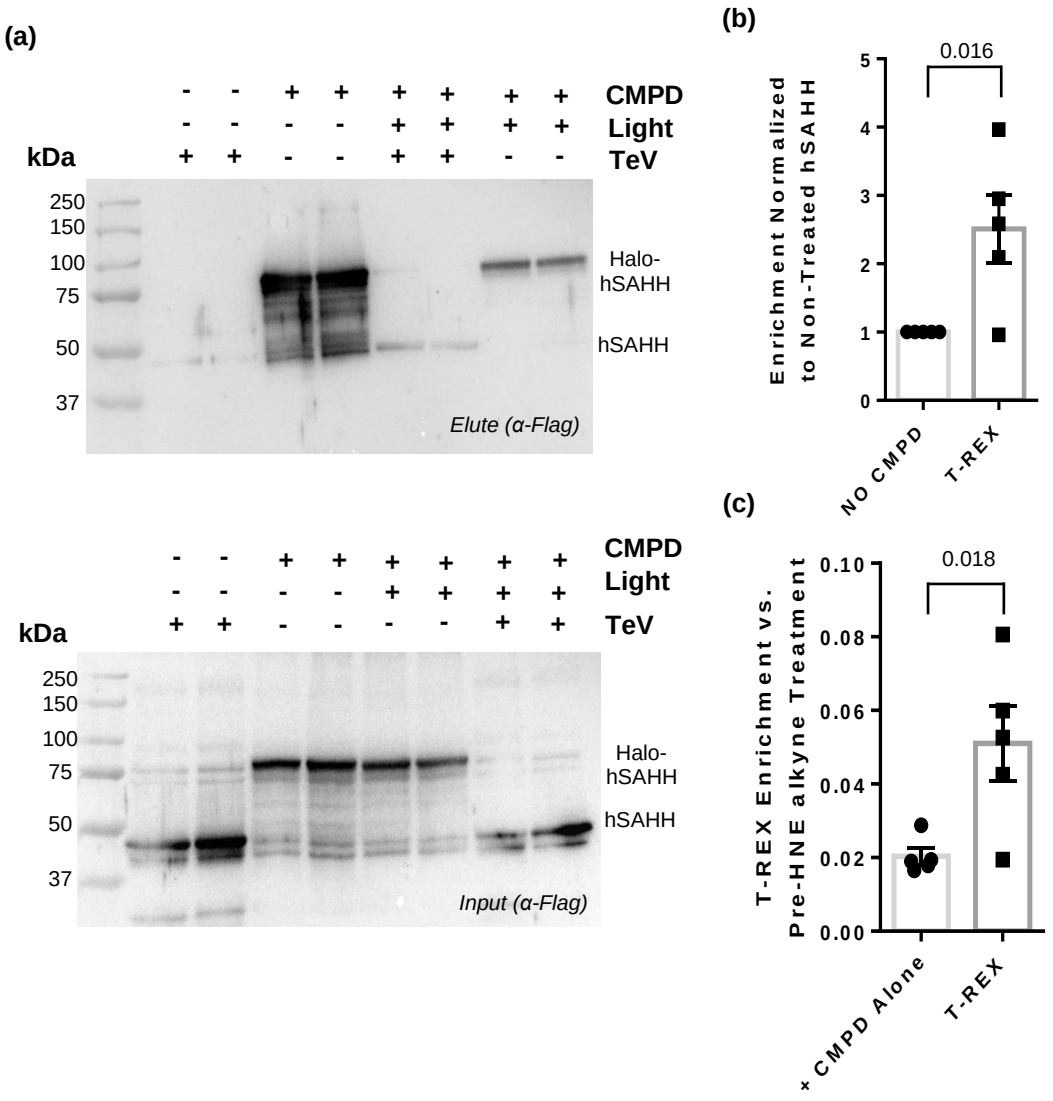

Figure 3-4. T-REX labeling of WT hSAHH in HEK293T. **(a)** Representative Western blot output of biotin-streptavidin enrichment of WT hSAHH following T-REX labelling (3.2.3). CMPD refers to the treatment RES compound (Ht-PreHNE alkyne). **(b)** Fold-enrichment of WT hSAHH following T-REX normalized to untreated hSAHH background. Error bars show SEM (n = 5) **(c)** Quantitation of HNE occupancy of WT hSAHH by comparison to signal from compound-alone hSAHH. Error bars show SEM (n = 5).

approximate labeling occupancy range of about 3-4% by comparison to pre-photouncaging samples; a low occupancy such as this is not unexpected of a REX-

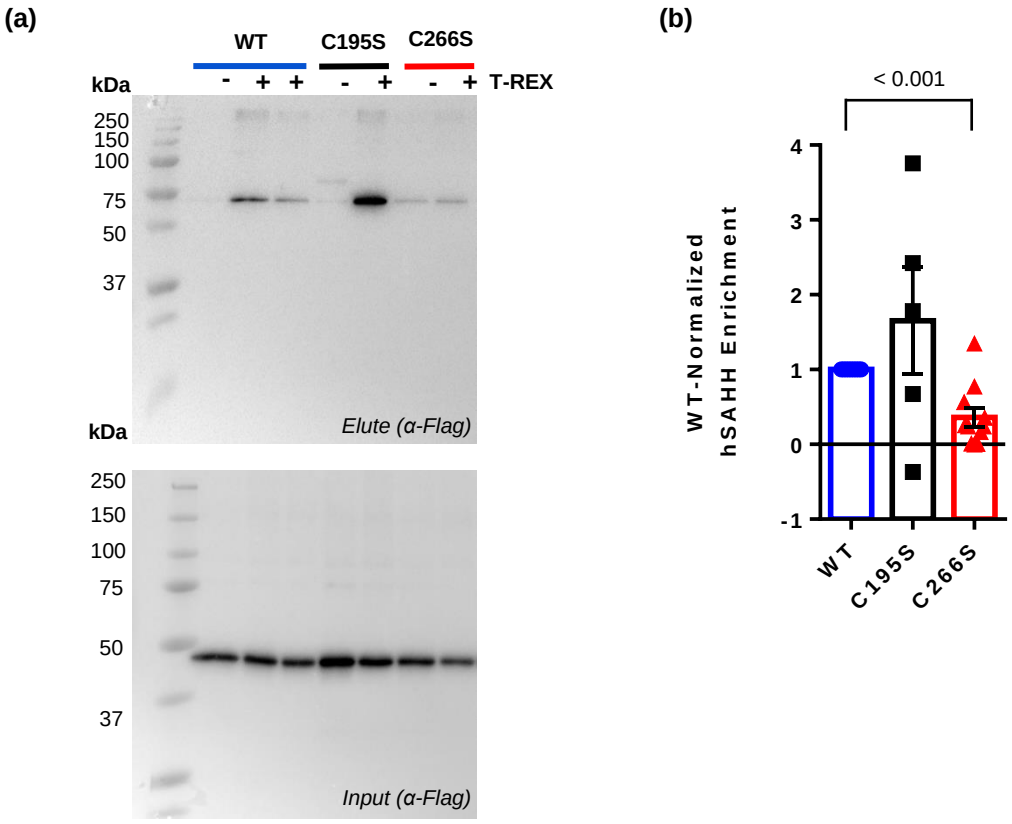

Figure 3-5. Differential T-REX labeling of hSAHH candidate loss-of-sensing mutants. **(a)** Representative Western blot output of biotin-streptavidin enrichment of relevant hSAHH sensing-deficient mutant candidates. All mutants were treated with Ht-PreHNE alkyne, with T-REX controlled by light exposure. **(b)** Quantitation of T-REX-driven enrichment of hSAHH WT and loss-of-sensing mutant candidates. Error bars show SEM ($n \geq 5$).

derived RES sensing candidate, nor does it preclude the enzyme from a significant change in downstream function.[13] Afterwards, we extended T-REX to the candidate loss-of-sensing mutants (**Figure 3-5**). Here, we observed that the C195S mutant did not lead to a significant loss of HNE sensing. However, HNE-derived enrichment of the C266S mutant was diminished by approximately 60% compared to WT after input normalization.

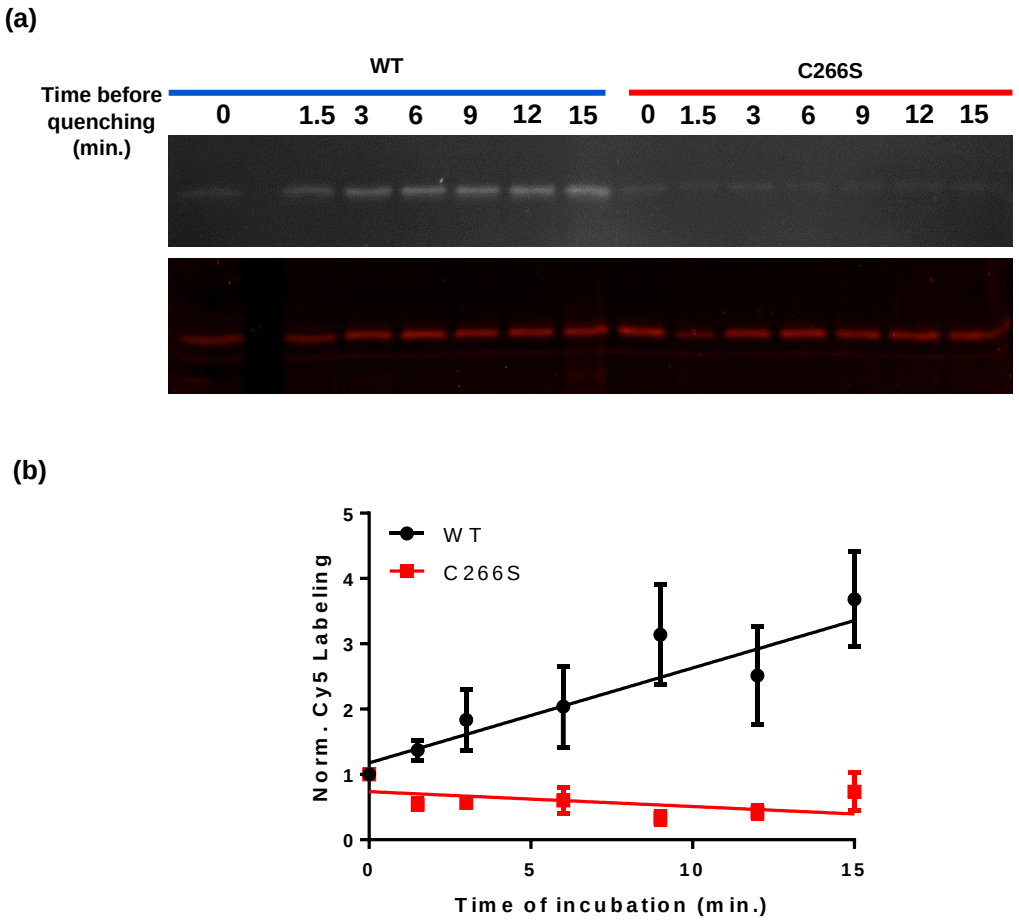

Figure 3-6. HNE-driven labeling of hSAHH i*n vitro*. **(a)** Cy5 visualization (top) of HNE-labelled recombinant hSAHH (WT and C266S) after exposure to HNE alkyne for variable lengths of time. Sypro Ruby staining (bottom) was used for normalization of [protein]. **(b)** Quantitation of HNE labeling of hSAHH, normalized to each respective zero time point. Error bars show SEM (n ≥ 5 per time point). *Performed with Sanjna Surya and Dr. Marcus Long*

We then further explored the sensing capability of C266 by time-variable exposure to bolus HNE-alkyne treatment (**Figure 3-6**). Recombinant WT and C266S hSAHH were treated with excess HNE-alkyne, with samples withdrawn and quenched at pre-determined time points. HNE binding was then evaluated by in-gel Cy5 fluorescent visualization at each time-point, normalized to total protein signal from

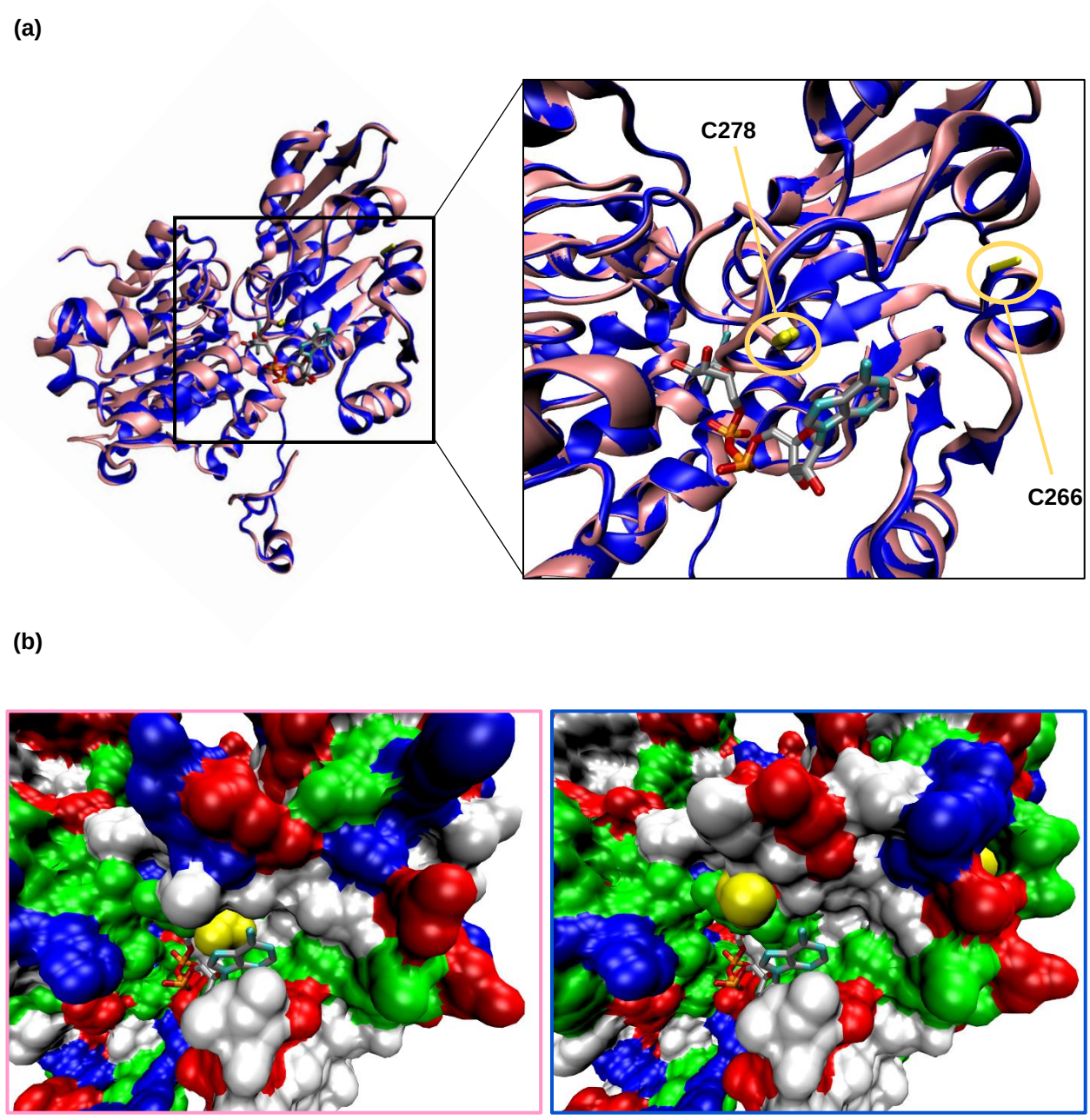

Figure 3-7. Comparative overlay of putative SAHH "redox-binding pocket." **(a)** Overlay of a single chain of hSAHH (PDB: 3NJ4; blue) and CeSahh (modelled using SWISS-MODEL homology suite via hSAHH template; pink). Positions of C266 and C278 relative to the NAD^+ cofactor are highlighted (inset). **(b)** Molecular surface render of CeSahh (left) and hSAHH (right) redox-binding region. Surface is colored by residue type (acidic resides are red, basic blue, polar green, and nonpolar white). C278 and C266 are highlighted in yellow.

follow-up Sypro Ruby treatment. At all time-points, HNE labeling of the C266S mutant was virtually undetectable compared to the WT counterpart. Such significant loss of HNE labeling without further compromise of structure nor basal function suggested that C266 was the primary RES sensor of hSAHH.

3.2.3 Conservation of structure – not primary sequence – of the SAHH RES-binding region

To date, no crystal structure has been identified for the CeSahh ortholog. Thus, we turned to structural homology modelling via the SWISS-MODEL server and repository system to determine the presence of a C266 equivalent in CeSahh.[14–19] Using the hSAHH crystal structure as a template (PDB 3NJ4[20]), we generated a model structure of a CeSahh subunit chain and overlaid the two structures in VMD visualization software (**Figure 3-7a**). From this overlay, no analogous residue for the human C266 was seen in the CeSahh structure. Our attention was instead drawn to the nearby surface-accessible cysteine residue C278, which itself was spatially conserved in CeSahh (C280 in the CeSahh primary sequence; both residues will be referred to as C278 for clarity). This C278 residue was positioned approximately 15-16 Å from C266 within the crystal structure – far closer to the NAD^+ cofactor – though its presence on a loop region could suggest a closer distance.

Taken together, the cysteine residues frame a region that could function as a RES binding pocket accessible to such species as HNE. We then speculated that C278 in

CeSahh may facilitate RES binding in this region in a manner analogous to C266 in hSAHH. As a prior exploratory measure, we generated the C278A loss-of-sensing hSAHH mutant (**Figure 3-3**), noting that, while still structurally unmodified and functional, the recombinant protein featured a notable lower basal activity than WT hSAHH. Interestingly, the human C278A mutant did not produce a significant loss of RES labelling compared to WT (see Figure 3-12); however, this further increased our curiosity about the behavior of C278 in the *C. elegans* ortholog. We performed T-REX using Halotag variants of WT and C278A loss-of-sensing CeSahh mutants (**Figure 3-8**); in doing so, we determined an approximate 60% reduction of HNE sensing. Thus, this leads to an interesting proposition: C278, while retained in both *C. elegans* and human orthologs, is the primary RES sensor only for the former, while remaining as a "deactivated" atavistic residue in the latter.

3.2.4 Phylogeny analysis reveals shift in sensing that parallels evolutionary history

The idea of a binding region within a protein undergoing optimization-driven changes across orthologs – particularly over the course of evolution – is not without precedent. This concept has been largely explored in the context of active or catalytic site binding, where structural conservation across orthologs had been maintained independently from primary sequence conservation. For example, shifts in the primary sequence location of the active-site lysine in rhodopsin did not compromise retinal

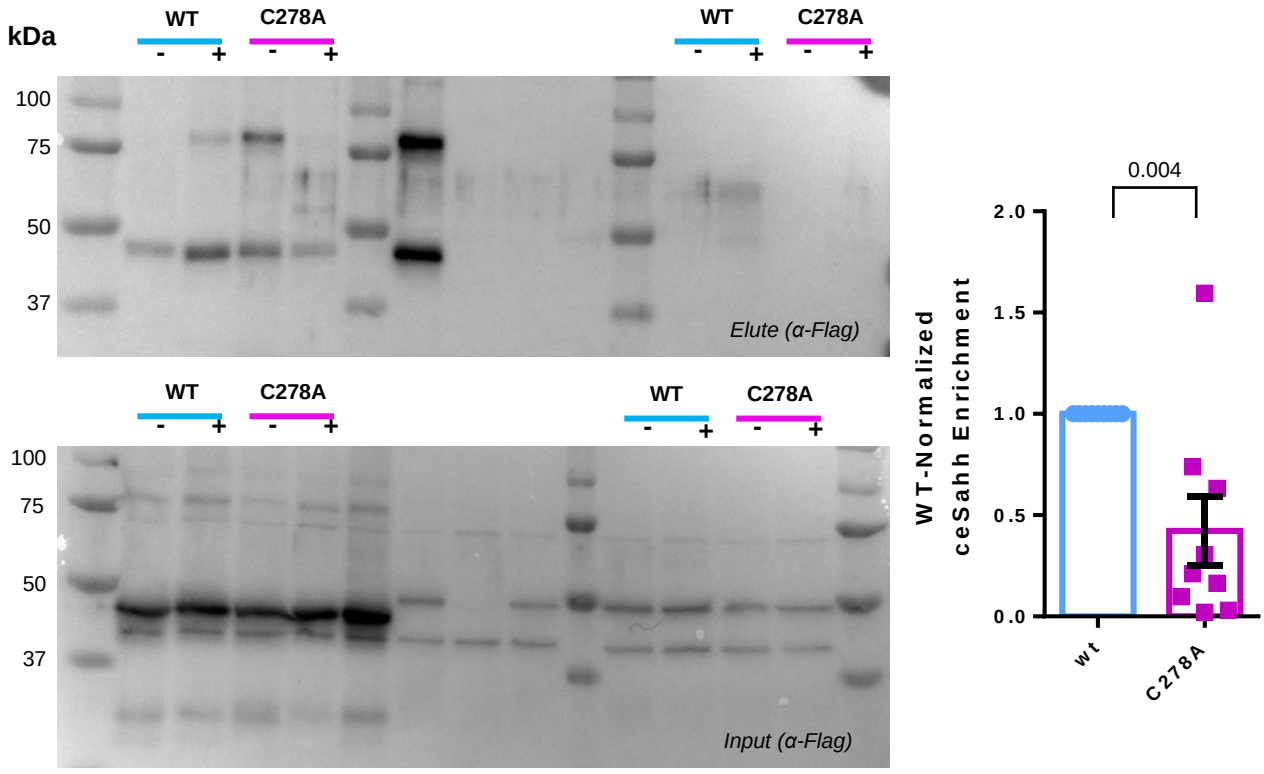

Figure 3-8. Differential T-REX labeling of CeSahh WT and C278A. **(a)** Representative Western blot output of biotin-streptavidin enrichment of WT and C278A CeSahh following T-REX labeling (3.2.3). Central unmarked lanes were discarded due to a discrepancy in associated input lanes. **(b)** Quantitation of T-REX labeling of C278A ceSahh by normalization to WT CeSahh enrichment (n = 9).

binding, [21] and active-site carboxylate residues have demonstrated significant plasticity with regards to primary sequence location across multiple different enzyme classes.[21,22] In many cases, evolutionary optimization of these sites is suggested by way of the presence of a discernable intermediate featuring several or all key residues, as the binding pocket undergoes a shift from one "primary" residue to another. The existence of a RES sensor site with multiple candidate nucleophilic residues is itself not unusual – the highly conserved Keap1 has multiple conserved cysteine sensors[23,24] – and as such,

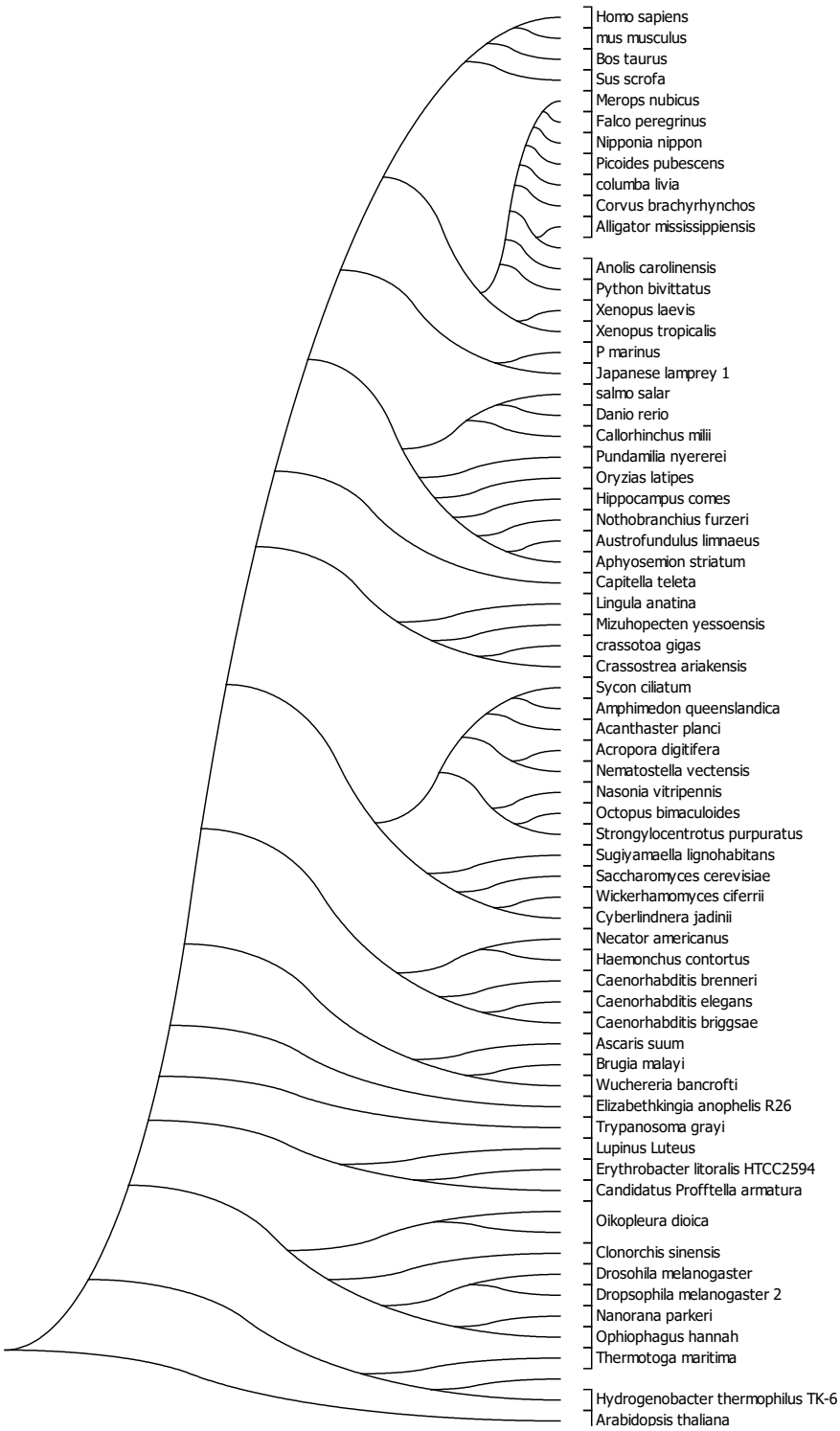

Figure 3-9. Molecular phylogeny analysis of a selection of representative species across the taxonomic ranking of *Homo sapiens*. Analysis was conducted within the Molecular Evolutionary Genetics Analysis (MEGA 7) software suite. *Performed with Dr. Marcus Long.*

the "hopping" of an active residue from one location to another within the binding region could point towards a similar evolutionary fine-tuning.

To explore this idea, we conducted a phylogenetic analysis focused on the evolutionary history of these 2 cysteine residues (**Figures 3-9 and 3-10**). For this analysis, 68 species were selected representing relevant taxa across the timeline of human evolution, and a phylogenetic tree was constructed via the maximum likelihood method using MEGA 7 software, illustrating the evolutionary history of the enzyme between higher eukaryotes and nematodes (**Figure 3-10**).[25–27] Additionally, we selected representative species spanning the transition from *C. elegans* to human SAHH and performed a sequence alignment using MUSCLE, focusing on C195, C266, and C278, as well as associated flanking residues (**Figure 3-10a**).[28] From this comparative analysis, we noticed that C195 – a previous RES sensor candidate – was not only missing from *C. elegans,* but also featured very little change in flanking primary sequence, a pattern that held when extended to the remaining species (**Figure 3-10b**). More importantly, the hypothetical conserved RES-sensing region showcased far more variability in primary sequence (**Figure 3-10c**) while appearing to transition through an "intermediate" state present in jawless fish (arctic lamprey, in this example). In this intermediate state, C266 appears in the region, and C278's immediate environment – featuring a positively charged 279 residue as far back as yeast orthologs – is maintained. Groups of species further along the human evolutionary timeline – including

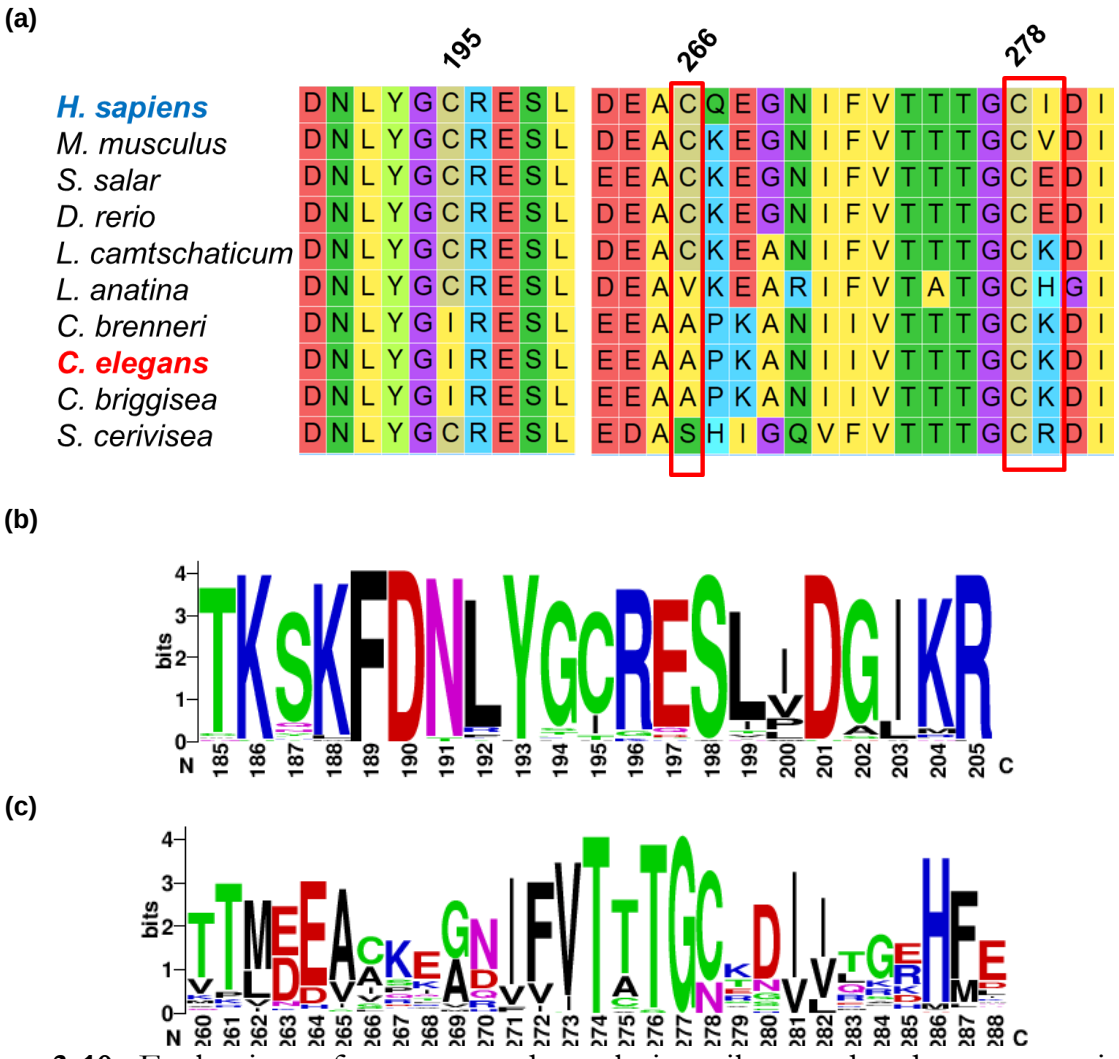

Figure 3-10. Evaluation of a conserved, evolutionarily tuned redox sensor site in hSAHH/CeSahh. **(a)** Multiple Sequence Comparison by Log-Expectation (MUSCLE) alignment of candidate cystine residues across SAHH orthologs of representative species along the evolutionary history between *C. elegans* and *H. sapiens*. **(b)** Sequence logo of C195 and surrounding residues constructed from 350 SAHH orthologs. **(c)** Sequence logo of C266 and C278 and surrounding residues constructed from 350 SAHH orthologs, generated using UC Berkeley's WebLogo tool. *Performed with Dr. Marcus Long*

teleost/ray-finned fish (such as zebrafish and Atlantic salmon) and higher eukaryotes – notably discard this positive 279 residue, with the latter adopting hydrophobic residues in its place.

The appearance of C266 coinciding with this meaningful change, as well as the presence of a transitional "intermediate" ortholog, suggests a change in the behavior of the otherwise-conserved RES sensing region from *C. elegans* to humans. Though C278 is retained in hSAHH, we demonstrated that it does not facilitate RES sensing to the same degree as in CeSahh. The changes to its microenvironment – primarily via the shift to a nonpolar residue at 279 – lead to a "deactivation" of C278, rendering it an "atavistic" sensor cysteine. Such atavistic residues are not uncommon in conserved regions that see this sort of residue hopping. [29] Instead, C266 is adopted as the primary sensor in the orthologs of humans and closely related eukaryotes.

3.2.5 Restoration of a "CeSahh-like" RES binding pocket in C266S sensing-deficient hSAHH

Given the modelled conservation of the RES binding region, as well as the evolutionary history of the cysteines of interest and surrounding residues, we posit that such a shift from C278 to C266 as the primary sensor should be demonstrably reversible. This should be accomplishable through basic point mutagenesis to restore the changes to the C278 microenvironment that correlate with its relegation to atavism – namely, the loss of K279. that end, we developed a CeSahh-like "rescue of sensing" hSAHH mutant (C266S, I279K). After validating the integrity of the rescue mutant (**Figure 3-3, b-c**), we utilized T-REX to determine the extent of HNE labeling that could be recovered in comparison to the loss-of-sensing C266S mutant. In doing so,

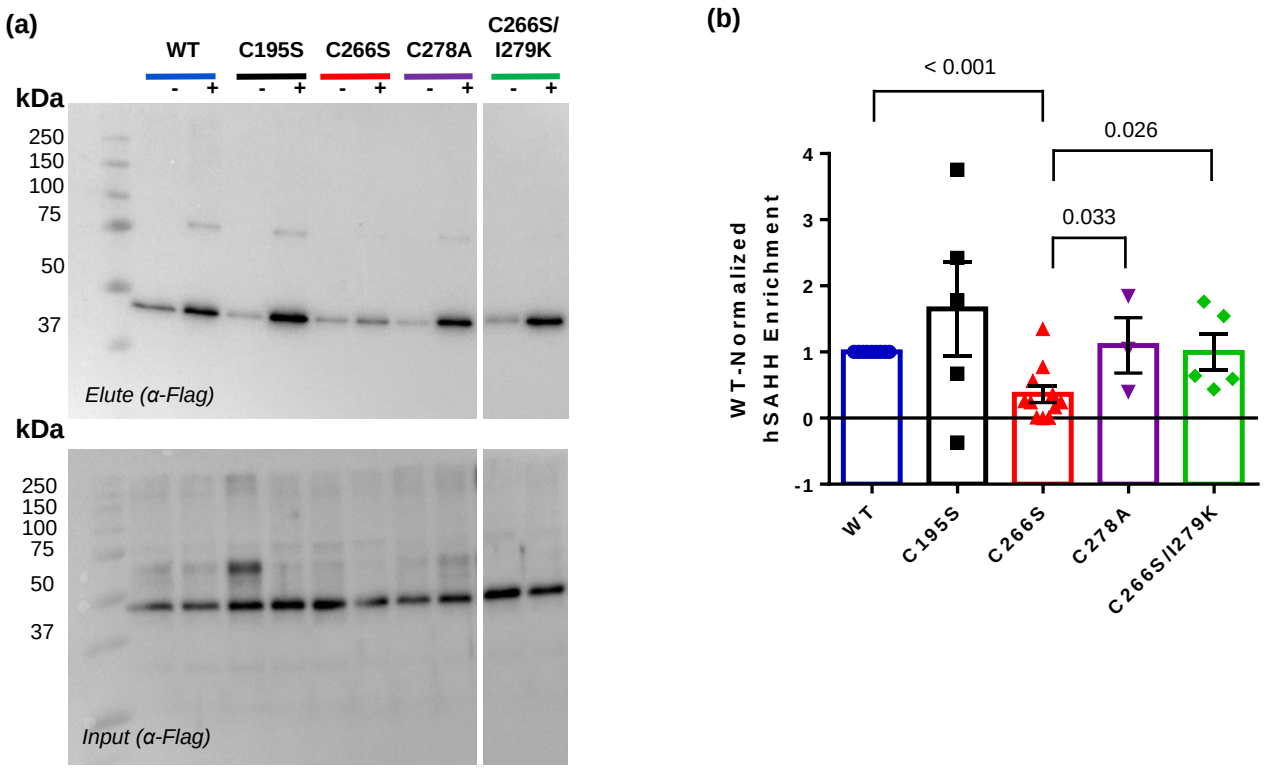

Figure 3-11. Recovery of RES labeling of the hSAHH C266S loss-of-sensing mutant via "restoration" of the CeSahh atavistic C278 sensor. **(a)** Representative Western blot output of biotin-streptavidin enrichment of relevant hSAHH sensing-deficient and sensing-recovery mutants. All mutants were treated with Ht-PreHNE alkyne, with T-REX controlled by light exposure. **(b)** Quantitation of T-REX-driven enrichment of hSAHH WT, sensing-deficient, and sensing-recovery mutants. Error bars show SEM ($n \geq 3$).

WT-like HNE-driven hSAHH enrichment was reestablished; observed HNE labeling did not significantly differ from WT, but was demonstrably elevated when compared to the original C266S loss-of-sensing mutant (**Figure 3-11**). That the restoration of the proximal charge state of the atavistic C278 led to an observable "reactivation" in the absence of a functional C266 lends weight to the proposed role of the local microenvironment as a RES-sensing enabler discussed earlier.

3.2.6 Emerging insights into the mechanism of redox-driven SAHH activity regulation

Elucidating the RES-sensing functionality of hSAHH carries significant implications in higher eukaryotes, given the established role of SAHH in facilitating methyltransferase activity and the pathologies associated with its misregulation. [1–7] Through SAHH, a RES-driven signal can be translated into a change in the balance of SAH and homocysteine, either of which carry critical implications for cell-level stress response. By determining the effect of HNE labeling on CeSahh and hSAHH activity, we aimed to discern the mechanistic consequences of SAHH sensing – and, by extension, a possible driver of RES-binding optimization. To do this, we adapted a well-established colorimetric catalytic activity assay to evaluate SAHH as a function of RES labeling, utilizing TNB absorbance at 412 nm as a readout for homocysteine production (**Figure 3-12, a-b**). [30] To prevent the reverse reaction from impeding the readout, we couple the assay with adenosine deaminase (AdoD) to deplete the adenosine side product (**Figure 3-12 c**). In instances were an inhibited control is required, we utilized 3-deazadenosine (DZA) (**Figure 3-12 d**).

Returning to the structural model of the RES binding site, we wondered if the close proximity to the NAD^+ cofactor may inform how HNE, or any RES binding partner, may tune the catalytic behavior of SAHH. We also wondered if NAD^+ could affect HNE binding or positioning within the site itself, especially in vitro without relevant biological context. NAD^+ has a nanomolar-range dissociation constant k_d with

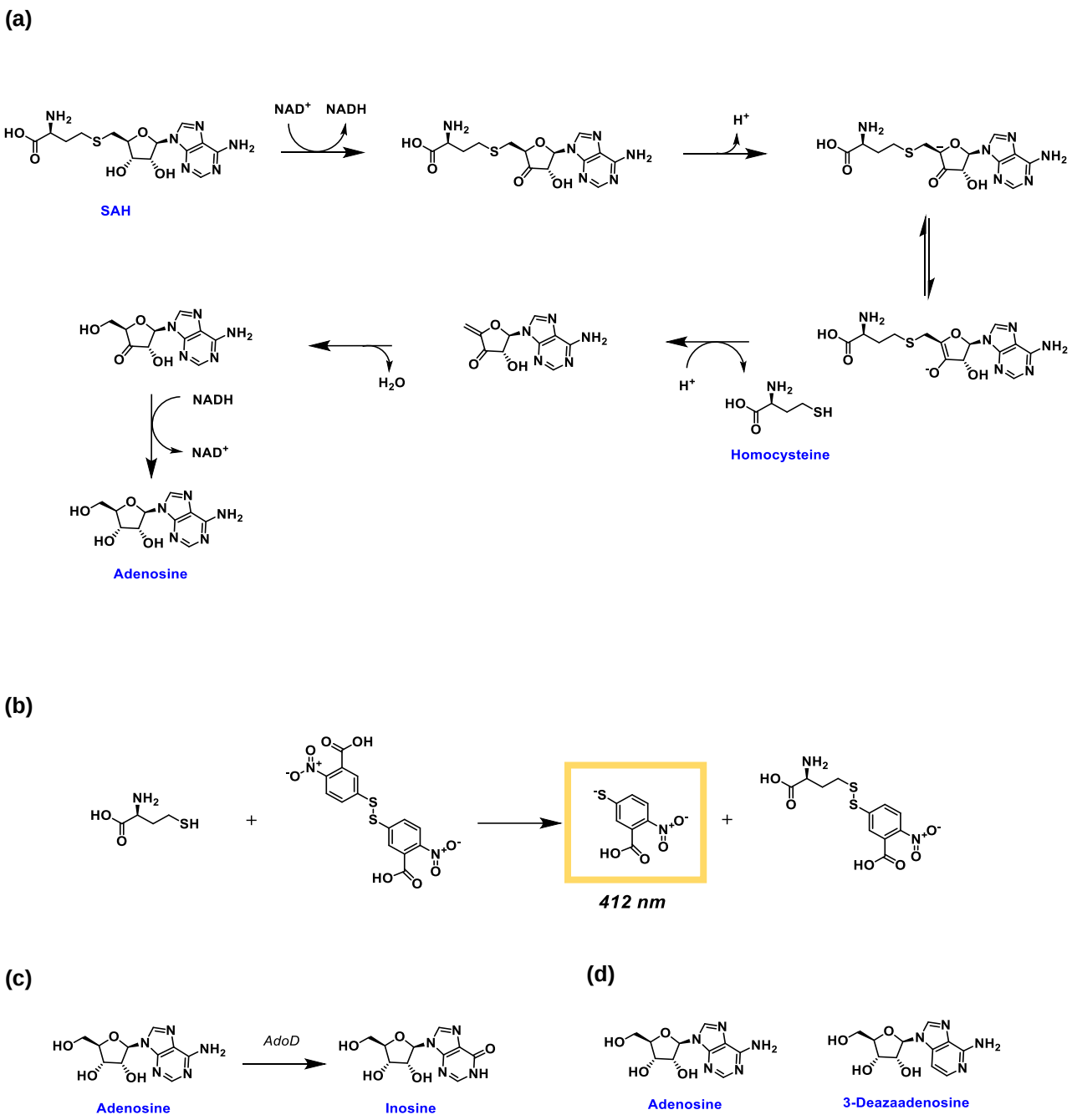

Figure 3-12 Overview of the colorimetric SAHH catalytic activity assay. **(a)** Hydrolysis of SAH to adenosine (Ado) and homocysteine. **(b)** Homocysteine reacts rapidly with DTNB (non-rate limiting) to produce TNB, which can be used as a colormetric readout at 412 nm. **(c)** SAHH is coupled with adenosine deaminase (AdoD) to limit the reverse synthesis of SAH (see Figure 3.2). **(d)** 3-deaazadenosine (DZA) is used as a potent inhibitor of SAHH to function as a background activity control.

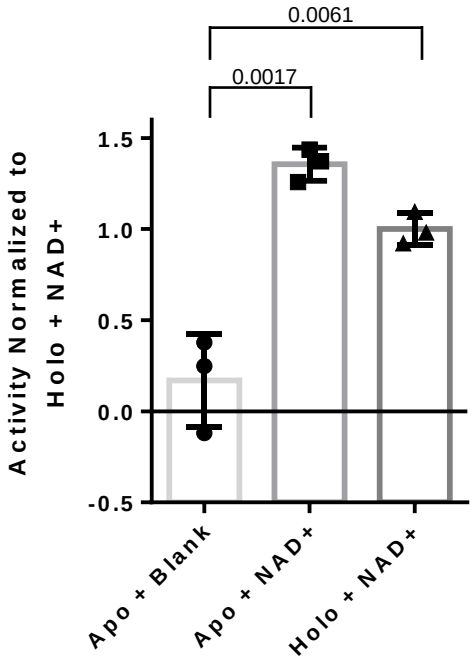

Figure 3-13. Catalytic activity validation of apo-hSAHH functionality upon restoration with excess NAD^+.

hSAHH and can survive Ni-NTA (among other metal-ion) purification, as well as extensive dialysis.[31] If the presence of a cofactor affected HNE labeling, it may affect the degree to which we can observe changes in activity against the background of a colorimetric kinetic assay; more interestingly, however, it would provide a possible clue into the mechanism by which HNE labelling interacted with SAHH activity, assuming we observed catalytic attenuation upon HNE sensing.

To pursue this avenue of thought, we generated apo-hSAHH via ammonium sulfate precipitation,[32] which we then validated via evaluation of its basal activity in comparison to the holoenzyme, as well as the apoenzyme after 30 minutes of NAD^+ treatment (**Figure 3-13**). To determine if the loss of NAD^+ affected HNE labeling, we

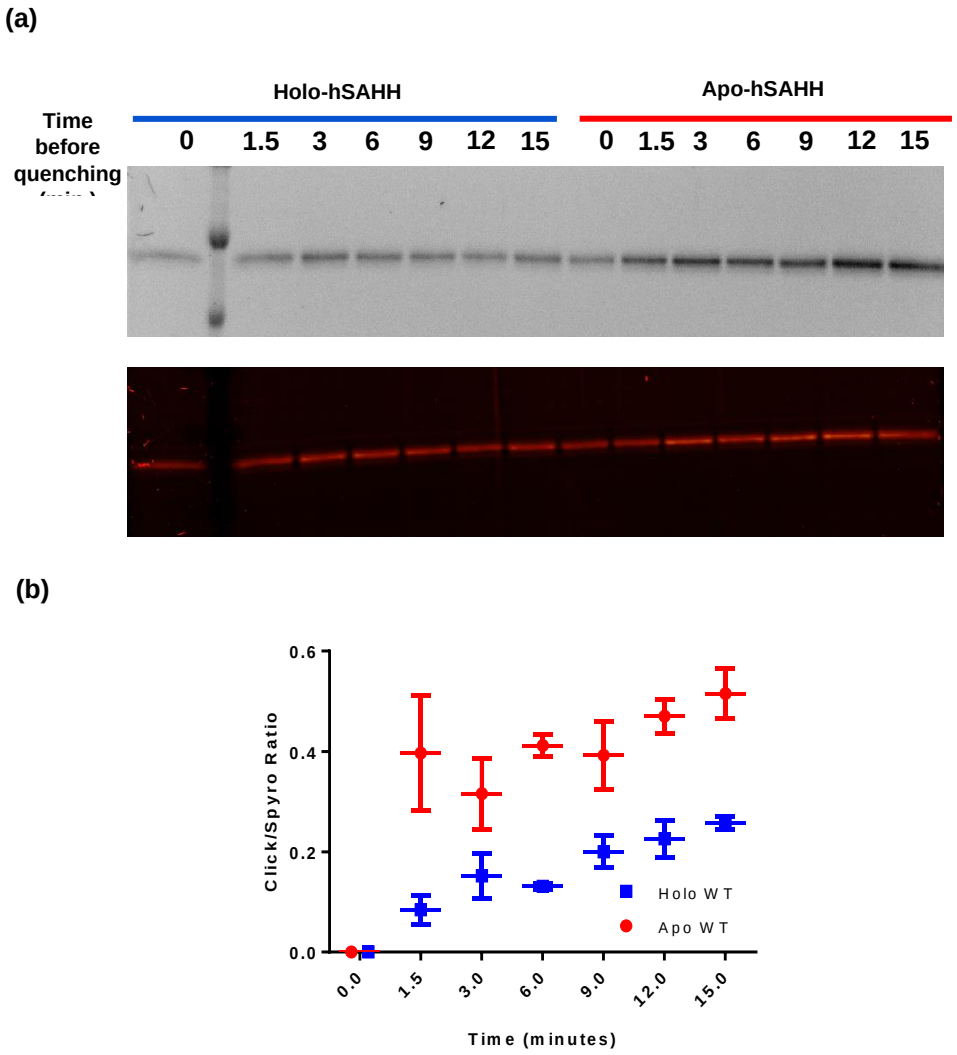

Figure 3-14. Demonstration of NAD$^+$/HNE interactivity in hSAHH via in-gel labeling. **(a)** Representative Cy5 visualization of HNE-labelled recombinant hSAHH (WT and C266S) after exposure to HNE alkyne for variable lengths of time. Sypro Ruby staining (bottom) was used for normalization of [protein]. **(b)** Quantitation of HNE labeling of holo-hSAHH and apo-hSAHH, with the zero time point zeroed in terms of signal ratio (n = 4). *Performed with Sanjna Surya and Dr. Marcus Long*

repeated the time-dependent HNE treatment assay demonstrated in Figure 3-6 to compare holo- and apo-hSAHH sensing (**Figure 3-14**). Consistent with our working hypothesis, we noticed that the apoenzyme was rapidly labeled in comparison to holo-

hSAHH. We then supposed that this might translate to an observable effect on catalytic activity if the apoenzyme were first treated with HNE before then introducing NAD^+ cofactor. Preliminary catalytic results seem to suggest that this is possible; titration of apoenzyme with HNE did appear to demonstrate an appreciable attenuation on SAHH activity that was not present when treating the holoenzyme, and NAD^+ titration of HNE-pretreated apo-hSAHH resulted in variable obtainable V_{max}. However, these results require further validation (See Appendix D).

3.2.7 Phenotypic consequences of CeSahh sensing deficiency in C. elegans

In order to fully validate our REX technology pipeline, we must be able to demonstrate biological consequences for RES labeling. In the context of SAHH and associated misregulation, lifespan and development have been consistent phenotypic targets. The consequences of methyltransferase disruption on lifespan and development in vertebrate eukaryotes has been studied for some time,[11,33] though SAHH misregulation has been more directly implicated in recent years. SAH accumulation has been linked to reduced lifespan,[9] and may be the underlying factor regarding hyperhomocysteinaemia's establishment as a risk factor leading to variable disease states.[2,3,7] Recent advances in our understanding of nematode methyltransferase regulation[8] suggest that phenotypic outcomes of CeSahh loss-of-sensing in *C. elegans,* while not directly transferable to higher eukaryotes, nonetheless can strongly implicate hSAHH sensing as equally – if not more – vital in humans.

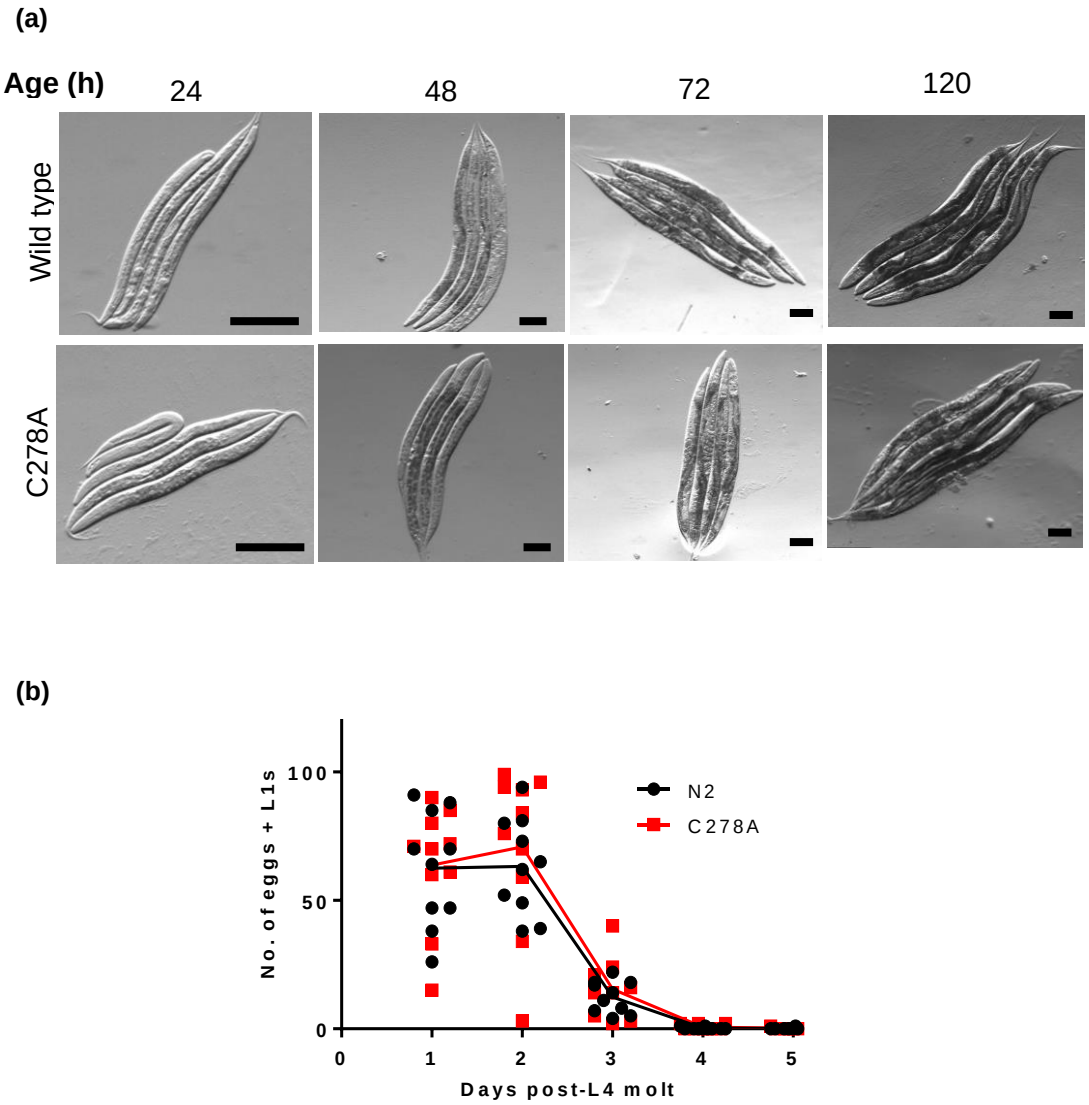

Figure 3-15. Growth and egg-laying behavior of N2 wild-type and *ahcy-1(syb7xxx) C. elegans* lines. **(a)** Representative images of sample *C. elegans* from each population at the marked time points. Black ruler represents 1 mm. **(b)** Daily egg counts from N2 and *ahcy-1(syb7xx) C. elegans* lines. Eggs were scored only upon subsequent successful production of healthy L1 progeny. *Performed with Jinmin Liu.*

Through nematode-adapted CRISPR/Cas-9 gene editing, we obtained triplicate strains of Bristol N2 background *C. elegans* featuring a C278A loss-of-sensing mutation [*ahcy-1(syb7xx)*]. We first evaluated the development of these worms in conjunction with unedited wild-type N2 *C. elegans* by way of anatomical comparison at pre-determined

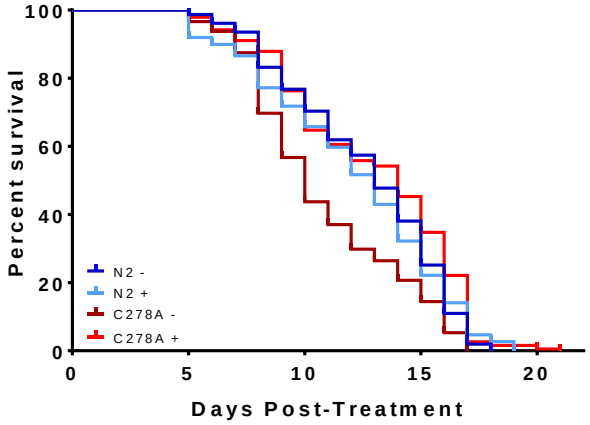

	Mantel-Cox – χ2	Mantel-Cox P value
All curves	44.55	< .0001
C278A - C278A+	38.65	<.0001
N2 – C278A -	19.45	<.0001
N2- N2+ C278A +	4.88	.0871

Figure 3-16. Impact of acute HNE treatment on maximal lifespan of N2 wild-type and *ahcy-1(syb7xx) C. elegans* lines. Survival curves for all conditions begin at the time of treatment (L4 stage). Mantel-Cox P values are listed for comparisons of select curves (right). -/+ indicate treatment with vehicle (-) or HNE (+) at L4 stage.

time points up to adulthood (**Figure 3-15a**). At no point did we observe any meaningful difference between the WT and *ahcy-1(syb7xx)* strains. A similar observance was made regarding offspring production in both strains (**Figure 3-15b**). The *ahcy-1(syb7xx)* worms did not demonstrate any discrepancy in egg-laying behavior, nor did their eggs vary in terms of viability, at least when we observed the offspring at L1 stage. While response to HNE dosing may have yielded a different result, we at least did not see a discernable change in *C. elegans* development related to loss of RES sensing in CeSahh.

A discrepancy between WT and *ahcy-1(syb7xx) C. elegans* did appear in our lifespan measurements, however (**Figure 3-16**). Populations of worms of both strains were age-synchronized, then treated with either HNE or a blank vehicle at L4 stage. Worms were seeded onto plates treated with floxuridine (FUDR) to prevent egg-laying, then scored

daily for total lifespan. In doing so, we did not notice any chance in the WT N2 worms related to HNE dosing. However, we did notice a significant die-off of *ahcy-1(syb7xx)* worms within the 7-10 day mark, with remaining worms maintaining lifespans similar to WT worms. Curiously, this die-off disappeared upon bolus HNE dosing; this may be explained as an obfuscation resulting from multiple off-target stress responses to bolus RES exposure. Regardless, the observation of, if not a lifespan decrease, at least a significant healthspan decrease in basal conditions is an intriguing result, considering the established implications of SAH accumulation in aging. It is possible that loss of endogenous RES sensing by CeSahh may instead manifest as a downstream methyltransferase misregulation, which itself has been shown to affect *C. elegans* lifespan through multiple avenues, including histone methylation.[11,34]

3.3 Conclusions

Through our work thus far, we have been able to identify unique primary cysteine sensors for both human and *C. elegans* SAHH orthologs. In doing so, we offer a model of RES-sensing conservation across species with a focus on the preservation of secondary structural elements that could be masked by a lack of primary sequence retention. In the immediate context of SAHH, we posit a potentially drug-targetable link that can facilitate the translation of endogenous RES flux into a disease-relevant downstream phenotypic outcome. It is possible that such a link may work through mechanisms affecting transmethylation and associated pathways, such as epigenetic

modification. Such a thought would provide a starting point in gauging the factors behind the evolutionary optimization of the RES binding pocket, though much additional work would be required to validate this idea.

In the broader scope of RES target discovery, progress towards the characterization of SAHH RES-sensing in two different orthologs – in terms of both enzymatic activity and physiological relevance – serves to complete the REX technology pipeline via validation of candidate privileged sensor proteins identified by G-REX profiling in variable biological environments. By altering the conditions of G-REX sensor profiling – such as utilizing a different species or pursuing a tissue-specific approach – one can explore multiple parameters to identify low-occupancy or low-concentration RES sensors otherwise missed through existing profiling methods. Then, through methods analogous to those in this chapter, the true RES-sensing capability (and associated consequence) of these new candidate sensors can be ascertained.

3.4 Experimental Details

3.4.1 SILAC/REX-Driven Screening of Candidate CeSahh RES Sensors

(Performed by Dr. Marcus Long, Dr. Souradyuti Ghosh, and Dr. Joseph Haegele)

For proteomics profiling, *C. elegans* lines expressing *tom70::mcherry::halo* and/or *gfp::halo* under the Hsp16 promoter were used. Approximately 2000-5000 adult worms were manually selected using the appropriate dominant fluorescent phenotypic markers.

Populations of worms are then supplemented with heavy or light arginine/lysine in M9 media, as well as SLE1 *E. coli* expressing *orn-1* RNAi. This allows for an adaptation of an *C. elegans* SILAC protocol published by Larance et. al.. [35] Following, populations are treated either with Ht-preHNE alkyne or vehicle as per the previously published protocol for worm T-REX [36] and those discussed in Chapter 2. Post-photouncaging, worms were washed twice in S complete buffer, then once in 50 mM HEPES (pH 7.6). Worm pellets are then spun down and frozen until ready to be used.

At a later time, heavy- and light-treated worms of equal pellet volume were lysed in a specialized lysis buffer [1.5% NP-40, 50 mM HEPES (pH 7.6), 0.5% deoxycholate, 2x Roche protease inhibitors, 0.30 mM TCEP] via freeze-thaw cycles and glass-bead beating. Roughly 10-20 mg of each lysate was then made up to 0.8 mg/mL and combined with the other. Lysates were then biotin-streptavadin enriched as described previously (See 2.4.8.2). Enriched eluates were run on an SDS-PAGE gel, which was then segmented into five parts, taking care to avoid the HaloTag band. These segments were then processed and analyzed by Cornell mass spectrometry services.

3.4.2 Generation of hSAHH/CeSahh Loss-of-Sensing Mutants

(Performed with Dr. Marcus Long, Dr. Joseph Haegele, and Sanjna Surya)

We designed our library of plasmids containing either hSAHH or CeSahh with the intent of establishing transient expression in mammalian HEK293T cell lines or inducible expression in BL21(DE3) *E. coli* depending on experimental context. To

generate the original HaloTag-Flag-hSAHH construct, ligase-free cloning was performed. For expression in HEK293T cell lines, we utilized pFN21a vector, which itself features a HaloTag appended to the inserted fusion gene partner. This construct's expression is governed by a CMV promoter, which results in constitutive expression in mammalian cell lines. For inducible expression of recombinant SAHH in BL21(DE3) via T7 expression system, we utilized pET28a vector. (See Appendix B)

3.4.3 T-REX-mediated Labeling of SAHH in Mammalian HEK293T Lines

Across all T-REX experiments, HEK293T cell lines were grown and maintained in 1X MEM + Glutamax™ media, supplemented with 10% FBS media, 1X NEAA solution, 1X sodium pyruvate, and 1X Pen-Strep solution. Active cell lines were stored at 37 C in humidified, 5% CO2 incubators. Cell lines were maintained through routine splitting at ~80% confluence, and seeded onto new plates at ~25% confluence. Cell lines with passage numbers of 6 or higher were not used for experiments and discarded.

To prepare cell lines for T-REX experiments, HEK239T cells were split into 3 cm culture dishes at ~0.5 x 10^6 cells/plate (approximately 40% confluency). After 24 h, cells were transfected with a transfection mix of 5.25% PEI by volume. 16-24 h post-transfection, cell media was replaced with fresh 10% FBS media and returned to incubation. Beyond this point, all steps were performed under red light. 36-48 h post-transfection, the cells, at approximately 70% confluence (~0.85 x 10^6 cells/plate), were treated with 20 μM Ht-PreHNE in serum-free media and incubated for another 2 h.

Afterwards, cells were rinsed with serum-free media three times, with 30 min of incubation between rinsings. These rinsings were performed carefully so as not to disturb the cell monolayer and lose cells. During incubation following the final rinsing, 365 nm UV lamps were powered on and left to warm up for a minimum of 20 min prior to light exposure. After this warm-up phase was complete, cells designated for light exposure were placed directly underneath the lamp for 5 min, with the dish lids removed such that the monolayers were directly exposed. The cells were then harvested after an additional 5 min post-exposure. The cell pellets were washed with ice-cold PBS twice, then once by 50 mM HEPES buffer (pH 7.6), then flash-frozen in liquid nitrogen before being stored in -80 C. Cells stored this way were generally used within 48 h, though they can be viably stored for up to a week.

3.4.4 Streptavadin-Biotin Enrichment of RES-Labeled SAHH from HEK293T Lysates

HEK239T cell pellets (see 3.4.3) were lysed using 2-4 volumes of Cell Lysis Buffer (**Table 3-2**), via three freeze-thaw cycles. For each cycle, cells were vortexed after buffer addition for 15 seconds, then flash-frozen in liquid nitrogen, then allowed to thaw at room temperature. Each successive cycle began as soon as thawing from the previous cycle was completed. After the final repeat, samples were centrifuged for 10 min at 20000 x g in a pre-chilled (4°C) centrifuge. Lysate supernatants were removed from each sample, and protein concentration was assessed via Bradford dye assay.

Table 3-2. Streptavadin-Biotin Enrichment Buffers

Buffer Name	Composition
Cell Lysis Buffer	50 mM HEPES (pH 7.6) 1% Triton OR 1% NP-40 1x Roche cOmplete tablet (EDTA-free)
Resolubilization Buffer	8% LDS 1 mM EDTA 50 mM HEPES (pH 7.6)

After concentration was determined, lysates were standardized to 2.0 mg/mL in 250 µL using Cell Lysis Buffer. To these sample volumes, TEV protease was added to a final concentration of 0.3 mg/mL. The samples were then incubated at 37°C for 30 min. Subsequently, each sample was made up to 350-600 mL final volume with 5% t-BuOH (added first), 1% SDS, 1 mM $CuSO_4$, 0.1 mM CuTBTA (added simultaneously via 10x master mix), 2 mM TCEP (added penultimately), and 0.2 mM biotin azide (added last). These samples were incubated further at 37°C for 30 m. Afterward, to precipitate all proteins, pre-chilled (-20°C) EtOH was added to each sample at a 4:1 EtOH:lysate ratio, followed by overnight storage at -80°C.

After overnight storage, the precipitated proteins were pelleted by centrifugation (20000 x g, 30 m, 4°C). The pellets were washed by resuspension in 70% EtOH, then 100% EtOH, then 100% acetone, followed by centrifugation in each instance (20000 x g, 30 m, 4°C). After the final wash, pellets were left exposed to open air until excess acetone had evaporated. Without leaving the pellet dry for a significant length of time, the pellets were resuspended in 50 µL protein Resolubilization Buffer (**Table 3-2**), and

then fully resolubilized via sonication for 10-15 m at 55°C. The samples were then centrifugated again (15000 x g, 5 m), and the samples were transferred to new, clean Eppendorf tubes, with a small portion removed from each sample to be used as an input control. The remainder of each sample was then diluted with 50 mM HEPES to a volume of 750 µL (0.53% LDS).

As the above was performed, streptavidin beads were withdrawn from a stock bottle and rinsed in ddH_2O (1:1 beads:ddH_2O) twice, then 50 mM HEPES buffer once (1:1 beads:HEPES) for a minimum of 30 m each. After each rinse, the beads were gently centrifugated (1500 x g, 1 m) and the rinse media was swapped. After the final rinse, beads were resuspended in 50 mM HEPES (1:1). 100 µL of this resuspension was then added to each sample, for a final volume of 800 µL + 50 µL bead volume. These samples were then incubated at room temperature on a rotator for 2 h. After this, the beads were washed twice with 0.5% LDS in 50 mM HEPES, then a third time with 0.75% LDS in 50 mM HEPES (1500 x g, 1 m centrifugation between washes). After the third wash, beads were resuspended in 2x Lamelli dye with 3% β-mercapthoethanol, then boiled at 98°C for 5 m to promote protein elution. The eluate was then analyzed via western blot, alongside the previously withdrawn inputs.

3.4.5 Homology Modelling and Phylogenetic Comparison Between hSAHH/CeSahh

3.4.5.1 Phylogenetic Analysis of SAHH Orthologs

(Performed with Dr. Marcus Long)

SAHH homolog sequences were obtained from a pool of species chosen from multiple kingdoms; additional emphasis was placed upon species that constitute an evolutionary timeline between the emergence of *C. elegans* and that of humans, with selections made that include common ancestors at varying taxonomic ranks). Ultimately, 68 species were selected with these criteria. The primary sequences for these homologs were then imported into MEGA7, where all subsequent phylogenetic analysis was performed. Next, the evolutionary history of the SAHH homologs was inferred by Maximum Likelihood method, based on the JTT matrix-based method (**Figure 3-10**). The subsequent phylogenetic tree generated was used to order the homologs within MEGA7, whose sequences were then aligned using MUSCLE sequence alignment algorithms.[28] Using this alignment, we identified a set of cysteine residues conserved across the selected species, as well as any cysteine residues present in the human ortholog that were not originally found in the aligned *C. elegans* sequence. For each conserved cysteine we identified that was solvent-exposed, we took note of flanking primary residues that had also changed or shifted, as well as any residues of note within the tertiary model (see 3.2.5.2), taking care to note significant changes in side chain polarity or charge.

3.4.5.2 Protein Modeling Analysis

Multiple crystal structures for hSAHH have been documented in the literature; for this visualization of a potential conserved RES binding pocket, PDB ID 3NJ4 was selected. [20] As no crystal structure yet exists for CeSahh, we used SWISS-MODEL online homology-modeling workspace to construct a comparable model for CeSahh, using 3NJ4 as the template structure. [20] The two models were then overlapped using UCSF Chimera visualization software, highlighting the candidate Cys residues in question as well as the nearby occupied NAD^+/NADH binding site.

3.4.6 Recombinant Expression of hSAHH/CeSahh and Putative Loss-of-Sensing Mutants

3.4.6.1 General Expression and Purification of His-Tagged Recombinant Protein

(Performed with Sanjna Surya)

All SAHH constructs were expressed using pET28a vectors to enable usage of the T7 expression system as well as appendage of N-terminal His6 tags onto the constructs for purposes of enabling Ni-NTA purification. The constructed plasmids were transformed into BL21(DE3) competent cells, with transformed cells selected for using LB agar plates treated with appropriate antibiotic via overnight growth at 37°C. From these plates, a single colony was selected and used to inoculate a starter culture of 5 mL antibiotic-treated LB media, grown overnight at 37°C (minimum growth time of 16 h) while agitated on an orbital shaker operating at 150 rpm. This starter culture

was then diluted into 1 L flasks antibiotic-treated LB media to be used for protein expression (1 mL starter culture per 1 L flask). These flasks were incubated at 37°C in an orbital shaker running at 200 rpm, and the OD600 of the media was evaluated every hour until reaching 0.7 ± 0.1. At this point, 1 mL of media was removed from each flask to use as negative controls for induction tests. Then, IPTG was added to a final concentration of 1 mM (from 1 M prepared stock), and the media was further incubated at 17°C overnight (16 h minimum). After this induction, < 1 mL of media was removed from each flask to use as positive controls for induction tests (exact volume was determined from OD600 measurements in order to ensure roughly equivalent amount of bacteria to negative controls). The remaining bacteria was harvested via centrifugation (4000 x g, 10 m), and the pellets were flash-frozen in liquid nitrogen and stored at -80°C for up to 2 weeks until purification can be performed.

From this point onward, all steps are carried out at 4°C or on ice, unless otherwise indicated. Before purification, cell pellets are removed from storage and allowed to thaw. During this time, Ni-NTA resin (7 mL of resin in storage buffer per 6 g of cell pellet) is prepared by rinsing the resin with 10 bed volumes (BV) of water, followed by 5 bed volumes of BL21 Lysis Buffer (**Table 3-3**). After the cell pellets thawed, they were resuspended in BL21 Lysis Buffer (6 mL per 1 g of pellet). Upon resuspension, they were incubated via end-to-end rotation at room temperature for 20 m. The suspension was then centrifugated at 20000 x g for 10 m, and the supernatant

Table 3-3. Buffers for SAHH Recombinant Expression and Purification

Buffer Name	Composition
BL21 Lysis Buffer *(*Add JUST before use)*	50 mM HEPES (pH 7.6) 5 mM imidazole 350 mM NaCl 150 μg/ml DNAse I* 5 μg/ml lysozyme* 1% NP-40, .1 mM PMSF* 5 mM BME (pH 7.5) DNAse I
Wash Buffer 1	50 mM HEPES (pH 7.6) 10 mM imidazole 350 mM NaCl 5 mM BME (pH 7.5)
Wash Buffer 2	50 mM HEPES (pH 7.6) 25 mM imidazole 350 mM NaCl 5 mM BME (pH 7.5)
Elution Buffer	50 mM HEPES (pH 7.6) 100 mM imidazole 350 mM NaCl 5 mM BME (pH 7.5)
Intermediate Buffer	50mM HEPES (pH 7.6) 250mM NaCl 10% glycerol 3mM TCEP-HCl (pH 7.5)
SAHH Storage Buffer	50mM HEPES (pH 7.6) 150mM NaCl 10% glycerol 3mM TCEP-HCl (pH 7.5)

was collected. The remaining pellets were resuspended in 10 mL lysis buffer, further incubated for 10 m, and then re-centrifugated at 20000 x g for 10 m. Both supernatants were combined and then added to the equilibrated Ni-NTA resin. The resulting

suspension was allowed to incubate either via end-over-end rotation in Falcon tubes or stirring in an appropriately sized flask for 20 m. After this, the suspension was loaded into a column, and the flowthrough was collected and set aside. The resin was then rinsed with Wash Buffer 1 (**Table 3-3**) 2 times, then by Wash Buffer 2 (**Table 3-3**) 2 times; all wash fractions were collected independently. Then, Elution Buffer (**Table 3-3)** was added at approximately 3-4 mL at a time, with 1.5 mL fractions of flow-through collected. Every other collected fraction was evaluated via Bradford dye analysis, and elution collection would continue until no significant protein could be detected. The fractions were then evaluated based on their $A_{280/260}$ profiles to confirm protein presence; fractions with suitable profiles were pooled and collected. This pool was then concentrated using a Centricon centrifugal filter unit (MWCO 30000) that has been pre-equilibrated with elution buffer. Afterwards, concentrated protein was loaded into a dialysis cassette or membrane tubing (MWCO 10000 or 30000) and dialyzed first in an Intermediate Buffer for 2 h, then in SAHH Storage Buffer overnight (**Table 3-3**).

hSAHH was further purified via size-exclusion chromatography (SEC). hSAHH designated for SEC purification was concentrated to a volume of < 5 mL as described above. The protein was loaded onto a GE HiLoad Superdex 200 column that had been pre-equilibrated with SAHH Storage Buffer. Elutions were collected in 2 mL fractions until an appropriate A280/260 peak could be resolved. Protein-containing fractions were then pooled and concentrated in a centrifugal filter unit until a desirable stock

concentration was achieved. The protein was then aliquoted and flash-frozen in liquid nitrogen before being transferred to -80°C storage.

3.4.6.2 Circular Dichroism Analysis

(Performed by Dr. Marcus Long and Sanjna Surya)

Wild-type (WT) hSAHH and C266S sensing-deficient mutants were diluted in SAHH Storage Buffer to a final concentration of 1 μM (47.7 μg/mL) and 3 μM (143.1 μg/mL). CD spectra of both enzymes were taken using an Aviv 400 Circular Dichroism Spectrometer, and a 150 W Suprasil Xenon lamp was used as a light source. 300 μL of each sample was analyzed at a time, using a wavelength range of 200-280 nm; measurements at each wavelength were taken with 5 s averaging times, and all measurements were taken at 25°C.

3.4.7 Generation of Apo-hSAHH via Protein Precipitation

1 mg of holo-hSAHH was used during each repeat of this procedure. To 1 volume of holo-hSAHH, 4 volumes of Precipitation Buffer 1 (**Table 3-4** Saturated NH4SO2 + 5 mM DTT in water) were added. The resulting mix was chilled on ice for 10 min, then spun down at 20000 x g for 20 min. Following removal of the supernatant, the precipitated protein was resuspended in 1 volume of Reconstitution Buffer 1 (**Table 3-4**). After resolubilization, 4 volumes of Precipitation Buffer 2 (**Table 3-4**) were added, and the sample chilling + spindown steps were repeated. After removal of the

Table 3-4. Ammonium Sulfate Precipitation Buffers for apo-SAHH generation

Buffer Name	Composition
Precipitation Buffer 1	Saturated NH_4SO_2 25 mM K_2HPO_4 5 mM DTT 1 mM EDTA pH 7.2
Precipitation Buffer 2	Saturated NH_4SO_2 50 mM K_2HPO_4 5 mM DTT 1 mM EDTA pH 7.2
Reconstitution Buffer 1	25 mM K_2HPO_4 5 mM DTT 1 mM EDTA pH 7.2
Reconstitution Buffer 2	50 mM K_2HPO_4 5 mM DTT 1 mM EDTA pH 7.2
Pre-Dialysis Buffer	10 mM K_2HPO_4 5 mM DTT

supernatant, the protein was resolubilized in 1 volume of Reconstitution Buffer 2 (**Table 3-4**). The solution was then loaded into dialysis tubing or a dialysis cassette (MWCO 30000) and dialyzed for 2 h in Pre-dialysis Buffer (**Table 3-4**), then overnight in SAHH storage buffer (see Appendix D). All dialysis occurred at 4°C.

3.4.8 Time-dependent RES Labeling of hSAHH in vitro

3.4.8.1 Differential Labeling Across hSAHH Mutants

(Performed with Dr. Marcus Long and Sanjna Surya)

Wild-type hSAHH and C266S sensing-deficient mutants were diluted in SAHH storage buffer to a final concentration of 12 μM (0.57 mg/mL), then split into aliquots based on the number of required time-points. To each, 12 μM of HNE-alkyne was added (with the exception of the zero time-point), and the protein mixes were allowed to incubate at room temperature for pre-determined amounts of time. At each time-point, the associated aliquot was quenched via 20-fold dilution with 50 mM HEPES, then further incubated with Cy5 click mix **(Table 3-2)** for 20 minutes at 37°C. The samples were then analyzed via SDS-PAGE in-gel fluorescence, using a follow-up Sypro Ruby stain to normalize for protein loading.

3.4.8.2 Time-dependent Labeling as a Function of NAD^+ Occupancy

(Performed with Dr. Marcus Long and Sanjna Surya)

Wild-type holo-hSAHH and apo-hSAHH were diluted in SAHH storage buffer to a final concentration of 12 μM (0.57 mg/mL), then split into aliquots based on the number of required time-points. All subsequent steps were performed similarly to 3.4.8.1.

3.4.9 Coupled Kinetic Activity Assays of hSAHH/CeSahh in vitro

3.2.9.1 SAHH Activity Assay General Protocol

(Performed with Dr. Marcus Long and Sanjna Surya)

During preparation and treatment of either recombinant protein or prepared lysates, an activity assay buffer was prepared containing 50 mM HEPES (pH 7.6), 1 mM DTNB, 1 mM EDTA, and 1 mM SAH. This assay buffer is set in a 37°C water bath as the protein/lysate is being prepared. Immediately before use, this assay buffer is supplemented with adenosine deaminase (AdoD) to a final concentration of 12 U/mL. Then, the buffer is split into a number of 150 μL aliquots in a pre-warmed (37°C) 96-well plate, depending on the conditions and replicates required in the particular assay. Afterwards, 10 μL of each lysate/protein condition is titrated into the assay buffer aliquots as quickly as possible using a multi-channel pipette. The 96-well plate is then immediately transferred into a pre-warmed BioTek Cytation 3 Cell Imaging Multi-Mode Reader. Subsequently, background-subtracted absorbance readings for each well were taken at 412 nm for up to 30 minutes at 37°C.

To determine the steady-state linear rate of each progress curve, a start time and end time was selected for each individual assay that best reflected the end of a pre-steady-state burst phase and the beginning of the curve plateauing. This range is then used to determine the linear rate of all SAHH reactions carried out during that assay.

3.4.9.2 Evaluation of HNE Inhibition of hSAHH *in vitro*

(Performed with Dr. Marcus Long and Sanjna Surya)

Portions of recombinant apo-hSAHH and holo-hSAHH were diluted to 5 μM with SAHH Storage Buffer (**Table 3-2**). Each was then split into aliquots and titrated

with HNE ranging from 0 to 500 μM. Each was left to incubate for 30 min. in a 37°C water bath. Afterwards, each aliquot was treated with excess NAD^+, then returned to 37°C for an additional minimum of 20 min.. After the final time point, activity assays were performed with each condition, and the resulting rates were analyzed.

3.4.9.3 Evaluation of NAD^+/HNE Pseudo-competition

A portion of recombinant apo-hSAHH was diluted to 5 μM with SAHH Storage Buffer (**Table 3-3**). This dilution was then split into three aliquots, each of which was treated with either 0, 250, or 500 μM HNE. Each was left to incubate for 30 min. in a 37°C water bath. Afterwards, each aliquot was further split, and each portion was treated with [NAD^+] ranging from 0 to 200 μM final concentration in solution. All split aliquots were then incubated at 37°C for another 20 minutes. Afterwards, activity assays were performed with each condition, and the resulting rates were fit to a Michaelis-Menten curve.

3.4.9.4 Evaluation of HNE Inhibition of CeSahh

Portions of dialyzed, non-SEC purified CeSahh (WT and C278A) were diluted to 50 μM with SAHH Storage Buffer (**Table 3-2**). The dilution was split into 10 aliquots; HNE was titrated at increasing concentrations, from 0 to 5 mM, into each aliquot. DZA and excess NAD^+ were added separately to the final two aliquots as controls. After 30 minutes at 37°C, each aliquot was treated with excess NAD^+, then returned to 37°C for an additional minimum of 20 min.. After the final time point,

activity assays were performed with each condition, and the resulting rates were analyzed.

3.4.10 Phenotypic Screening of Loss-of-Sensing CeSahh Knock-in Mutant C. elegans Line

3.4.10.1 Generation of CeSahh Loss-of-sensing Knock-in Mutant Line

Generation of the *C. elegans* loss-of-sensing CeSahh knock-in mutant lines (C280A) were conducted by SunyBiotech Co. using CRISPR/Cas9 genome editing. Three identical, independently generated lines were created and used in equal proportion across all phenotypic assays detailed here {*ahcy-1(syb748)[C280A], ahcy-1(syb749)[C280A], ahcy-1(syb750)[C280A]*}. For brevity, this mixed line population will be referred to as *ahcy-1(syb7xx).* (See Appendix B)

3.4.10.2 Larval Development of *C. elegans* WT and Mutant Lines

(Performed with Jinmin Liu)

C. elegans from separate wild-type and *ahcy-1(syb7xx)* populations were synchronized and allowed to arrive to L1 arrest overnight at room temperature (see General Methods). After synchronization, L1 larval worms from both populations were transferred onto OP50-seeded NGM plates and allowed to recover. Afterwards, worms from both populations were transferred to clean NGM plates with no OP50 lawn to allow for shedding of excess bacteria. During this time, 3% agarose pads were prepared

on clean glass slides, and a solution of levamisole was prepared to a final concentration of 1 mM. Once prepared, a number of individual worms were selected and transferred to agarose pads that had been prepared with several drops of levamisole for immobilization of the worms. Once the worms were deposited into the levamisole droplet, the worms were mounted using a glass cover slip, and imaged using a Leica M205FA stereomicroscope. The remaining worms from both populations were allowed to continue growing at 20°C. This process is then repeated every 24 hours; images from both sets of worms were then compared to identify any potential phenotypic deviations.

3.4.10.3 Viable Egg-lay Assays of *C. elegans* WT and Mutant Lines

(Performed with Jinmin Liu)

As in the previous section, worms from both wild-type and *ahcy-1(syb7xx)* populations were L1-synchronized overnight, then allowed to recover on OP-50-seeded NGM plates. Once recovered, worms were maintained at 20°C until reaching L4 stage. At this point, a minimum of 10 L4 worms from each population were taken and transferred to individual NGM plates and stored at 20°C for 24 hours. After 24 hours, each worm was moved to a fresh NGM plate, and the number of eggs produced on each of the previous NGM plates were counted. These previous plates were then retained at 20°C.

After 24 hours, the previous NGM plates are checked for hatched L1 worms; these worms are counted to indicate the number of eggs that were viable from the

previous day's count. Then, the active worms are each transferred to a third set of plates, and the second set's eggs are counted in an identical manner to the first set. The plates from this second set are then retained so that hatched L1s can be counted in an identical fashion. This process was continued until all worms have stopped laying eggs for a full 24 hrs.

3.3.10.4 Lifespan of *C. elegans* WT and Mutant Lines as a Function of HNE Treatment

Large populations of both wild-type and *ahcy-1(syb7xxx)* (minimally 10 confluent 10 cm plates per line) were synchronized to L1 overnight at room temperature. After recovery, these worms were then allowed to grow to L4 stage at 20°C; once grown, the worms were then split into two sub-populations, each in a 1.5 mL Eppendorf tube containing 750 μL liquid M9 media. One of each sub-population was treated with excess (1 mM final) HNE, and the other with an equivalent volume of DMSO vehicle. These volumes where then incubated on a rotator for 1 hr. After incubation, the worms were pelleted and washed a minimum of three times with M9 media, then plated.

After allowing for recovery, a minimum of 150 worms from each sub-population was then transferred to NGM plates (a maximum of 10 worms per plate) that had been pre-treated with 50 mM FUDR. Once plated, all worms were stored at 20°C, then evaluated every 24 hr. post-treatment for survival. Worms were checked for mobility to determine survival; worms that were immobile or otherwise lethargic were touched with

a platinum pick and scored as dead if no touch response could be observed. Instances where worms had died of unnatural causes, including desiccation by crawling to the edge of the plate, were discarded from the sample population. This process continued until all worms had died, at which point survival curves for each of the sub-populations were produced and analyzed. Statistically significant deviances in lifespan were determined by the Mantel-Cox test, with a p value of < 0.05 considered significant.

3.5 References

1. Turner, M. A. *et al.* Structure and function of S-adenosylhomocysteine hydrolase. *Cell Biochem. Biophys.* **33**, 101–125 (2000).
2. Graham, I. Homocysteine in health and disease. *Annals of Internal Medicine* vol. 131 387–388 (1999).
3. Shen, W. *et al.* Homocysteine-methionine cycle is a metabolic sensor system controlling methylation-regulated pathological signaling. *Redox Biol.* **28**, 101322 (2020).
4. Wang, Y. *et al.* Regulation of S-adenosylhomocysteine hydrolase by lysine acetylation. *J. Biol. Chem.* **289**, 31361–31372 (2014).
5. Belužić, L. *et al.* Knock-down of AHCY and depletion of adenosine induces DNA damage and cell cycle arrest. *Sci. Rep.* **8**, 1–16 (2018).
6. Vryer, R. & Saffery, R. *Metabolic regulation of DNA methylation in mammalian cells. Handbook of Epigenetics: The New Molecular and Medical Genetics* (Elsevier Inc., 2017). doi:10.1016/B978-0-12-805388-1.00019-5.
7. Barić, I. Inherited disorders in the conversion of methionine to homocysteine. *J. Inherit. Metab. Dis.* **32**, 459–471 (2009).
8. Yu, G., Wu, Q., Gao, Y., Chen, M. & Yang, M. The epigenetics of aging in invertebrates. *Int. J. Mol. Sci.* **20**, (2019).
9. Parkhitko, A. A. *et al.* Tissue-specific down-regulation of S-adenosyl-homocysteine via suppression of dAhcyL1/dAhcyL2 extends health span and life span in Drosophila. *Genes Dev.* **30**, 1409–1422 (2016).
10. Ma, S. & Gladyshev, V. N. Molecular signatures of longevity: Insights from cross-species comparative studies. *Semin. Cell Dev. Biol.* **70**, 190–203 (2017).
11. Parkhitko, A. A., Jouandin, P., Mohr, S. E. & Perrimon, N. Methionine metabolism and methyltransferases in the regulation of aging and lifespan extension across species. *Aging Cell* **18**, 1–18 (2019).
12. Yuan, C. S., Ault-Riché, D. B. & Borchardt, R. T. Chemical modification and site-directed mutagenesis of cysteine residues in human placental S-adenosylhomocysteine hydrolase. *J. Biol. Chem.* **271**, 28009–28016 (1996).
13. Long, M. J. C., Urul, D. A. & Aye, Y. *REX technologies for profiling and decoding the electrophile signaling axes mediated by Rosetta Stone proteins. Methods in Enzymology* vol. 633 (Elsevier Inc., 2020).

14. Studer, G. *et al.* QMEANDisCo-distance constraints applied on model quality estimation. *Bioinformatics* **36**, 1765–1771 (2020).

15. Benkert, P., Biasini, M. & Schwede, T. Toward the estimation of the absolute quality of individual protein structure models. *Bioinformatics* **27**, 343–350 (2011).

16. Bertoni, M., Kiefer, F., Biasini, M., Bordoli, L. & Schwede, T. Modeling protein quaternary structure of homo- and hetero-oligomers beyond binary interactions by homology. *Sci. Rep.* **7**, 1–15 (2017).

17. Waterhouse, A. *et al.* SWISS-MODEL: Homology modelling of protein structures and complexes. *Nucleic Acids Res.* **46**, W296–W303 (2018).

18. Bienert, S. *et al.* The SWISS-MODEL Repository-new features and functionality. *Nucleic Acids Res.* **45**, D313–D319 (2017).

19. Guex, N., Peitsch, M. C. & Schwede, T. Automated comparative protein structure modeling with SWISS-MODEL and Swiss-PdbViewer: A historical perspective. *Electrophoresis* **30**, (2009).

20. Lee, K. M. *et al.* X-ray crystal structure and binding mode analysis of human S-adenosylhomocysteine hydrolase complexed with novel mechanism-based inhibitors, haloneplanocin A analogues. *J. Med. Chem.* **54**, 930–938 (2011).

21. Devine, E. L., Oprian, D. D. & Theobald, D. L. Relocating the active-site lysine in rhodopsin and implications for evolution of retinylidene proteins. *Proc. Natl. Acad. Sci. U. S. A.* **110**, 13351–13355 (2013).

22. Schrag, J. D., Winkler, F. K. & Cygler, M. Pancreatic lipases: Evolutionary intermediates in a positional change of catalytic carboxylates? *J. Biol. Chem.* **267**, 4300–4303 (1992).

23. Parvez, S. *et al.* T-REX on-demand redox targeting in live cells. *Nat. Protoc.* **11**, 2328–2356 (2016).

24. Lin, H.-Y., Haegele, J. a., Disare, M. T., Lin, Q. & Aye, Y. A Generalizable Platform for Interrogating Target- and Signal-Specific Consequences of Electrophilic Modifications in Redox-Dependent Cell Signaling. *J. Am. Chem. Soc.* **137**, 6232–6244 (2015).

25. Felsenstein, J. Evolutionary trees from DNA sequences: A maximum likelihood approach. *J. Mol. Evol.* **17**, 368–376 (1981).

26. Jones, D. T., Taylor, W. R. & Thornton, J. M. The rapid generation of mutation data matrices from protein sequences. *Bioinformatics* **8**, 275–282 (1992).

27. Kumar, S., Stecher, G. & Tamura, K. MEGA7: Molecular Evolutionary Genetics

Analysis Version 7.0 for Bigger Datasets. *Mol. Biol. Evol.* **33**, 1870–1874 (2016).

28. Edgar, R. C. MUSCLE: A multiple sequence alignment method with reduced time and space complexity. *BMC Bioinformatics* **5**, 1–19 (2004).

29. Todd, A. E., Orengo, C. A. & Thornton, J. M. Plasticity of enzyme active sites. *Trends Biochem. Sci.* **27**, 419–426 (2002).

30. Lozada-Ramírez, J. D., Martínez-Martínez, I., Sánchez-Ferrer, A. & García-Carmona, F. A colorimetric assay for S-adenosylhomocysteine hydrolase. *J. Biochem. Biophys. Methods* **67**, 131–140 (2006).

31. Cai, S. *et al.* Comparative kinetics of cofactor association and dissociation for the human and trypanosomal S-adenosylhomocysteine hydrolases. 3. Role of lysyl and tyrosyl residues of the C-terminal extension. *Biochemistry* **49**, 8434–8441 (2010).

32. Brzezinski, K., Bujacz, G. & Jaskolski, M. Purification, crystallization and preliminary crystallographic studies of plant S-adenosyl-L-homocysteine hydrolase (Lupinus luteus). *Acta Crystallogr. Sect. F Struct. Biol. Cryst. Commun.* **64**, 671–673 (2008).

33. López-Otín, C., Blasco, M. A., Partridge, L., Serrano, M. & Kroemer, G. The hallmarks of aging. *Cell* **153**, 1194 (2013).

34. Greer, E. L. *et al.* Members of the H3K4 trimethylation complex regulate lifespan in a germline-dependent manner in C. elegans. *Nature* **466**, 383–387 (2010).

35. Larance, M. *et al.* Stable-isotope labeling with amino acids in nematodes. *Nat. Methods* **8**, 849–851 (2011).

36. Long, M. J. C. *et al.* Precision Electrophile Tagging in Caenorhabditis elegans. *Biochemistry* **57**, 216–220 (2018).

CHAPTER 4

REDOX-SENSING CHARACTERIZATION OF HSPB7, A CARDIOVASCULAR SMALL HEAT-SHOCK PROTEIN

PREFACE

Figures and data from the following chapter have appeared in a previously published work. They have been adapted for presentation in this work with permission from ACS Chemical Biology (Copyright 2018 American Chemical Society):

Surya, S. L.; Long, M. J. C.; Urul, D. A.; Zhao, Y.; Mercer, E. J.; Elsaid, I. M.; Evans, T.; Aye, Y. Cardiovascular Small Heat Shock Protein HSPB7 Is a Kinetically Privileged Reactive Electrophilic Species (RES) Sensor. ACS Chem. Biol. 13, 1824–1831 (2018). (doi: 10.1021/acschembio.7b00925)

4.1 Introduction

4.1.1 Identification of zebrafish Hspb7 via a medium-throughput T-REX-enabled screen

Thus far we have shown that discovery of novel RES-sensing candidate proteins via the REX technology pipeline can be supplemented with phylogenetic analysis to connect results found through proteomic profiling in disparate species to biologically relevant redox sensing in humans. Specifically, we have been able to identify evolutionarily conserved RES-binding regions through a combination of sequence conservation analysis with homology modeling. However, such an approach must be generalizable across distinct species that have been integrated into the REX platform as model organisms. By identifying a novel sensor in a unique REX-compatible species and characterizing an evolutionarily-conserved binding residue retained through a human ortholog, we can further validate the approach used in our studies of SAHH and extend such a strategy to RES-sensing candidates identified in future proteomic profiling studies.

Concurrent with our work on SAHH characterization, our group identified a novel *D. rerio* redox-sensor candidate through a medium-throughput screen established prior to the development of the G-REX platform.[1] This screen employed the commercially available Halo ORF clone library as a starting ground; this library enabled us to probe an extensive variety of readily Halo-tagged proteins using our T-REX

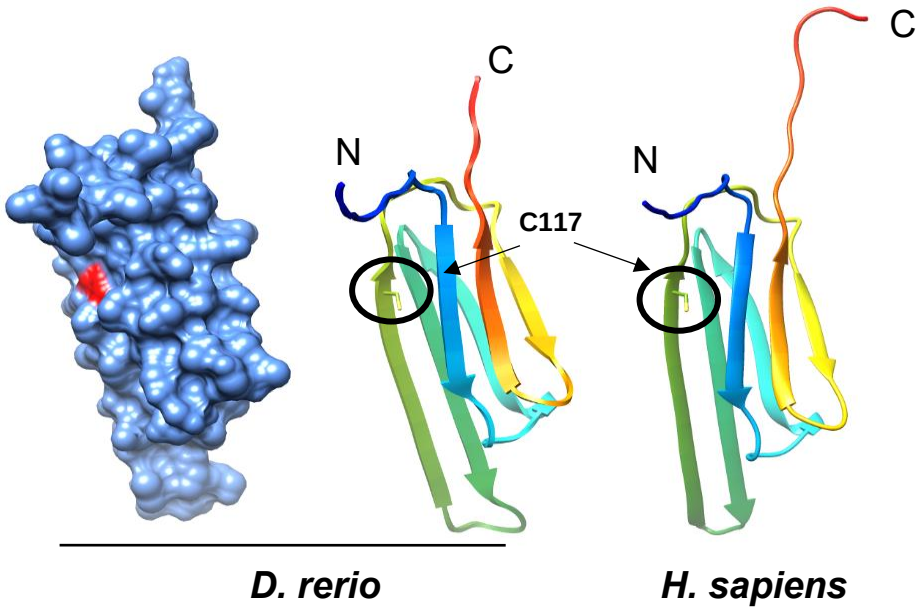

Figure 4-1. Structural homology models of zHspb7 (*D. rerio)* and hHSPB7 (*H. sapiens).* The left-most zHspb7 model is a surface-accessible map, with C117 highlighted in red. All models were constructed using human HSPB6 as a template (PDB ID: 5LTW). *Performed by Dr. Marcus Long.*

platform, from which we could focus on promising RES-sensor candidates. One such emergent sensor was zebrafish heat shock protein family B member 7 (zHspb7) (**Figure 4-1**). These, along with other small heat shock proteins (sHSPs), are known primarily to function as energy-independent molecular chaperones,[2,3] and though they are not well characterized as individual proteins, they are collectively seen to have significant roles in cellular stress response.[4,5] zHspb7 is among those sHSPs with an implicit role in stress response and disease states, as misregulation has been associated with cardiac abnormalities and stress-induced fatality.[6,7] While the associated mechanisms are not well understood, it is possible that a novel RES-sensing function may offer a key insight into such behavior.

4.1.2 zHspb7/hHSPB7 as a bridge between REX-mediated target discovery and in vitro biochemical characterization

zHspb7 represents a novel case among known redox sensors, including Keap1[8–10] and Akt3.[1] zHspb7 is a small, non-enzymatic protein (~18 kDa) featuring only 2 total cysteines. However, non-enzymatic proteins of similar size and cysteine content have recently been uncovered through pilot G-REX profiling in HEK293T cells, such as Ube2V2.[11] Validation of zHspb7, therefore, would reinforce a predictive model by which kinetically privileged cysteine sensors can inform RES sensing capability independent of many other characteristics, including cysteine richness, size, or mode of action. Such a model would be consistent with the specificity required of kinetically-privileged sensors operating through low-occupancy RES modification and subsequent downstream signal amplification.

A significant contributor to this predictive model, as alluded to earlier, involves phylogenetic analysis of identified RES sensor proteins native to our model species; this would allow for the identification of conserved regions that may offer insight into kinetically-privileged cysteine sensor residues. In this specific instance, there is a high degree of conservation across the sHSPs, including zHspb7 and its human ortholog (hHSPB7) (**Figure 4-2a**). Intriguingly, comparing these two species reveals that, of the two zHspb7 cysteines, one appears highly conserved with a few identifiable residue shifts (C117), whereas the other is omitted from hHSPB7 entirely (C49) (**Figure 4-2b**).

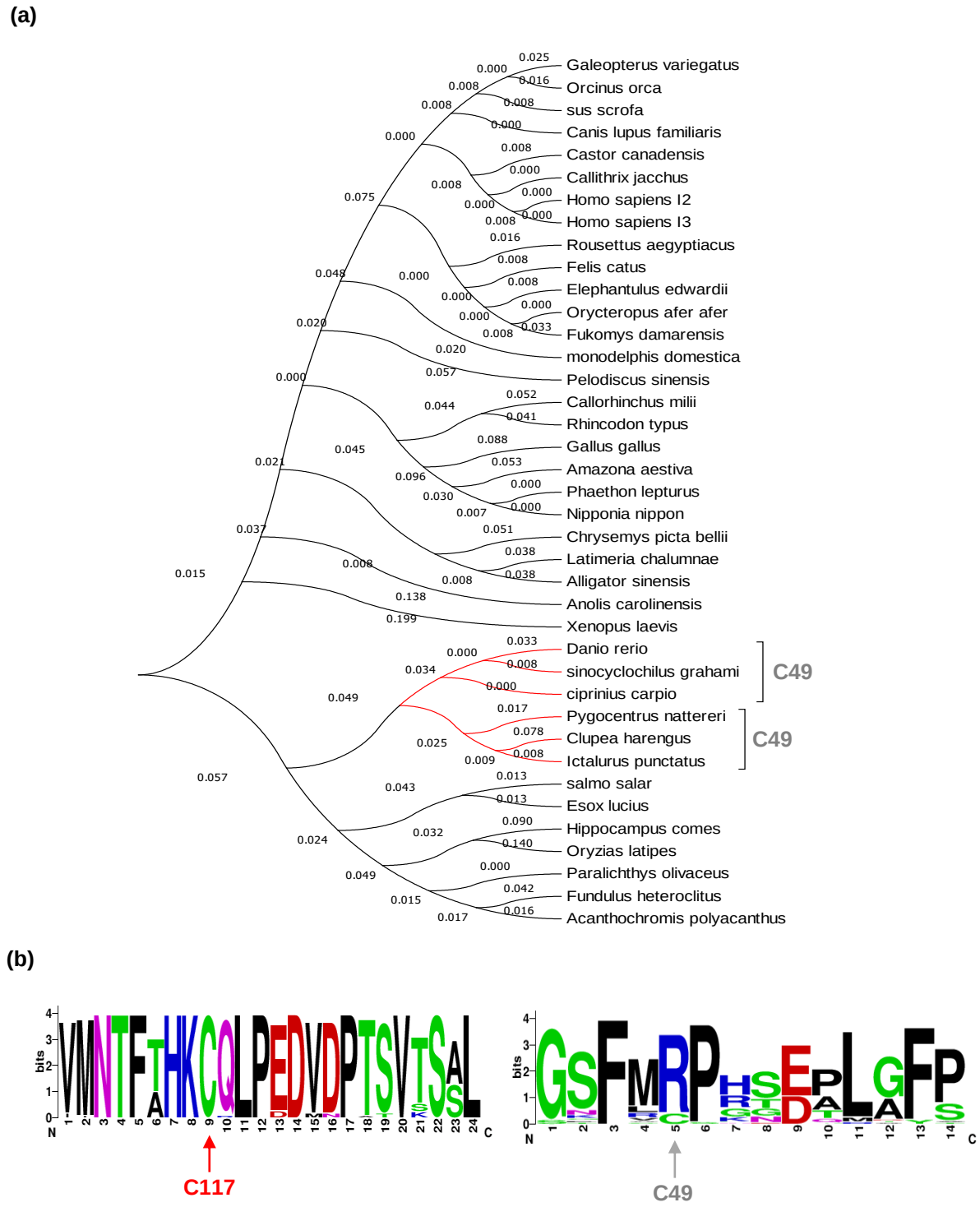

Figure 4-2. Evaluation of the conservation of zHspb7 cysteine residues. **(a)** Molecular phylogeny analysis of known HSPB7 orthologs. Analysis was conducted within the Molecular Evolutionary Genetics Analysis (MEGA 7) software suite. **(b)** Sequence logos of the zHspb7 cysteine residues across all known orthologs. *Performed with Dr. Marcus Long.*

Comparing the redox-sensing efficacy of these cysteines in zHspb7 may offer further insight into interpreting these conserved regions, keeping in mind both the primary sequence conservation and the three-dimensional context offered by homology modeling (**Figure 1**). With this in mind, we sought to identify the RES sensing capability of either zHspb7 cysteine, evaluate the HNE-modification kinetics of zHspb7 itself, and further explore the ramifications of residue shifts – if any – near the identified RES-sensing cysteine from the zebrafish to the human ortholog.

4.2 Results and Discussion

4.2.1 Identification of C117 as the first-responder redox sensor of zHspb7

The fact that zHspb7 contains only two cysteines permits the practical use of site-directed mutagenesis to individually determine the redox-sensing capability of each such cysteine. As such, each possible permutation of zHspb7 sensing-deficient mutant (C49S, C117S, C49S/C117S) was generated for analysis in this study. Though confocal microscopy, the mutants were determined to express and localize in a similar fashion within HeLa cells (**Figure 4-3a**), suggesting that the functionality and behavior of the non-enzymatic zHspb7 was likely preserved in these mutants. With this established, each mutant was HNEylated via T-REX (**Figure 4-3b**). Upon assessing degrees of HNEylation, we found that there was no discernable perturbation of labeling by the C49S mutant; however, the C117S and C49S/C117S mutants demonstrated total or at

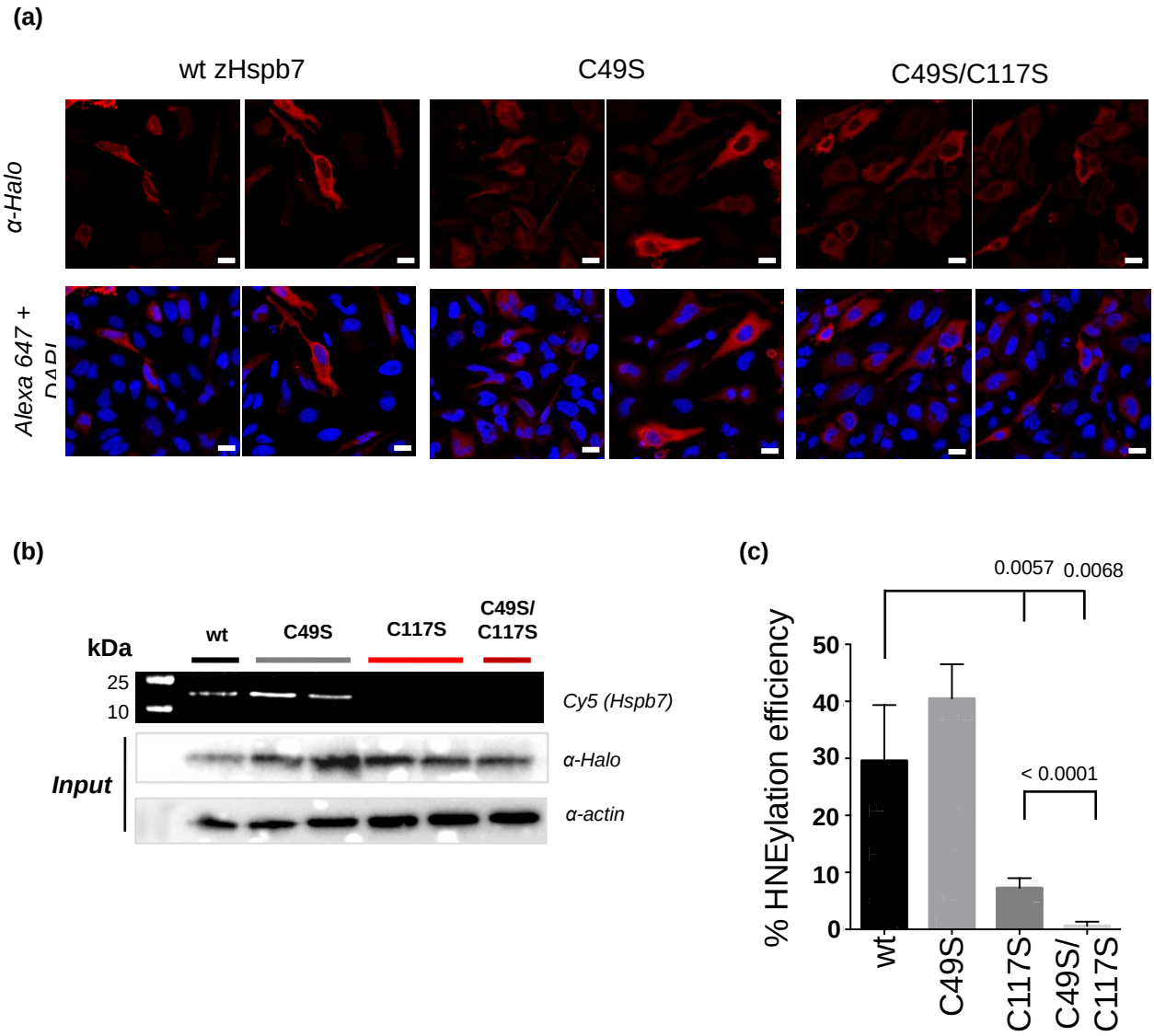

Figure 4-3. Identification of the primary cysteine sensor residue of zHspb7. **(a)** Immunofluorescent evaluation of expression and localization of *Halo::tev::zHspb7* and associated sensing-deficient mutant candidates in HeLa cells. Cells were analyzed by confocal imaging after MeOH fixation and IF antibody treatment 2 days post-transfection. **(b)** In-gel fluorescent evaluation of wild-type and sensing-deficient zHspb7 mutant candidates following T-REX in HEK293T cells. Expression was normalized via follow-up Western blots. **(c)** Quantitation of T-REX-mediated zHspb7 labeling across sensing-deficient mutant candidates. Error bars show SEM. *Performed by Dr. Marcus Long and Sanjna Surya.*

least considerable HNE modification, strongly implicating C117 as the primary redox-sensing cysteine residue in zHspb7 (**Figure 4-3c**).

4.2.2 Structural dynamics of C117 labeling offer mechanistic insight

As zHspb7 is non-enzymatic, and any assayable downstream targets that may be affected by zHspb7 – and, by extension, many other sHSPs – are not well characterized, we sought other means by which to assess zHspb7 response to HNE modification. Structural perturbation was one such parameter; many molecular chaperones are regulated by redox-driven structural modification.[12] With this in mind, we used cicular dichroism analysis to determine any structural changes incurred as a function of HNE modification (**Figure 4-4**). Initial CD analysis of WT zHspb7 revealed a significant degree of β-sheet structure (~33%) compared to α-helix (<6%), which was consistent with our homology model (**Figure 4-1**). Upon incubation with a stoichiometric equivalent of HNE (30 min., 37°C), the WT protein secondary structure trended further towards β-sheets (~50%). Repeating this treatment with each of the zHspb7 sensing-deficient mutants revealed a similar, albeit attenuated, shift in the C49S mutant; the C117S and C49S/C117S mutants, however, reported significant and total loss of this structural shift, respectively. This further implicated C117 as the primary redox sensor, whose modification possibly induces a functionally relevant modification to zHspb7 structure.

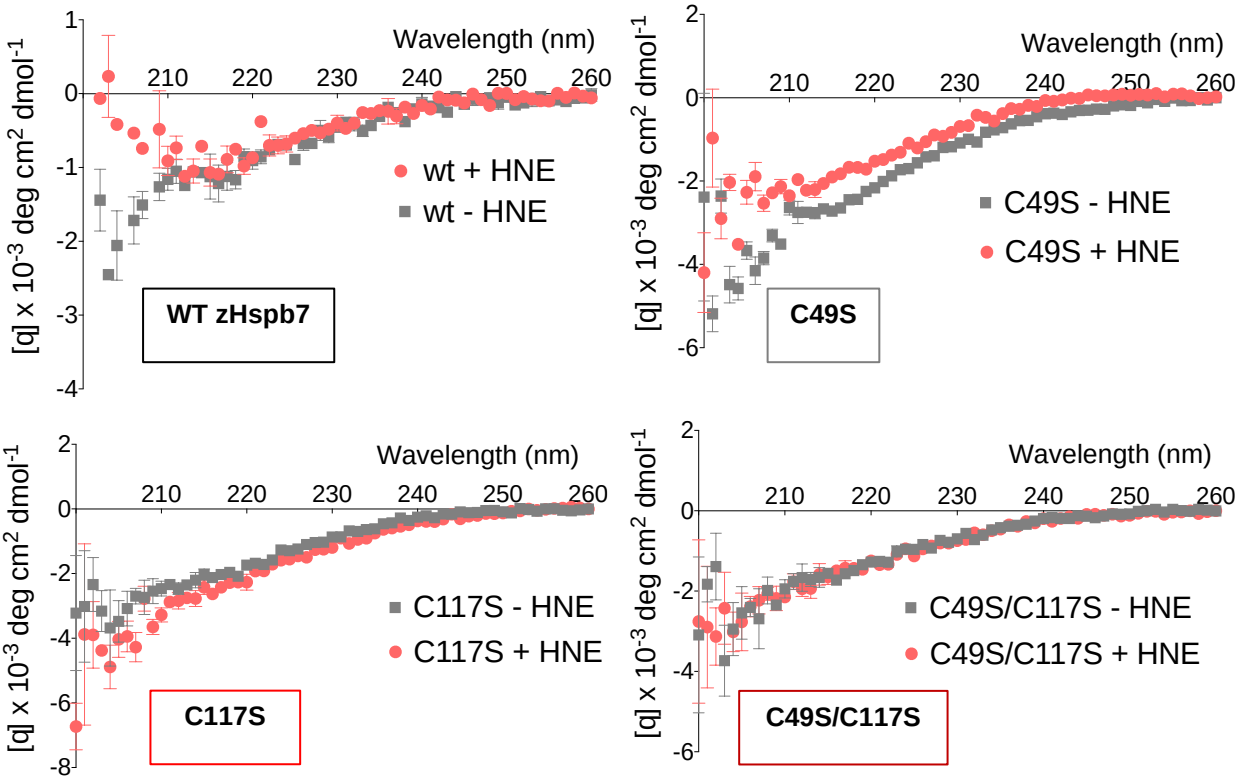

Figure 4-4. Circular dichroism analysis of zHspb7 secondary structural changes as a function of RES labelling. CD data for the wild-type was obtained with 2.8 μM zHspb7 after pre-treatment with 1 equivalent HNE or DMSO vehicle (30 min., 37°C); data for the mutants was obtained with 1.85 μM protein and 6 equivalents of HNE or vehicle (30 min., 37°C). *Performed by Dr. Marcus Long and Sanjna Surya.*

4.2.3. Comparison of zHspb7 RES modification kinetics to established sensor proteins

As previously discussed, zHspb7 occupies a unique niche among RES sensors evaluated and characterized through T-REX due to its low cysteine content and size. Despite this, the presence of a kinetically privileged sensor – putatively C117 at this stage – should be sufficient for zHspb7 to demonstrate efficient RES modification *in vitro* in the presence of freely available HNE, in line with known known redox-sensor

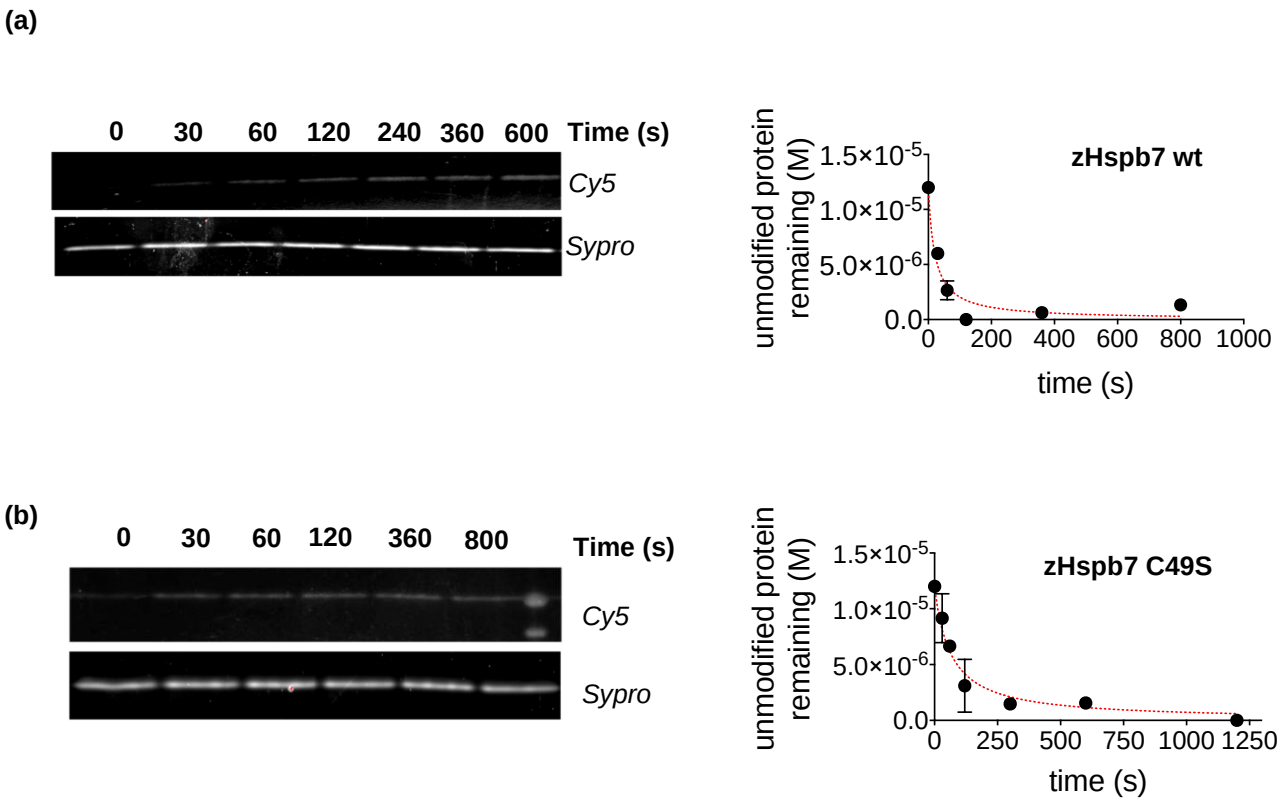

Figure 4-5. Evaluation of time-dependent HNEylation of zHspb7 *in vitro*. **(a)** In-gel fluorescent evaluation of zHspb7 HNEylation *in vitro*. 12 μM aliquots of zHspb7 were treated with 12 μM of HNE (alkyne) before being quenched by dilution into chilled buffer at each time point. Cy5 signal was normalized to follow-up Sypro Ruby staining. **(b)** Quantitation of time-dependent HNEylation of zHspb7, fitted to a homodimerization equation. Error bars show SEM. *Performed with Dr. Marcus Long.*

proteins. To evaluate this claim, we treated WT zHspb7 with a stoichiometric equivalent of HNE (alkyne) and evaluated the rate of zHspb7 labeling (**Figure 4-5a**). Upon doing so, we observed near-total saturation of the protein within 5 minutes. Repeating this assay with the C49 mutant yielded a similar rate (**Figure 4-5b**), further implicating C117 as the primary residue driving zHspb7 RES sensitivity.

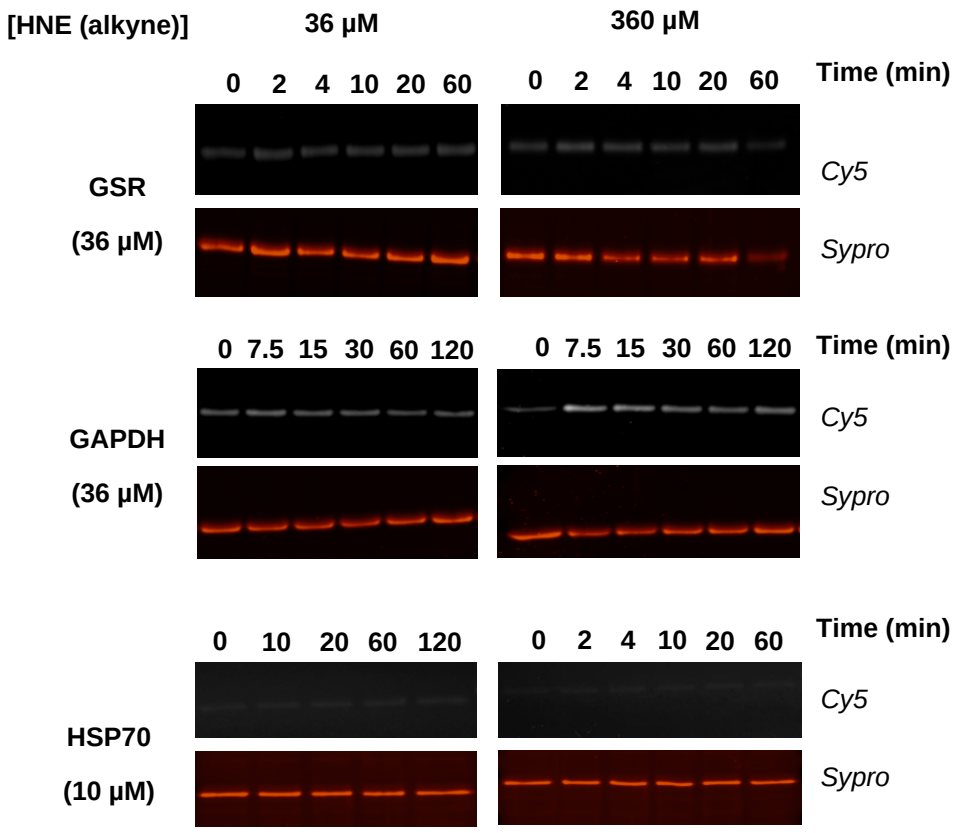

Figure 4-6. Qualitative evaluation of time-dependent *in vitro* labeling of known HNE sensors comparable to zHspb7. Labeling experiments were performed with 1:1 and 1:10 protein:HNE ratios for GSR and GAPDH, and 1:3.6 and 1:36 ratios for HSP70. *Performed with Dr. Marcus Long.*

These observed rates were comparable to a variety of redox sensors with well-characterized HNEylation behavior in the literature: glutathione-S-reductase (GSR),[13] human glyceraldehyde-3-phosphate dehydrogenase (GAPDH) [14], and human HSP70.[15] To directly assess zHspb7 against this sampling of known RES sensors, we assayed each of these three using the identical *in vitro* stoichiometric labeling protocol (**Figure 4-6**). In all, the collection of proteins assayed demonstrated slower labeling rates than zHspb7 within identical time-frames. However, to validate the reliability of this assay in

correctly assessing known RES sensors, we further probed GSR by increasing incubation times up to 60 min. and by replicating the assay in excess HNE (alkyne), mimicking bolus-dosing conditions. Doing so produced an apparent second-order rate constant slightly above 10 M^{-1} s^{-1} in stoichiometric editions. While this is markedly below literature HNE-driven inhibition rates (~500 M^{-1} s^{-1}), it is important to note that *in vitro* modification of a RES-sensing cysteine may differ significantly in mechanism from the reported two-step HNE inhibition pathway of GSR *in vivo*. More importantly, this observed rate was still faster than that of GAPDH – which produced observable HNE modification only in excess conditions – while HSP70 was hardly labeled in the same timeframe. This rate order corresponds with reported observations in the literature, and was independent of cysteine content, reducing the concern of nonspecific labeling. Therefore, the rapid HNE adduction observed with zHspb7 is likely to be real.

4.2.4 Conservation of C117 as a primary RES sensor in hHSPB7

Phylogenetic analysis of the HSPB7s revealed near-total conservation of C117 across the evaluated orthologs (**Figure 4-2**). Interestingly, C49 appears only within *D. rerio* and closely associated species within its clade (red species in Figure 4-2). Thus, hHSPB7 only features the one C117 cysteine (C126 in hHSPB7 numbering). If our evolutionary model pertaining to conserved RES sensing motifs holds, we would assume that hHSBP7 should be susceptible to HNE modification, facilitated primarily through C117. A simple HNE (alkyne) treatment of HEK233T cells expressing FLAG-

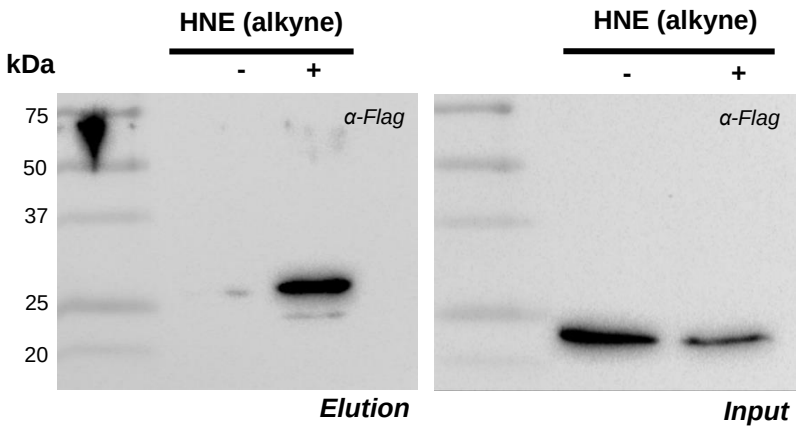

Figure 4-7. HNEylation of hHSPB7 in HEK239T cells in bolus-dosing conditions. Cells transfected with *hHSPB7::myc::Flag* were treated with 20 μM HNE (alkyne) for 2 hr. prior to harvesting. MW discrepancy is likely due to biotinylation or intramolecular cross-linking. *Performed with Dr. Marcus Long.*

tagged hHSPB7 – followed by biotin-streptavidin enrichment – confirmed this susceptibility (**Figure 4-7**).

Interestingly, however, the changes to flanking residues of C117 between zHspb7 and hHSPB7 suggest – purely from a primary-sequence perspective – that C117 labeling would be affected, if not attenuated outright, in hHSPB7. For example, R118 in zHspb7 becomes Q118 (Q127) in humans, and T114 becomes A114 (A123). These would suggest a transition away from a charged microenvironment around the C117 residue, which we have discussed before in the context of attenuating RES sensing (see Chapter 3). However, this was not observed in our work; evaluation of these residues' positions relative to C117 in the constructed homology models suggests that they may

not contribute to the stereoelectronic environment of C117 due to their distance and placement along the β-sheet.

4.2.5 Structural context for C117 redox sensing behavior in zHspb7/hHSPB7

If changes to the primary sequence over an evolutionary timespan did not affect susceptibility of C117 to RES modification, then it is worth turning our attention to the residues nearby in a three-dimensional environment that were preserved. In this case, one such nearby residue is H115, which points towards C117 in the constructed model (**Figure 4-8a**). Searching the Catalogue of Somatic Mutations in Cancer (COSMIC) database revealed H115D as a potential oncogenic mutation, revealing a possible link between RES signaling misregulation and cancer occurrence. To evaluate this, we generated the H115D sensing-deficient mutant, hypothesizing that this mutation would inactivate C117. After validating expression and localization of the H115D mutant (**Figure 4-8b**), we assessed HNE sensitivity of the C117 residue compared to WT zHSPB7 via T-REX (**Figure 4-8c**). Quantitation of the Cy5 signal output revealed that HNE modification was significantly reduced in the H115D mutant to a level comparable to that of C117S knockout itself (**Figure 4-8d**).

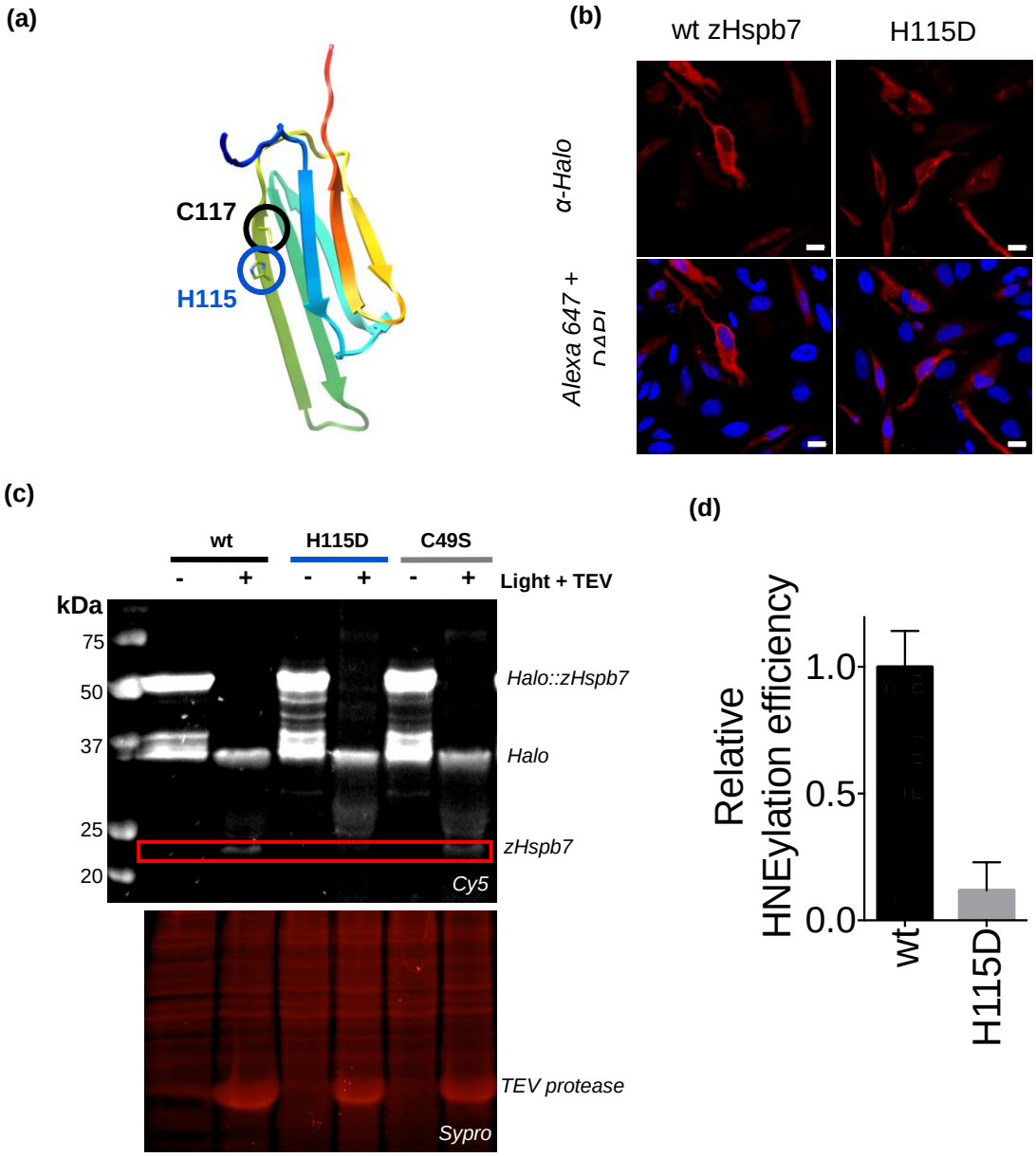

Figure 4-8. Reduction of zHspb7 RES sensing via perturbation of the spatially proximal H115D. **(a)** Relative locations of C117 and H115 in the proposed zHspb7 homology model. **(b)** Immunofluorescent evaluation of expression and localization of *Halo::tev::zHspb7* and H115D mutant in HeLa cells. Cells were analyzed by confocal imaging after MeOH fixation and IF antibody treatment 2 days post-transfection. **(c)** In-gel fluorescent evaluation of the wild-type and H115D zHspb7 mutant following T-REX in HEK293T cells. Lysates were normalized via follow-up Sypro Ruby staining. **(d)** Quantitation of T-REX-mediated zHspb7 labeling of the WT and H115D mutant. Error bars show SEM. *Performed with Dr. Marcus Long and Sanjna Surya.*

4.3 Conclusions

Taken together, this data supports the role of C117 as a kinetically privileged sensor in zHspb7, one that is preserved between orthologs up to and including hHSPB7. The differences between the HSPB7s and other T-REX-validated RES sensors we have covered in this work serve to highlight the individual significance of kinetically privileged cysteine sensors in bestowing redox signal interpretation upon their respective proteins. Further, given that the H115D mutant demonstrated near-complete similarity with wild-type in terms of cell localization and expression, it is possible that RES sensing can provide an assayable condition to evaluate proteins whose misregulation may otherwise be difficult to detect, despite leading to oncogenesis or other disease states.

In the broader scope of our overall work, we have presented an evolutionarily conserved RES sensor whose HNE affinity is affected, not simply by changes in flanking primary sequence, but by local stereoelectric changes in a three-dimensional environment. It is possible that the significant overlap of function and significance between zHspb7 and hHSPB7 with respect to their respective species indicated that changes or optimizations to a hypothetical RES binding region would yield no benefit; contrast this outcome with hSAHH/CeSahh, where changes pertaining to the complexity and significance of post-translational modifications and methylation cycles may have necessitated an optimization of RES-sensing capability. In either case,

phylogenetic analysis can provide a bridge between the species of the G-REX toolbox and the human homologs whose redox-sensing functionality can be further ascertained.

4.4 Experimental Details

4.4.1 Generation of Plasmids for Expression of HaloTag-hHSPB7/zHspb7 Wild-type and Cysteine-sensor Mutants

(Performed by Dr. Marcus Long, Sanjna Surya, and Islam Elsaid)

Plasmids designed for this project were made with the intent of establishing transient expression in HEK293T cell lines or inducible expression in BL21(DE3) *E. coli* depending on experimental context. Ligase-free cloning was performed to generate all hHSPB7/zHspb7 constructs, including *halo::tev::zHapb7, His6::zHspb7* and *flag::myc::hHSPB7*. zHspb7 mutants (C117S, C49S, C49S/C117S, H115D) were created via site-directed mutagenesis. For expression in HEK239T and HeLa cell lines, the pCS2+8 vector was utilized, featuring an SP6 promoter system. For inducible expression of recombinant zHspb7/hHSPB7 in BL21(DE3) via T7 expression system, we utilized pET28a vector. (See Appendix B)

4.4.2 Recombinant Expression of zHspb7/hHSPB7 and Associated Mutants

4.4.2.1 General Purification of His-tag Recombinant Protein

(Performed by Sanjna Surya)

All zHspb7 constructs were expressed using pET28a vectors to enable usage of the T7 expression system as well as appendage of N-terminal His6 tags onto the constructs for purposes of enabling Ni-NTA purification. The constructed plasmids were transformed into BL21(DE3) competent cells, with transformed cells selected for using LB agar plates treated with appropriate antibiotic (kanamycin) via overnight growth at 37°C. From these plates, a single colony was selected and used to inoculate a starter culture of 5 mL antibiotic-treated LB media, grown overnight at 37°C while agitated on an orbital shaker operating at 200 rpm. This starter culture was then diluted into 1 L flasks antibiotic-treated LB media to be used for protein expression (1 mL starter culture per 1 L flask). These flasks were incubated at 37°C in an orbital shaker running at 200 rpm, and the OD600 of the media was evaluated every hour until reaching 0.5 ± 0.1. Then, IPTG was added to a final concentration of 1 mM (from 1 M prepared stock), and the media was further incubated at 17°C overnight (16 h minimum). The remaining bacteria was harvested via centrifugation (5000 x g, 10 m), and the pellets were flash-frozen in liquid nitrogen and stored at -80°C for up to 2 weeks until purification can be performed.

From this point onward, all steps are carried out at 4°C or on ice, unless otherwise indicated. Before purification, cell pellets are removed from storage and allowed to thaw. During this time, Ni-NTA resin (8 mL of resin in storage buffer per

10 g of pellet) is prepared by rinsing the resin with 37 mL of water, followed by 20 mL of BL21 Lysis Buffer (**Table 4-1**). After the cell pellets thawed, they were resuspended in BL21 Lysis Buffer (2.5 mL per 1 g of pellet). Upon resuspension, they were incubated via end-to-end rotation at room temperature for 20 min. The suspension was then centrifugated at 20000 x g at 4°C, and the supernatant was collected. The supernatant was then added to the pre-equilibrated resin, and the resulting suspension was allowed to incubate either via end-over-end rotation in Falcon tubes or stirring in an appropriately sized flask for 20 min at 4°C. After this, the suspension was loaded into a column, and the flowthrough was collected and set aside. The resin was then rinsed three times with Wash Buffer (**Table 4-1**). Then, Elution Buffer (**Table 4-1**) was added 5 mL at a time, with each 5 mL fraction collected separately. Every 10 mL, the concentration of imidazole within the Elution Buffer was increased, from 20 mM, to 40 mM and then to 60 mM, 80 mM, 120 mM, and finally 250 mM (at this concentration, six 5 mL fractions were collected). The fractions were then evaluated based on Bradford assay readouts and SDS-PAGE gel analysis to confirm protein presence; fractions with suitable profiles were pooled and collected. Afterwards, the pooled protein was loaded into dialysis membrane tubing (MWCO 10000) and dialyzed in 2L of HSPB7 Dialysis/Storage Buffer (**Table 4-1**) with 3 mM TCEP for one hour. Afterwards, the HSPB7 Dialysis/Storage Buffer (with TCEP) was replaced, and dialysis continued for another hour.

Table 4-1. Buffers for HSPB7 Recombinant Expression and Purification

Buffer/Media Name	**Composition**
BL21 Lysis Buffer *(*Add JUST before use)*	50 mM HEPES (pH 7.6) 5 mM imidazole 350 mM NaCl 5 μg/ml DNAse I* 150 μg/ml lysozyme* 1% NP-40 1X Roche EDTA-free Protease inhibitor cocktail 4 mM βME (pH 7.5)
Wash Buffer	50 mM HEPES (pH 7.6) 5 mM imidazole 350 mM NaCl 1% NP-40 4 mM βME (pH 7.5)
Elution Buffer *(*Increase over the course of elution)*	50 mM HEPES (pH 7.6) 20-250 mM imidazole* 350 mM NaCl 1% NP-40 4 mM βME (pH 7.5)
HSPB7 Dialysis/Storage Buffer	50 mM HEPES (pH 7.6) 350 mM NaCl 15% glycerol (v/v) 3mM TCEP-HCl (pH 7.5)

After this, the dialyzed protein was concentrated down to a volume of ≤ 13 mL by a centrifugal filter unit (10000 MWCO) to be further purified by SEC. The protein was loaded onto a GE HiLoad Superdex 75 column that had been pre-equilibrated with HSPB7 Dialysis/Storage Buffer. Elutions were collected in 2 mL fractions until an appropriate A280/260 peak could be resolved. Protein-containing fractions were then pooled and concentrated in a centrifugal filter unit until a desirable stock concentration

was achieved. The protein was then aliquoted and flash-frozen in liquid nitrogen before being transferred to -80°C storage.

4.4.2.2 Immunofluorescent Analysis of zHspb7 Mutant Localization

(Performed by Dr. Marcus Long and Sanjna Surya)

HeLa cells to be used for imaging were grown to 50% confluence on glass-backed plates using complete MEM media. Upon reaching 50% confluence, cells were transfected with the appropriate plasmids using TransIT-2020 transfection reagent mix, using a fixed ratio across all plasmids (2.5 μg plasmid per 7.5 μL TransIT-2020). 48 h after transfection, cells were fixed with MeOH (-20°C, 20 min.) after a wash with cold PBS media. Following, cells were w ashed with PBS media once more, then stored in a cold room under dark conditions. When ready for use, cells were washed via incubation with 3% BSA and 0.2% Triton X-100 in PBS for 1 hr. Then, after cells were washed two more times with PBS media, cells were stained with the primary antibody with 1% BSA and 0.02% Triton X-100 in PBS for 3-4 h at room temperature. Then, after three additional PBS media rinses, cells were incubated with the secondary antibody 1% BSA and 0.02% Triton X-100 in PBS for 1 h at room temperature. Finally, after a PBS rinse, cells were stained with DAPI for 5 min., then washed twice again with PBS and stored on ice until they can be imaged via confocal microscopy.

4.4.3 T-REX-mediated Labeling of zHspb7 in HEK293T Cells

(Performed by Dr. Marcus Long and Sanjna Surya)

Across all T-REX and bolus-dosing experiments, HEK293T cell lines were grown and maintained in 1X MEM + Glutamax™ media, supplemented with 10% FBS media, 1X NEAA solution, 1X sodium pyruvate, and 1X Pen-Strep solution. Active cell lines were stored at 37 C in humidified, 5% CO2 incubators. Cell lines were maintained through routine splitting at ~80% confluence, and seeded onto new plates at ~25% confluence. Cell lines with passage numbers of 6 or higher were not used for experiments and discarded.

To prepare cell lines for T-REX experiments, HEK239T cells were split into 3 cm culture dishes at ~0.5 x 10^6 cells/plate (approximately 40% confluency). After 24 h, cells were transfected with a TransIT-2020 transfection reagent mix containing the target plasmid construct at the manufacturer's recommended concentration. Beyond this point, all steps were performed under red light. 24-36 h post-transfection, the cells were treated with 20 μM Ht-PreHNE in serum-free media and incubated for another 2 hr. Afterwards, cells were rinsed with serum-free media three times, with 30 min of incubation between rinsings. These rinsings were performed carefully so as not to disturb the cell monolayer and lose cells. During incubation following the final rinsing, 365 nm UV lamps were powered on and left to warm up for a minimum of 20 min prior to light exposure. After this warm-up phase was complete, cells designated for

light exposure were placed directly underneath the lamp for 5 min, with the dish lids removed such that the monolayers were directly exposed. The cells were then harvested after an additional 5 min post-exposure. The cell pellets were washed with ice-cold PBS twice, then once by 50 mM HEPES buffer (pH 7.6), then flash-frozen in liquid nitrogen before being stored in -80 C. Cells stored this way were generally used within 24-48 hr.

4.4.4 In-gel Fluorescent Evaluation of HNEylated Proteins

(Performed with Dr. Marcus Long)

Cells from T-REX or bolus-dosing experiments were harvested and lysed using 50 μL (per plate) of Cell Lysis Buffer (**Table 4-2**) via three freeze-thaw cycles. For each cycle, cells were vortexed after buffer addition for 15 seconds, then flash-frozen in liquid nitrogen, then allowed to thaw at room temperature. Each successive cycle began as soon as thawing from the previous cycle was completed. After the final repeat, samples were centrifuged for 10 min at 20000 x g in a pre-chilled (4°C) centrifuge. Lysate supernatants were removed from each sample, and protein concentration was assessed via Bradford dye assay.

Following, portions of lysate were removed and made up to 1.0 mg/mL protein by dilution with 50 mM HEPES (pH 7.6) and 0.3 mM TCEP. To these volumes, TEV protease was added to a final concentration of 0.2 mg/mL, such that the final total volume in each sample was 21 μL. The samples were then incubated at 37°C for 30 min. Subsequently, Cy5 click reactions were performed with each lysate, with t-BuOH

Table 4-2. Assorted Buffers for HEK293T Cell Lysis and HSPB7 Res Modification Assays

Buffer/Media Name	Composition
Cell Lysis Buffer	50 mM HEPES (pH 7.6) 1% NP-40 1X Roche cOmplete tablet (EDTA-free) 0.3 mM TCEP-HCl (pH 7.5)
10X Cy5 Click Mix	10% SDS 10 mM $CuSO_4$ 1 mM Cu(TBTA) 50 μM Cy5 azide. 17 mM TCEP-HCl (pH 7.5)
Resolubilization Buffer	8% LDS 1 mM EDTA 50 mM HEPES (pH 7.6)

and Cy5 Click Mix (Table 4-2) added such that each sample contained 5% t-BuOH and a final volume of 25 μL. These samples were incubated further at 37°C for 30 min., after which they were quenched with 8 μL of 4X Laemmeli dye containing 6% βME. After a further 5 min. at 37°C, lysates were analyzed by SDS-PAGE gel and follow-up Western blot or staining (Sypro Ruby or Coomassie), depending on context.

4.4.5 Homology Modeling and Phylogenetic Comparison Between HSPB7 Orthologs

4.4.5.1 Protein Modeling Analysis

(Performed by Dr. Marcus Long)

As no crystal structure yet exists for either zHapb7 or hHSPB7, the SWISS-MODEL online homology-modeling workspace was used to construct a comparable model for both orthologs, using human HSPB6 (PBD ID: 5LTW) as the template structure.[16–21]

4.4.5.2 Phylogenetic Analysis of HSPB7 Orthologs

(Performed with Dr. Marcus Long)

The primary sequences for all known HSPB7 homologs were imported into MEGA7, where all subsequent phylogenetic analysis was performed. Next, the evolutionary history of the SAHH homologs was inferred by Maximum Likelihood method, based on the JTT matrix-based method (**Figure 4-3a**). The subsequent phylogenetic tree generated was used to order the homologs within MEGA7, whose sequences were then aligned using MUSCLE sequence alignment algorithms, discarding positions with gaps or missing data within individual sequences.[22] Using these alignments, sequence logos of the primary sequence regions containing C49 and C119 within the zHspb7 sequence were generated using UC Berkeley's WebLogo tool.

4.4.6 Circular Dichroism Analysis of HNEylated zHspb7

(Performed by Dr. Marcus Long and Sanjna Surya)

Before analysis, zHspb7 was diluted in HSPB7 Dialysis/Storage Buffer (**Table 4-1**) to 2.8 μM (0.05 mg/mL). CD spectra of both enzymes were taken using an Aviv

400 Circular Dichroism Spectrometer, and a 150 W Suprasil Xenon lamp was used as a light source. 300 μL of each sample was analyzed at a time, using a wavelength range of 300-195 nm; measurements at each wavelength were taken with 5s averaging times, and all measurements were taken at 25°C. When measuring the CD spectra of HNElyated zHspb7, the protein was first incubated with an equivalent of HNE for 30 min. at 37°C, after which dilution was performed using a blank that contained the same final concentration of HNE. CD spectra for all zHspb7 mutants were taken similarly, but at a protein concentration of 1.85 μM and with 6 equivalents of HNE.

4.4.7 Evaluation of hHSPB7 HNEylation Under Bolus-Dosing Conditions

4.4.7.1 Bolus-Dose Labeling of hHSPB7 in HEK293T Cell Lines

(Performed with Dr. Marcus Long and Sanjna Surya)

To prepare cell lines for bolus-dosing experiments, HEK239T cells were split and grown in 10 cm plates to 60% confluence. Once at 60% confluence, cells were transfected using a PEI solution (7.5 μg plasmid, 21 μL 1 mg/mL PEI in 400 μL Opti-MEM media per plate). 24 hr. post-transfection, cells were treated with either 20 μM HNE-alkyne or DMSO for 2 hr. in serum-free media. Following, cells were rinsed twice in serum-free media, then harvested. The cell pellets were washed with ice-cold PBS twice, then once by 50 mM HEPES buffer (pH 7.6), then flash-frozen in liquid nitrogen before being stored in -80 C. Cells stored this way were generally used within 24-48 hr.

4.4.7.2 Biotin-Streptavidin Enrichment of HNEylated hHSPB7

(Performed with Dr. Marcus Long and Sanjna Surya)

Cell pellets, when ready to be used, were lysed using 200 μL of Cell Lysis Buffer (**Table 4-2**), via three freeze-thaw cycles. For each cycle, cells were vortexed after buffer addition for 15 seconds, then flash-frozen in liquid nitrogen, then allowed to thaw at room temperature. Each successive cycle began as soon as thawing from the previous cycle was completed. After the final repeat, samples were centrifuged for 10 min at 20000 x g in a pre-chilled (4°C) centrifuge. Lysate supernatants were removed from each sample, and protein concentration was assessed via Bradford dye assay.

After concentration was determined, 1 mg of each lysate was standardized to 2.0 mg/mL using Cell Lysis Buffer. To these sample volumes, TEV protease was added to a final concentration of 0.2 mg/mL. The samples were then incubated at 37°C for 45 min. Subsequently, Biotin click reactions were performed with each lysate, with final concentrations of 5% t-BuOH (added first), 1% SDS, 1 mM CuSO4, 0.1 mM CuTBTA (added simultaneously via 10x master mix), 2 mM TCEP (added penultimately), and 0.2 mM biotin azide (added last). These samples were incubated further at 37°C for 30 min. Afterward, to precipitate all proteins, pre-chilled (-20°C) EtOH was added to each sample at a 4:1 EtOH:lysate ratio, followed by overnight storage at -80°C.

After overnight storage, the precipitated proteins were pelleted by centrifugation (20000 x g, 30 min., 4°C). The pellets were washed by resuspension in 70% EtOH, then

100% EtOH, then 100% acetone, followed by centrifugation in each instance (20000 x g, 30 min., 4°C). After the final wash, pellets were left exposed to open air until excess acetone had evaporated. Without leaving the pellet dry for a significant length of time, the pellets were resuspended in 50 µL protein Resolubilization Buffer (**Table 4-2**), and then fully resolubilized via sonication for 10-15 m at 51°C. The samples were then centrifugated again (20000 x g, 5 min.), and the samples were transferred to new, clean Eppendorf tubes, with a small portion removed from each sample to be used as an input control. The remainder of each sample was then diluted with 50 mM HEPES to a volume of 750 µL (0.53% LDS).

As the above was performed, streptavidin beads were withdrawn from a stock bottle and rinsed in ddH_2O (1:1 beads:ddH_2O) twice, then 50 mM HEPES buffer once (1:1 beads:HEPES) for a minimum of 30 min. each. After each rinse, the beads were gently centrifugated (1500 x g, 1 m) and the media was swapped. After the final rinse, beads were resuspended in 50 mM HEPES (1:1). 100 µL of this resuspension was then added to each sample, for a bead volume of 50 µL per lysate sample. These samples were then incubated at room temperature on a rotator for 2-3 hr. After this, the beads were gently spun down and – after removing the supernatant- were washed three times with 0.5% LDS in 50 mM HEPES using 30 min. of end-over-end rotation (500-750 x g, 1 min. centrifugation between washes). After the third wash, beads were resuspended in 4x Lamelli dye with 6% βME, then boiled at 98°C for 5 m to promote protein elution.

The eluate was then analyzed via western blot, alongside the previously withdrawn inputs.

4.4.8 In vitro Time-dependent HNEylation of zHspb7 and Comparable HNE-sensing Proteins

(Performed with Dr. Marcus Long)

Purified protein in storage buffer (12 μM in 100 μL) was treated with an equivalent of HNE alkyne and incubated at 37°C. At each time-point, 1.5 μL of the protein was removed and quenched by dilution with chilled 30 μL of 50 mM HEPES with 1% Triton X-100. After the final time-point was withdrawn, all aliquots were treated with Cy5 click mix (**Table 4-2**) for 15 minutes at 37°C. The samples were then quenched by Laemelli buffer and analyzed via SDS-PAGE in-gel fluorescence, using a follow-up Sypro Ruby stain to normalize for protein loading.

Analyses of GSR and GAPDH were performed similarly with 36 μM protein and either 36 μM (one equivalent) or 360 μM (six equivalents) HNE-alkyne. Proteins treated with 360 μM HNE-alkyne were diluted into 90 μL pre-chilled dilution buffer instead of 30 to minimize interference from non-insignificant amounts of unbound HNE-alkyne. Click reactions for HSP70 were performed at 10 μM protein and either 36 μM (3.6 equivalents) or 360 μM (36 equivalents) HNE-alkyne; aliquots taken from both were diluted in 60 μL dilution buffer.

4.5 References

1. Long, M. J. C. *et al.* Akt3 is a privileged first responder in isozyme-specific electrophile response. *Nat. Chem. Biol.* **13**, 333–338 (2017).
2. Narberhaus, F. α-Crystallin-Type Heat Shock Proteins: Socializing Minichaperones in the Context of a Multichaperone Network. *Microbiol. Mol. Biol. Rev.* **66**, 64–93 (2002).
3. Elicker, K. S. & Hutson, L. D. Genome-wide analysis and expression profiling of the small heat shock proteins in zebrafish. *Gene* **403**, 60–9 (2007).
4. Eyles, S. J. & Gierasch, L. M. Nature's molecular sponges: Small heat shock proteins grow into their chaperone roles. *Proc. Natl. Acad. Sci. U. S. A.* **107**, 2727–2728 (2010).
5. Hilton, G. R., Lioe, H., Stengel, F., Baldwin, A. J. & Benesch, J. L. P. Small Heat-Shock Proteins: Paramedics of the Cell. in *Molecular Chaperones* (ed. Jackson, S.) 69–98 (Springer Berlin Heidelberg, 2013). doi:10.1007/128_2012_324.
6. Christians, E. S., Ishiwata, T. & Benjamin, I. J. Small heat shock proteins in redox metabolism: implications for cardiovascular diseases. *Int. J. Biochem. Cell Biol.* **44**, 1632–45 (2012).
7. Mercer, E. J., Lin, Y. F., Cohen-Gould, L. & Evans, T. Hspb7 is a cardioprotective chaperone facilitating sarcomeric proteostasis. *Dev. Biol.* **435**, 41–55 (2018).
8. Lin, H.-Y., Haegele, J. a., Disare, M. T., Lin, Q. & Aye, Y. A Generalizable Platform for Interrogating Target- and Signal-Specific Consequences of Electrophilic Modifications in Redox-Dependent Cell Signaling. *J. Am. Chem. Soc.* **137**, 6232–6244 (2015).
9. Parvez, S. *et al.* Substoichiometric Hydroxynonenylation of a Single Protein Recapitulates Whole-Cell-Stimulated Antioxidant Response. *J. Am. Chem. Soc.* **137**, 10–13 (2015).
10. Parvez, S. *et al.* T-REX on-demand redox targeting in live cells. *Nat. Protoc.* **11**, 2328–2356 (2016).
11. Zhao, Y., Long, M. J. C., Wang, Y., Zhang, S. & Aye, Y. Ube2V2 Is a Rosetta Stone Bridging Redox and Ubiquitin Codes, Coordinating DNA Damage Responses. *ACS Cent. Sci.* **4**, 246–259 (2018).
12. Barford, D. The role of cysteine residues as redox-sensitive regulatory switches. *Curr. Opin. Struct. Biol.* **14**, 679–686 (2004).

13. Jagt, D. L. V. *et al.* Inactivation of glutathione reductase by 4-hydroxynonenal and other endogenous aldehydes. *Biochem. Pharmacol.* **53**, 1133–1140 (1997).

14. Hiratsuka, A., Hirose, K., Saito, H. & Watabe, T. 4-Hydroxy-2(E)-nonenal enantiomers: (S)-selective inactivation of glyceraldehyde-3-phosphate dehydrogenase and detoxification by rat glutathione S-transferase A4-4. *Biochem. J.* **349**, 729–735 (2000).

15. Carbone, D. L., Doorn, J. A., Kiebler, Z., Sampey, B. P. & Petersen, D. R. Inhibition of Hsp72-mediated protein refolding by 4-hydroxy-2-nonenal. *Chem. Res. Toxicol.* **17**, 1459–1467 (2004).

16. Guex, N., Peitsch, M. C. & Schwede, T. Automated comparative protein structure modeling with SWISS-MODEL and Swiss-PdbViewer: A historical perspective. *Electrophoresis* **30**, (2009).

17. Benkert, P., Biasini, M. & Schwede, T. Toward the estimation of the absolute quality of individual protein structure models. *Bioinformatics* **27**, 343–350 (2011).

18. Bertoni, M., Kiefer, F., Biasini, M., Bordoli, L. & Schwede, T. Modeling protein quaternary structure of homo- and hetero-oligomers beyond binary interactions by homology. *Sci. Rep.* **7**, 1–15 (2017).

19. Bienert, S. *et al.* The SWISS-MODEL Repository-new features and functionality. *Nucleic Acids Res.* **45**, D313–D319 (2017).

20. Waterhouse, A. *et al.* SWISS-MODEL: Homology modelling of protein structures and complexes. *Nucleic Acids Res.* **46**, W296–W303 (2018).

21. Studer, G. *et al.* QMEANDisCo-distance constraints applied on model quality estimation. *Bioinformatics* **36**, 1765–1771 (2020).

22. Edgar, R. C. MUSCLE: A multiple sequence alignment method with reduced time and space complexity. *BMC Bioinformatics* **5**, 1–19 (2004).

APPENDIX A

General Materials

Table A-1. Common reagents used across all projects in this work.

Manufacturer	Reagent
Thermo Scientific	Phusion Hotstart II polymerase
	BSA
New England Biolabs	All restriction enzymes
IDT	All primers
Roche	cOmplete EDTA-free protease inhibitor
	AdoD
BioRad	Bradford dye
	PVDF membrane
	Gel ladders
Lumiprobe	(Cy5)-azide
	Cu(TBTA)
Goldbiochem	Dithiothreitol
	Streptomycin Sulfate
	Ampicillin
	Kanamycin
	IPTG
	TCEP-HCl
Promega	HaloTag® TMR-Ligand
Quanta Biodesign	Biotin-dPEG®11-azide
Pierce	High-capacity Streptavidin agarose
JT Baker	$MnCl_2$
	$ZnSO_4$
	$CuSO_4$
	$MgSO_4$
	Sodium Citrate
Fisher	K_2HPO_4
	KH_2PO_4
	BSA
	BME
	EDTA
	Glycerol

	Methanol
	Agar
	NP-40 / Triton X-100
	Dialysis plasticware
Life Technologies	Penicillin/streptomycin
	Nystatin
	PBS
	Sodium pyruvate
	DMEM / OptiMEM media
	NEAA
EMD	NaCl
Chem-Impex	Tris base
	HEPES
Invitrogen	BL21(DE3)–RIL starter cells
American Type Culture Collection	HEK293T / HeLa starter cells
University of Minnesota Caenorhabditis Genetics Center	*C. elegans* N2 wild-type lines
	OP50 starter cells
ClonTech	TALON resin
	His_6 Ni-NTA resin
Mirus	TransIT-2020 transfection reagent
Polysciences	PEI
VWR	Agar plate dishes
	Tryptone
CellTreat	Sterile plasticware
Millipore	Centricon plasticware
GE	Sephadex resin
Qiagen	Plasmid Mini/Maxiprep kits
Sigma	All other materials

Table A-2. Antibodies used in Chapter 2.

Antibody	Catalog Number	Dilution
Mouse monoclonal anti-β-Actin	A4700; Sigma	1:5000 – 1:10000
Rabbit polyclonal anti-Halo	G9281; Promega	1:1000

Mouse monoclonal anti-Halo	G921A; Promega	1:1000
Mouse monoclonal anti-Keap1	Ab119403, Abcam	1:1000
Mouse monoclonal anti-GFP	Sc-9996; Santa Cruz Biotechnology	1:1000
Secondary antibody to rabbit IgG, HRP linked	7074; Cell Signaling Technology	1:5000-1:10000
Secondary antibody to mouse IgG, HRP linked	Ab6789; Abcam	1:5000

Table A-3. Antibodies used in Chapter 3.

Antibody	Catalog Number	Dilution
Rabbit polyclonal anti-Halo	G9281; Promega	1:1000
Rabbit polyclonal anti-Flag	PA1-984B; Fisher	1:2000
Secondary antibody to rabbit IgG, HRP linked	7074; Cell Signaling Technology	1:5000-1:10000
Anti actin-HRP	Sigma	1:30000

Table A-4. Antibodies used in Chapter 4.

Antibody	Catalog Number	Dilution (WB/IF)
Rabbit polyclonal anti-Halo	G9281; Promega	1:1000/1:500
Rabbit polyclonal anti-Flag	PA1-984B; Fisher	1:2000/1:500
Secondary antibody to rabbit IgG, HRP linked	7074; Cell Signaling Technology	1:5000-1:10000 (WB)
Anti actin-HRP	Sigma	1:30000 (WB)
Donkey anti rabbit-Alexa 647	Abcam; AB150075	1:700 (IF)

Table A-5. List of laboratory equipment common to all projects.

Manufacturer	Equipment
Leica	M205 FA stereomicrosope
Spectroline	XDS-1000 UV power sensor
	ENF240C handheld UV lamp
	XX15N UV lamp
BioRad	Chemi-Doc MP imaging system
	Electrophoresis chambers
BioTek	Cytation 5 plate reader
GE	Superdex filtration columns
VWR	*C. elegans* benchtop incubators
Percival Scientific	*C. elegans* 13°C incubator

Table A-6. List of specialty software common to all projects.

Publisher/Developer	Software
Graphpad	Prism 6
Leica	Leica Application Suite X
BioRad	Image Lab
Pennsylvania State University	Molecular Evolutionary Genetics Analysis
University of Illinois: Urbana-Champaign	Visual Molecular Dynamics
University of California, San Francisco	UCSF Chimera
National Institutes of Health	ImageJ
GSL Biotech	SnapGene
University of Basel	SWISS-MODEL web server

Table A-7. Table of compounds originally synthesized within the Aye group.

Probe	Structure	Originally Synthesized By:
Ht-preHNE (alkyne)	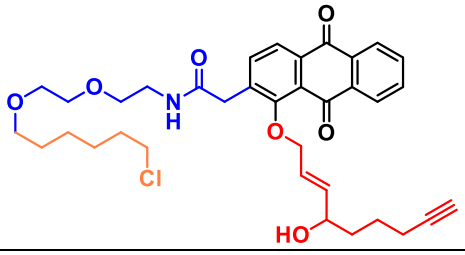	Dr. Xinqiang Fang Dr. Hong-Yu Lin Dr. Yi Zhao Dr. Joseph Haegele Yiran Wang
Ht-preHNE	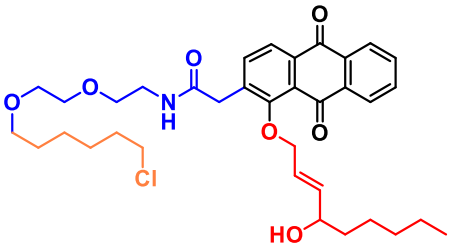	Dr. Xinqiang Fang Dr. Hong-Yu Lin Dr. Yi Zhao Dr. Joseph Haegele Yiran Wang
Ht-PredHNE (alkyne)	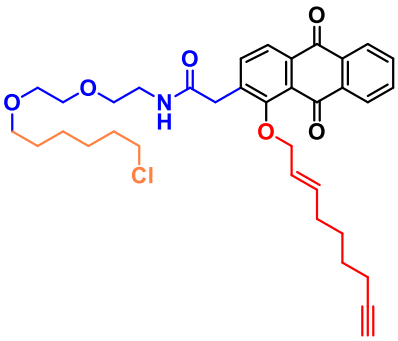	Dr. Hong-Yu Lin
Ht-PreHDE (alkyne)	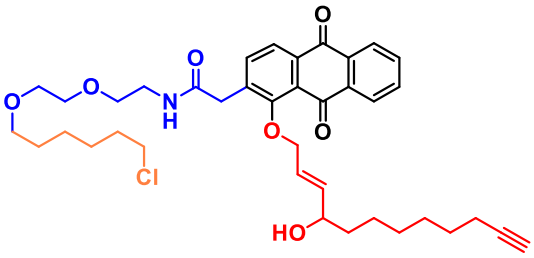	Dr. Hong-Yu Lin
HNE (alkyne)	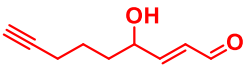	Dr. Xinqiang Fang Dr. Hong-Yu Lin Dr. Yi Zhao Dr. Joseph Haegele Yiran Wang

Ht-TMR (Homemade HaloTag-TMR ligand)	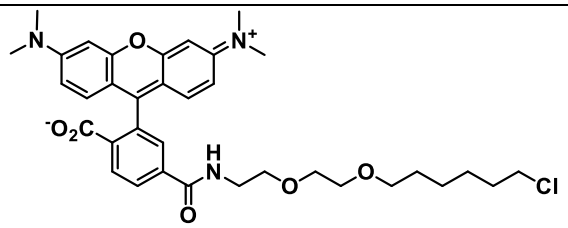	Dr. Souradyuti Ghosh Dr. Yi Zhao Shivansh Chawla

APPENDIX B

Plasmid Construction and Primer Sequences

General Plasmid Construction Protocol

For any plasmid not acquired directly from an outside source, ligase-free cloning was utilized. To subclone a target fusion gene into a new vector of choice, the target gene is first PCR-amplified from the original plasmid using the appropriate forward (fwd-1) and reverse (rev-1) primers. Then, the PCR product was extended using the appropriate fwd-2 and rev-2 primers (and, subsequently, fwd-3/rev-3, if necessary). The megaprimer is then inserted into the target vector via PCR after linearization via the appropriate restriction enzyme.

To verify that the cloning protocol produced the correct gene insert, all plasmids were verified via sequencing before use. Sequencing was performed via Cornell Institute of Biotechnology (at Cornell) or Microsynth AG (at EPFL). The quality of all traces were manually evaluated prior to use. Upon adding a plasmid to our library (**Table B-1**), any subsequent preparation/regeneration of that plasmid is checked with sequencing before use to ensure the integrity of the insert.

Constructs and Primer Sequences

Table B-1. Table of plasmids/constructs used.

Plasmid	Promoter	Gene Insert
pET28a	T7	*his$_6$::halo::tev::keap1*
		his$_6$::halo::flag::hsahh(WT)
		his$_6$::halo::flag::hsahh(C195S)
		his$_6$::halo::flag::hsahh(C266S)
		his$_6$::halo::flag::hsahh(C278A)
		his$_6$::halo::flag::hsahh(C266S/I279K)
		his$_6$::halo::flag::cesahh(WT)
		his$_6$::halo::flag::cesahh(C278A)
		his$_6$::halo::tev::zhspb7(WT)
		his$_6$::halo::tev::zhspb7(C49S)
		his$_6$::halo::tev::zhspb7(C117S)
		his$_6$::halo::tev::zhspb7(C49S/C117S)
		hhspb7::myc::flag
pRK793	Tac	*mbp::his$_6$::tev_protease**
pMIR (dsRed-IRES)	CMV	*his$_6$::halo::tev::keap1*
pFN21a	CMV	*his$_6$::halo*
		his$_6$::halo::flag::hsahh(WT)
		his$_6$::halo::flag::hsahh(C195S)
		his$_6$::halo::flag::hsahh(C266S)
		his$_6$::halo::flag::hsahh(C278A)
		his$_6$::halo::flag::hsahh(C266S/I279K)
		his$_6$::halo::flag::cesahh(WT)
		his$_6$::halo::flag::cesahh(C278A)
pCS2+8	SP6	*his$_6$::halo::tev::zhspb7(WT)*
		his$_6$::halo::tev::zhspb7(C49S)
		his$_6$::halo::tev::zhspb7(C117S)
		his$_6$::halo::tev::zhspb7(C49S/C117S)
		his$_6$::halo::tev::zhspb7(H115D)
		hHSPB7::myc::flag
Lig778	Hsp-16.41	*his$_6$::halo*

		his$_6$::halo::tev::keap1
		gfp::halo
		tom70::mcherry::halo
pJKL-502	hlh8	*gfp::halo*

Table B-2. Table of primers used in Chapter 2

Primer name	Sequence	Primer Type
hkeap1-Lig778-rev	ATGACAGCGGCCGATGCGGAGCTCTTATC AACAGGTACAGTTCTGCTGGTCAAT	rev-1
Lig778-His$_6$-Fwd-Met_Fix	TTGTGAAATTAGAAATCTTCAAACTATAATC ATCTCACTATGGGCAGCAGCCATCATCAT	fwd-1
Halo_Rev_UTR	ATGACAGCGGCCGATGCGGAGCTCTTAGC CGGAAATCTCGAGCG	rev-1
*gfp*_Fwd_Lig778	AAATTAGAAATCTTCAAACTATAATCATCAC TATGGTGAGCAAGGGCG	fwd-1
*gfp*_fwd_*hlh*	AACTGACCGATTTCAAATATGATTTTCACA GATGGTGAGCAAGGGCG	fwd-1
Lig778_TOM70	GAAATTAGAAATCTTCAAACTATAATCATCT CACTATGAAGAGCTTCATTACAAGGAACA	fwd-1
Lig778_fwd extender	TACCGAACAACATTTGCTCTAATTGTGAAA TTAGAAATCTTCAAACTATAATCATCTCAC	fwd-2
Lig778_UTR extender	TTGGACTTAGAAGTCAGAGGCACGGGCGC GAGATGGCGATCTGATGACAGCGGCCGAT GC	rev-2
*halo*_rev_*hlh*_UTR	TAGAAGTCAGAGGCACGGGCGCGAGATGT TAGCCGGAAATCTCGAGCG	rev-2
*hlh*_fwd_extender	TGTGTTACTTTTCATATGTTTATTACTTGAA CTGACCGATTTCAAATATGATTTTCACAG	fwd-2
Rev_extender_*hlh*_UTR	GAAAGAGCATGTAGGGATGTTGAAGAGTA ATTGGACTTAGAAGTCAGAGGCACGGGC	rev-2

Table B-3. Table of primers used in Chapter 3

Primer name	Sequence	Primer Type
Human C266S-AHCY-Fwd	GTGACCACCATGGATGAGGCCTCTCAGGAG	fwd-1
Human C266S-AHCY-Rev	ACAAAGATGTTGCCCTCCTGAGAGGCCTCATC	rev-1
Human C195S-AHCY-Fwd	AAGTTTGACAACCTCTATGGCTCCCGGGAGT	fwd-1
Human C195S-AHCY-Rev	CCATCTATGAGGGACTCCCGGGAGCCATAG	rev-1
Human C278A-AHCY-Fwd	CAACATCTTTGTCACCACCACAGGCGCTATTGACATCATCCTTGGCCGGCACTTTG	fwd-1
Human C278A-AHCY-Rev	CAAAGTGCCGGCCAAGGATGATGTCAATAGCGCCTGTGGTGGTGACAAAGATGTTG	rev-1
Human I279K-AHCY-Fwd	GGCAACATCTTTGTCACCACCACAGGCTGTAAAGACATCATCCTTGGCCGGCACTTTGAG	fwd-1
Human I279K-AHCY-Rev	CTCAAAGTGCCGGCCAAGGATGATGTCTTTACAGCCTGTGGTGGTGACAAAGATGTTGCC	rev-1
Human AHCY into pEt28a – fwd	TGGTGCCTCGTGGTAGCCATATGTCTGACAAACTGCCCTACAAAGTC	fwd-2
Human AHCY into pEt28a - rev	CTCAGCTTCCTTTCGGGCTTTGTTATCAGTAGCGGTAGTGATCCGGCTT	rev-2
C. elegans AHCY into pEt28a - fwd	TGGTGCCTCGTGGTAGCCATATGGCCCAGTCTAAGCCAGCTTACAAG	fwd-2
C. elegans AHCY into pEt28a - rev	CTCAGCTTCCTTTCGGGCTTTGTTATTAATATCTGTAGTGGTCTGGCTTGTATG	rev-2
pet28a forward extender	ATGGGCAGCAGCCATCATCATCATCATCACAGCAGCGGCCTGGTGCCTCGTGGTAGCCAT	fwd-3
pet28a reverse extender	TAT GCT AGT TAT TCA GCG GTG GCA GCAGCCAACTCAGCATCCTTTCGGGCTTTGTTA	rev-3

Table B-4. Table of primers used in Chapter 4

Primer name	Sequence	Primer Type
HSPB7_C49S_fwd	GACTTTGGATCTTTCATGAGTCCGAAGGATGCTTTGGGATTT	fwd-1
HSPB7_C49S_rev	AAATCCCAAAGCATCCTTCGGACTCATGAAAGATCCAAAGTC	rev-1
HSPB7_C117S_fwd	AACACTTTCACCCATAAAAGCCGGCTACCAGAAGATGTGGAC	fwd-1
HSPB7_C117S_rev	GTCCACATCTTCTGGTAGCCGGCTTTTATGGGTGAAAGTGTT	rev-1
HSPB7pet28afwd	TGGTGCCTCGTGGTAGCCATATGAGCGCGAGCAATTCTTC	fwd-1
HSPB7pet28arev	CTCAGCTTCCTTTCGGGCTTTGTTACTAGATTTTGATCTCTGTGCGGAAC	rev-1
pet28a forward extender	ATGGGCAGCAGCCATCATCATCATCATCACAGCAGCGGCCTGGTGCCTCGTGGTAGCCAT	fwd-2
pet28a reverse extender	TATGCTAGTTATTCAGCGGTGGCAGCAGCCAACTCAGCATCCTTTCGGGCTTTGTTA	rev-2

APPENDIX C

Miscellaneous General Methods

Protein/Lysate quantitation

Bradford Quantitation: 1 mL aliquots of Bradford reagent are set aside (3 per sample, including buffer blank). Then, to each, 1 μL of each protein/lysate is added to each aliquot of Bradford dye accordingly. The aliquots are then mixed and distributed in 200 μL volumes onto a 96-well plate in technical duplicate. The plate is then read and quantitated on a Cytation 5 plate reader.

A280 Quantitation: 2 μL of purified protein samples and blank were loaded in duplicate onto a BioTek Take3 micro-volume plate. The plate was then loaded into a Cytation 5 reader and quantitated accordingly.

Antibody validation

Upon usage of any antibodies for Western blot analysis or immunofluorescence studies, an additional condition where the target protein is not present or expressed is used as a negative control. For cells, this consists of a non-transfected population. For *C. elegans,* this consists of transgenic worms who have not undergone heat-shock; if the transgene is constitutively expressed, wild-type N2 worms are used instead. The resultant signal is compared to a positive control to determine antibody quality.

SDS-PAGE gel preparation and staining

For in-gel fluorescence detection, gel staining, or Western blot analysis, SDS-PAGE gels are prepared within the lab (10 or 15% SDS, depending on target protein size). For LC-MS/MS submissions, individually packaged gradient (4-20% SDS) gels were instead purchased from BioRad and carefully maintained to minimize contamination.

After electrophoresis, SDS-PAGE gels are rinsed with ddH_2O briefly to wash out excess detergent. At this stage, non LC-MS/MS gels are either imaged (fluorescent detection), transferred to PVDF membranes (see Western Blotting Protocol below). In the former case, after imaging, all gels are stained either with Coomassie Brilliant Blue solution (2-4 hrs. staining; overnight destain in ddH_2O) or Sypro Ruby solution (manufacturer's protocols followed for fixing/staining/washing using Basic Protocol), depending on the required detection range.

Western blotting protocol

All Western blot transfers were performed on ice in a 4°C cold room, with cold packs added to the chamber to prevent any fluctuation in temperature. Transfers were then performed at low voltage (typically 20-40 V depending on power source) overnight. After transfer, membranes were incubated with 5% milk in TBST media for 1 hr. at a minimum. Following this, membranes were treated with primary antibodies in 1% milk in TBST media (see **Table A-2 - 4** for antibody dilutions) for a minimum

of 2 hrs. at room temperature (longer in cases where low global detection was anticipated; overnight incubations are conducted at 4°C). Then, following triplicate TBST rinses, membranes were incubated with HRP-conjugated secondary antibodies in a similar fashion (45 min., room temperature). Afterwards, membranes were washed twice with TBST, once with TBS, then imaged using HRP detection reagents.

If a second epitope tag was to be detected on the membrane using appropriately different secondary antibodies, the bound HRP was subjected to sodium azide deactivation (100 mM NaN_3, 2 hr, minimum) before washing and incubation with the next primary antibody. If not, the membrane was instead stained with Coomassie (5 min.) and left to dry.

C. elegans *synchronization protocol*

Whenever a worm population required age synchronization, that population is first raised on OP50 plates until it was close to reaching food scarcity (many adult worms and many eggs are visible). The plate was rinsed and the worms were collected in M9 media into a 15 mL conical tube. Following, the worms were pelleted and washed three times with fresh M9 media. The pellet was then treated with a 20% alkaline hypochlorite solution for 5 minutes; during this time, the tube was periodically agitated and monitored under a light microscope. After 5 minutes, if only eggs were largely visible, the tube was spun down, the solution removed, and the remaining egg pellet diluted in M9 media. After 2 more washes, the egg pellet was resuspended in 0.5 mL

M9 media, transferred to a 1.5 mL tube, and placed on an end-to-end rotator overnight to allow the eggs to hatch and the resultant worms arrest at L1 state. The following day, the L1 worms were plated and evaluated to synchronicity and apparent health.

C. elegans ***fluorescent imaging protocol***

Glass slides for imaging were prepared in advance by seeding each slide with several drops of freshly prepared 3% agarose in ddH_2O, forming a pad atop the slide. To these slides, several drops of 1 mM levamisole were added immediately prior to imaging. Then, worms to be imaged were transferred using a sterilized Pt pick into the levamisole droplet. A glass cover slip was gently placed atop the droplet, completing the mounting process. Parameters for imaging all samples in a given group were then determined using a wild-type and transgenic worm sample.

Common statistical methods

All statistical analyses were performed using GraphPad Prism version 6. Signal quantitations of Western blots and fluorescence gels were performed using ImageJ v. 1.50i. Data presented throughout this work is expressed in terms of mean and standard error of the mean unless specified otherwise. Comparative analyses of groups used two-tailed unpaired t tests unless specified otherwise, with a p value of < 0.05 treated as significant. No method of pre-determination was used to determine sample sizes.

APPENDIX D

Preliminary Insights into SAHH Catalytic Attenuation Upon HNE Labeling

Before experimenting with the apoenzyme, we first sought to measure any discernable impact of HNE labeling on hSAHH activity by comparing WT and C266S post T-REX labeling via direct assaying of the cell lysate. However, attempting to gauge the activity of labelled Halo-Flag-hSAHH in HEK239T lysate did not lead to an observable effect on SAH hydrolysis after accounting for lysate background (**Figure F-1 a**). This was not unexpected given the low occupancy of hSAHH by HNE we had determined prior, coupled with the elevated background activity from HEK293T lysate. However, when we attempted exploratory exposure of recombinant hSAHH to excess HNE, we did not notice a significant change in activity, despite elevated [hSAHH] (**Figure F-1 b**).

To see if our observations regarding apo-hSAHH RES binding **(Figure 3-14)** translated to a readable change in catalytic activity, we titrated the recombinant holo-hSAHH and apo-hSAHH with HNE; when measuring activity at each HNE concentration, we were able to discern a loss of activity in the apoenzyme, whereas such behavior was not replicated in holo-hSAHH (**Figure F-2 a, b**). We followed this with an NAD^+ titration of the apoenzyme pre-treated with various concentrations of HNE; doing so, we noticed that we could achieve a variable V_{max} depending on the HNE pre-treatment (**Figure F-2 c**). The combination of increased sensitivity to HNE labeling

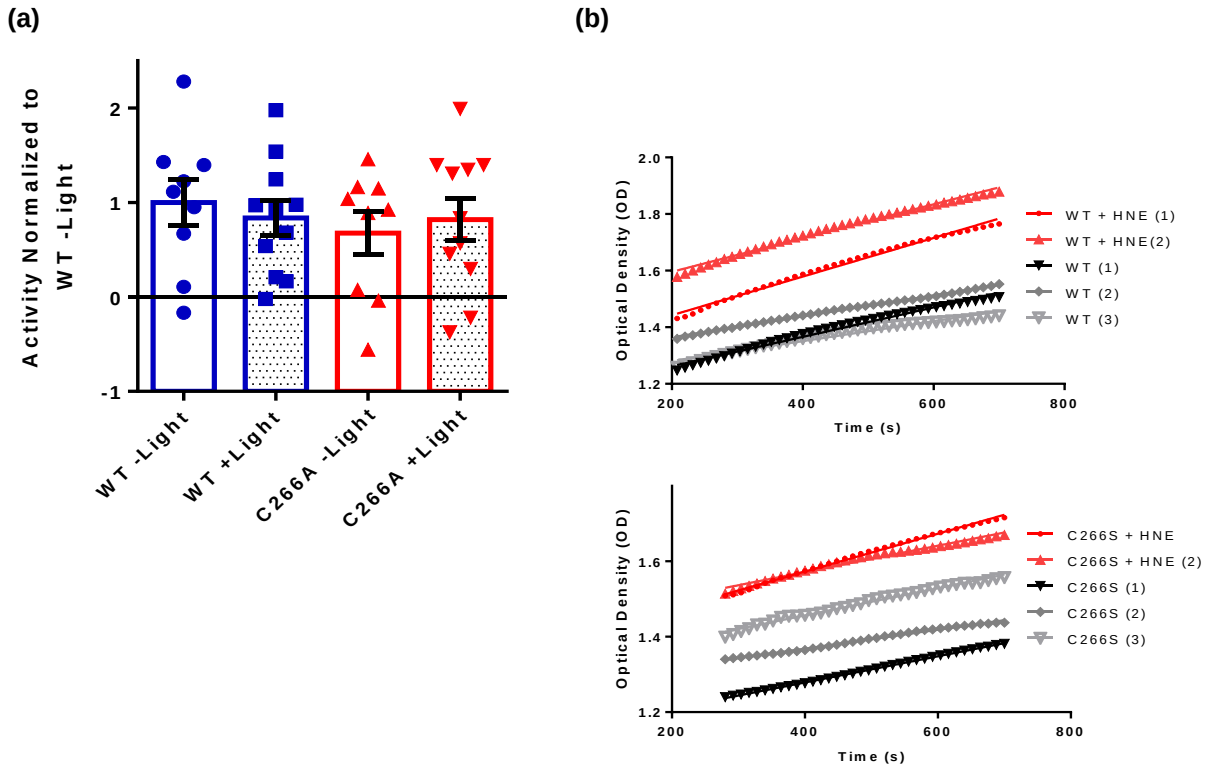

Figure D-1. **(a)** T-REX of WT and C266A hSAHH in HEK293T cells, measured as a function of activity normalized to non-light exposed WT activity. **(b)** Representative steady-state time frames of raw progress curves of WT and C266S hSAHH with and without HNE bolus dosing. Optical density was measured at 412 nm.

and activity attenuation upon labelling suggest a possibility of a pseudo-competitive system between a bound RES and NAD^+ that translates celluar RES levels into SAHH activity flux. Further testing of hSAHH mutants would be required to confirm this theory, however.

Regardless of the accuracy of this "pseudo-competitive" system, however, there exists the requirement to showcase a similar post-RES labeling behavior in CeSahh to further connect the orthologs. Complicating our analysis was the relative instability of the C278A upon SEC purification; while induction and Ni-NTA purification of the two

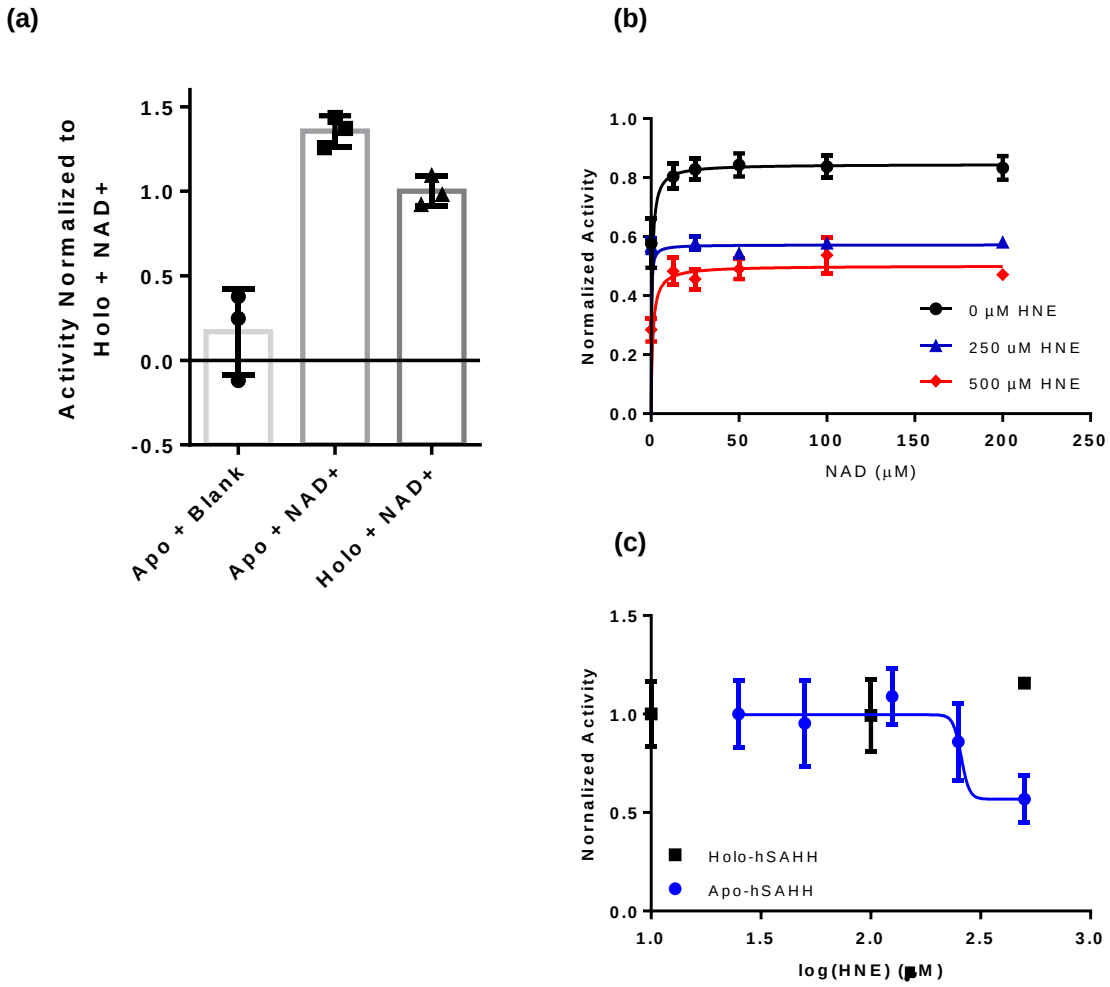

Figure D-2. Demonstration of NAD^+/HNE interactivity in in the SAHH redox binding pocket. **(a)** Validation of apo-hSAHH activity recovery upon titration of NAD^+. Activity was normalized to the holo-enzyme. Error bars show SEM (n = 3). **(b)** NAD^+ titration of apo-hSAHH following direct HNE treatment. V_{max} of each treatment was as follows: .845 ± .078 for untreated hSAHH, .572 ± .117 at 250 µM, .501 ± .049 at 500 µM. **(c)** Quantitation of comparative sensitivity of holo-hSAHH and apo-hSAHH to direct HNE treatment, following addition of 25 µM NAD^+. IC50 of HNE with regards to the apo protein was determined to be ~253 µM, with maximum inhibition of ~43%.

CeSahh enzymes proceeded without issue (**Figure F-3**), follow-up SEC purification produced consistently inactive protein. We instead opted to follow up Ni-NTA

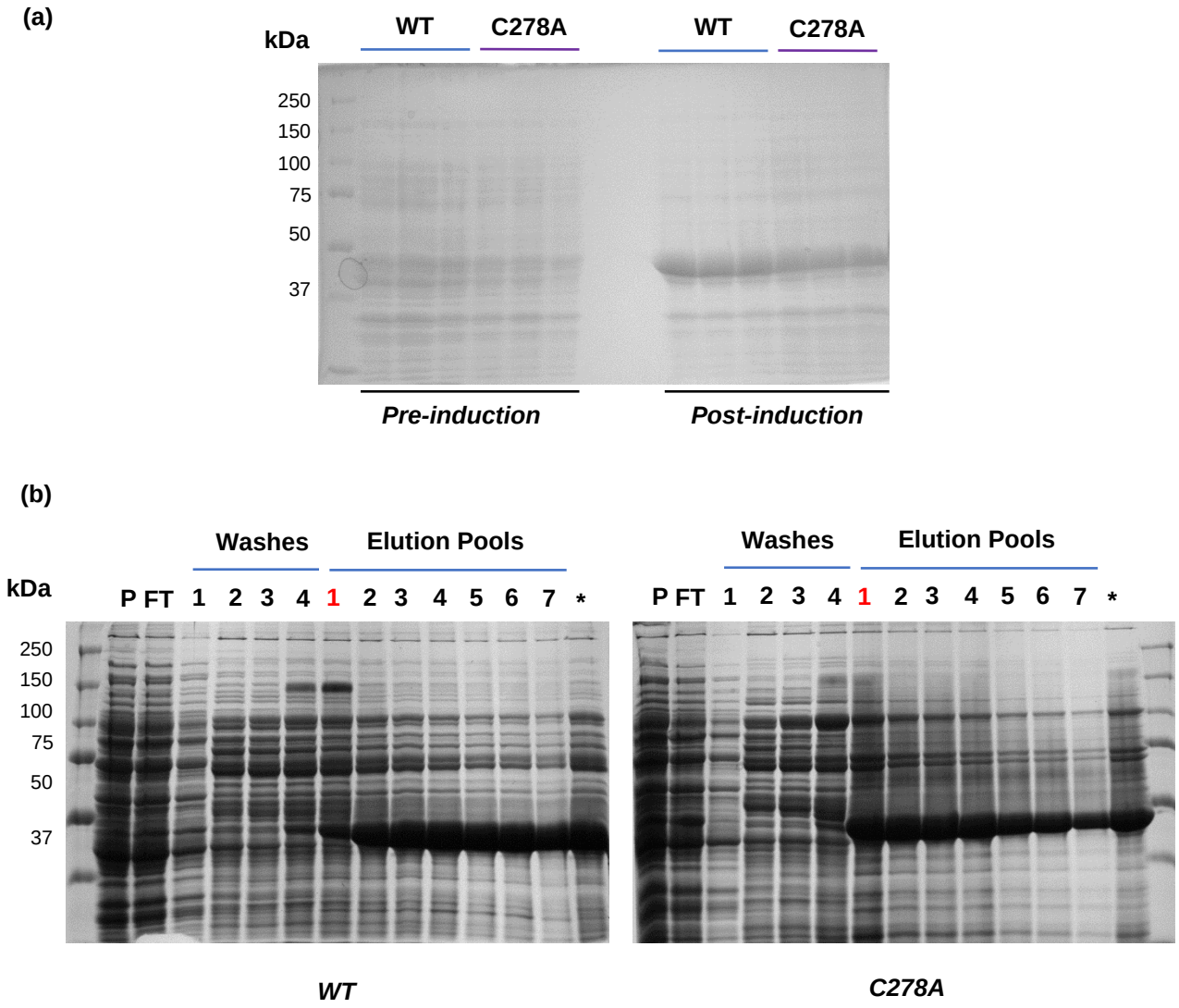

Figure D-3. Generation of recombinant CeSahh and the C278A loss-of-sensing mutant. **(a)** Coomassie stain gel of representative induction test of WT and C278A loss-of-sensing CeSahh mutant in BL21 DE3 lysate. **(b)** Representative Ni-NTA purification of WT (left) and C278A (right) CeSahh, followed by concentration and overnight dialysis in SAHH storage buffer (see lane marked *).

purification with overnight dialysis into storage buffer. We were able to then titrate the resultant enzyme with HNE (**Figure F-4**). In doing so, we were able to determine a

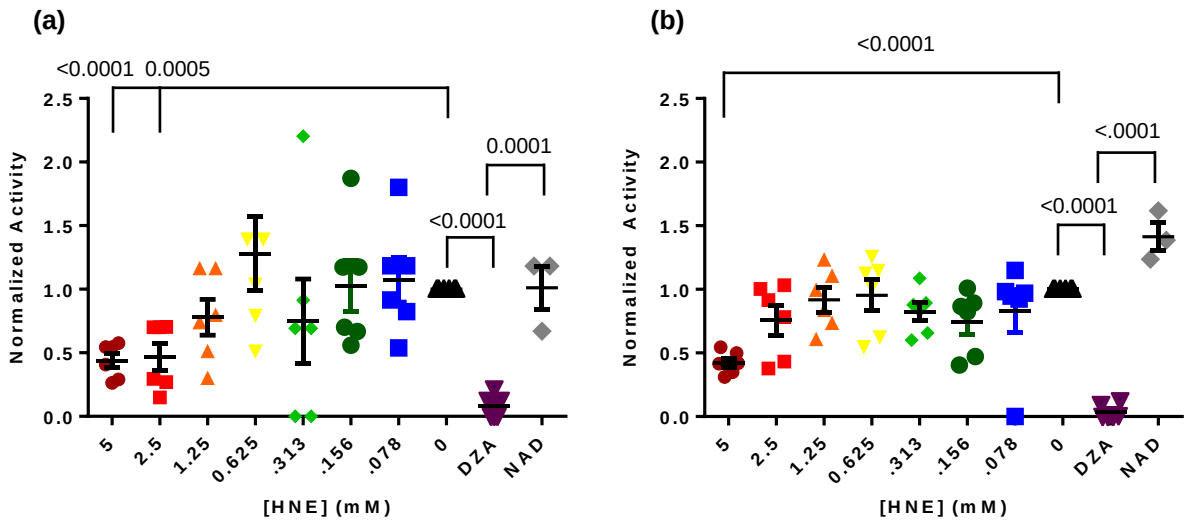

Figure D-4. HNE-driven inhibition of high-concentration CeSahh. **(a)** Titration of HNE into WT CeSahh. Activity is normalized to untreated CeSahh. DZA and supplemental NAD^+ controls are included (n = 3 for NAD^+; n = 6 otherwise). **(b)** Titration of HNE into loss-of-sensing C278A CeSahh. Activity is normalized to untreated CeSahh. DZA and supplemental NAD^+ controls are included (n = 3 for NAD^+; n = 6 otherwise).

reduced – but not altogether eliminated – sensitivity to high-concentration HNE dosing in the C278A mutant, when contrasted to the WT enzyme.

It is difficult to directly compare the results obtained from stable, purified recombinant hSAHH to that of high-concentration CeSahh evaluated in the manner shown here. At a minimum, analysis of the catalytic response to HNE labeling of hSAHH mutants – namely C266S and C266S/I279K – is required, as is an evaluation of apo-CeSahh labelling for both WT and the C278A mutant. However, the data thus far offers a promising start to establishing a model of pseudo-competition between a bound RES and NAD^+ cofactor, wherein the presence of elevated RES perturbs NAD^+

binding in such a manner that SAHH activity is attenuated. It is possible that shifting the primary cysteine sensor away from NAD^+ allows for increased sensitivity to lower [RES]; the presence of tightly-bound NAD^+ may preclude any RES binding and accumulation at C278, whereas binding at C266 may permit an incoming RES to sterically interact with NAD^+ in such a manner as to increase dissociation.